Investigation of Unsteady Flow Conditions at Dam Bottom Outlet Works Due to Air Entrainment During Gate Closure

VOLUME II: COMPUTATIONAL MODELLING

Gerrit Basson (Editor)

WATER RESEARCH COMMISSION

TT 529/12

INVESTIGATION OF UNSTEADY FLOW CONDITIONS AT DAM BOTTOM OUTLET WORKS DUE TO AIR ENTRAINMENT DURING GATE CLOSURE

Volume II: Computational Modelling

GERRIT BASSON (Editor)

Report to the

Water Research Commission

by

Institute for Water and Environmental Engineering

Department of Civil Engineering

University of Stellenbosch

WRC Report No. TT 529/12

July 2012

WATER RESEARCH COMMISSION

UNIVERSITEIT·STELLENBOSCH·UNIVERSITY
jou kennisvennoot • your knowledge partner

OBTAINABLE FROM

Water Research Commission
Private Bag X03
Gezina, 0031
Republic of South Africa

orders@wrc.org.za or download from www.wrc.org.za

The publication of this report emanates from a project entitled *Hydraulic Testing of the Outlet Works of the Berg River Dam* (WRC Project No. K5/1914//1).

This report forms part of a series of two reports. The other report in the series is *Investigation of unsteady flow conditions at dam bottom outlet works due to air entrance during gate closure* (WRC Report No. TT 528/12)

ISBN 978-1-4312-0287-4
Set No. 978-1-4312-0288-1
Printed in the Republic of South Africa

SYNOPSIS

The Berg River Dam is equipped with the first multi-level draw off environmental flood release outlet in South African and can release flows of up to 200 m^3/s. The outlet is controlled by a radial gate and is protected by a vertical emergency gate. Commissioning tests of the emergency gate in 2008 found that large volumes of air were expelled from the air supply shaft designed to reduce expected negative pressures in the conduit during emergency gate closure.

In 2009 Stellenbosch University was first commissioned by the WRC to investigate this phenomenon. The 2009 study, comprising of tests on a 1:40 scale physical model and a two-dimensional numerical computational fluid dynamics (CFD) analysis, was inconclusive on the cause of the large air releases. This report (Volume II) covers subsequent study using three-dimensional CFD analyses. The accompanying Volume I covers subsequent study using a 1:14.066 scale physical model.

A three-dimensional CFD model was successfully created and results of steady-state simulations of various fixed gate opening were studied in detail and compared to physical model simulations (see Volume I). The flow patterns shown in the CFD model were very similar to those seen in the physical model and the graphical representation of flows provided by the CFD analysis helped give a clear understanding of the flow, although the discharge through the CFD model was found to be greater than that in the physical model.

The model was then successfully adapted to perform a closing gate transient simulation. However, the excessive computational time required by the solver meant that only a single simulation of a very fast gate closure could be completed. Further, comparison of pressure results with those from the physical model showed that energy losses are significantly underestimated by the CFD model. The CFD model, therefore, could not aid in explaining the airshaft expulsions experienced in the commissioning tests.

ACKNOWLEDGEMENTS

The research in this report emanated from a project funded by the SA Water Research Commission entitled:

INVESTIGATION OF UNSTEADY FLOW CONDITIONS AT DAM BOTTOM OUTLET WORKS DUE TO AIR ENTRAINMENT DURING GATE CLOSURE.

The Reference Group responsible for this project consisted of the following persons:

Mr W Nomquphu	WRC (chairperson)
Mr L Furstenburg	Knight Piésold
Mr S Malan	Goba/BRC
Prof G Pegram	University of KwaZulu-Natal
Dr P Roberts	SANCOLD/Consultant
Dr M Shand	Aurecon
Mr T Tente	TCTA
Dr P Wessels	DWA

The following persons also attended a Reference Group meeting and contributed towards a better understanding of what happened during the 2008 commissioning tests at Berg River Dam:

Mr R Fraser	Aurecon/BRC
Mr J Metcalf	Goba
Mr L Mills	Knight Piésold /BRC

The financing of the project by the Water Research Commission and TCTA, and the contribution of the members of the Reference Group are gratefully acknowledged.

This report was edited by Prof Gerrit Basson of the University of Stellenbosch.

Co-authors of this report were Ms R Kime and Ms D Pulle of the University of Stellenbosch. Co-workers on this project, all from the University of Stellenbosch, were, Mr J Calitz, Mr W Kamish, Mr H Schwedhelm, Ms L Schulze, Mr D van den Heever, Mr C Visser and Ms A Vos.

TABLE OF CONTENTS

LIST OF FIGURES

LIST OF TABLES

LIST OF ABBREVIATIONS

A	Area (m^2)
B	Gate width (m)
BWP	Berg Water Project
CFD	Computation fluid dynamics
D	Conduit diameter or height
DWA	Department of Water Affairs
F_r	Froude number
Fr_c	Froude number at vena contracta
g	Gravitational constant (m/s^2)
G	Percentage of gate opening
h	Full size of gate opening
Hz	Hertz
km	Kilometre
L	Tunnel length
m	Metre
m^2	Metre square
mA	Milli-ampere
masl	Meters above sea level
mm	Millimetre
p	Prototype
Q_a	Air flow (m^3/s)
Q_W	Water flow (m^3/s)
R_e	Reynolds number
s	Seconds
T	Top width of flow passage (m)
TCTA	Trans-Caledon Tunnel Authority
V	Mean flow velocity (m/s)
V	Volt
v	Kinematic viscosity of water
W_e	Webber number
y	Flow depth
y_e	Effective flow depth (m)
β	Air demand ratio
Ω	Ohm
γ_w	Water specific weight
ΔP	Sub-atmospheric pressure after gate
ρ_w	Water density

1. INTRODUCTION

1.1 Berg Water Project

Water is of critical importance to protect and maintain healthy ecosystems as well as to provide for basic human needs. It also supports South Africa's mines, power generation and industries, and it is used for recreational purposes. Water is the key to development and a good quality of life.

The Berg Water Project (BWP) is the result of a 14-year strategic integrated planning process carried out by the Department of Water Affairs (DWA) to identify suitable measures to address the increasing water demand in the Greater Cape Town region. The BWP includes the Berg River Dam (previously known as the Skuifraam Dam) and supplement scheme. The supplement scheme pumps a portion of the winter high flows from downstream tributaries back into the Berg River Dam to augment the water from the Berg River as an additional water supply to the Greater Cape Town region and to supply environmental requirements. The Berg River Dam is situated in the La Motte plantation, about 6 km west of Franschhoek, and the supplement scheme is located approximately 10 km downstream of the dam (TCTA, 2008).

1.2 Berg River Dam

The Berg River Dam on the Berg River forms the major part of the Berg Water Project. The dam is operational alongside the Theewaterskloof Dam, situated in the Breede River catchment. The Riviersonderend inter-basin transfer tunnel, constructed through the Franschhoek Mountain range, links the two dams to provide water to the Greater Cape Town area (**Figure 1-1**) (TCTA, 2008).

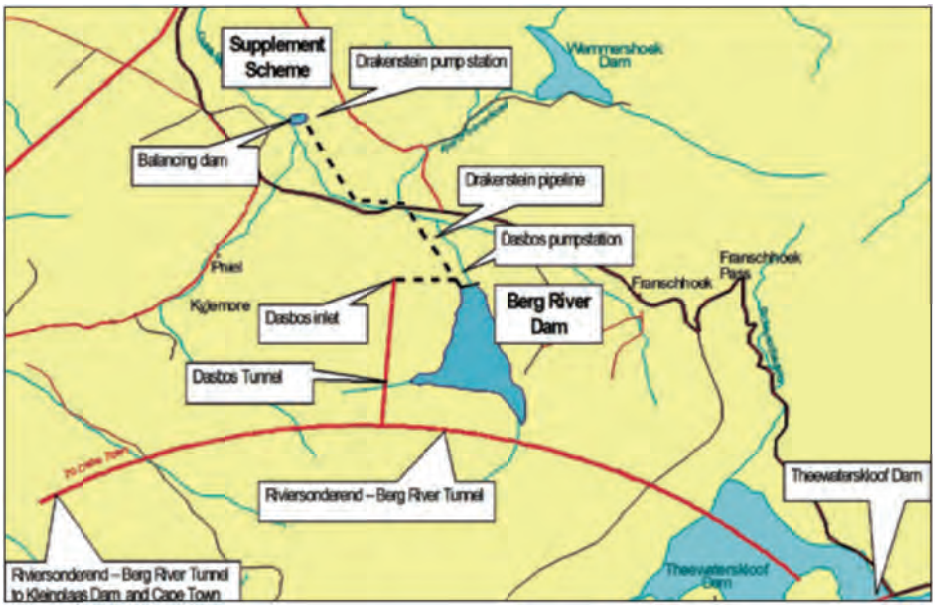

Figure 1-1: Scheme layout

The Berg River Dam is a concrete-faced rockfill embankment, approximately 65 m high and 990 m wide, with a base width of 220 m, and is shown in **Figure 1-2** (TCTA, 2008). It has a gross storage capacity of 130 million m^3.

Figure 1-2: Berg River Dam

The Berg River Dam is the first of its kind in South Africa, comprising structures that permit the release of both low and high flows, the latter up to 200 m^3/s. The Ecological Reserve water release,

downstream of the dam, had been determined beforehand for the BWP, which ensures that the aquatic ecosystems downstream of the dam are protected. This reserve prescribes low and high flow releases, as well as the quality of the water released (TCTA, 2006).

The Berg River Dam was designed to cater for the Ecological Reserve, and this is made possible by the intake tower. The intake tower is divided into a north and south section. The north section is a dry well equipped with multi-level inlets, pipes and valves, which provide the facilities for extracting water from the dam into the supply system to the Greater Cape Town region, as well as making provision for low flow environmental releases (less than 12 m^3/s). The southern section of the intake tower is an open vertical wet well with multi-level gates designed to draw water from the dam for high flows, which imitate the occurrence of natural flood events (up to 200 m^3/s). The wet well is connected to the concrete bottom outlet underneath the dam embankment. This system for releasing high floods is a requirement of the Ecological Reserve and is unique to the Berg River Dam. Surplus water spills over the 40 m side spillway with modified Roberts splitters and flows down the concrete chute to the ski-jump (TCTA, 2006). **Figure 1-3** shows a cross-sectional view of the intake tower of the Berg River Dam.

The outflow for the environmental flood release is controlled by a radial gate at the end of the outlet conduit. If this gate should fail, the dam would empty, giving rise to hazardous conditions as a result of downstream river bank erosion. An emergency gate therefore is provided that can close under its own weight if the radial gate fails. The design speed of this closure is 12 minutes (Van Vuuren, 2003).

The Berg River Dam and its appurtenant structures were the first large water resource infrastructure project in South Africa to be subjected to the National Water Act of 1998 (Act 36) and the World Commission on Dams (WCD) Report of 2000 (Abban et al., 2008). It is anticipated that a prerequisite for future dam-related projects in South Africa will be that they have to make provision for ecological or environmental flow releases to maintain the integrity of the rivers and to ensure a healthy ecosystem. Therefore it is fundamental that lessons learned from the BWP are shared with the engineering industry.

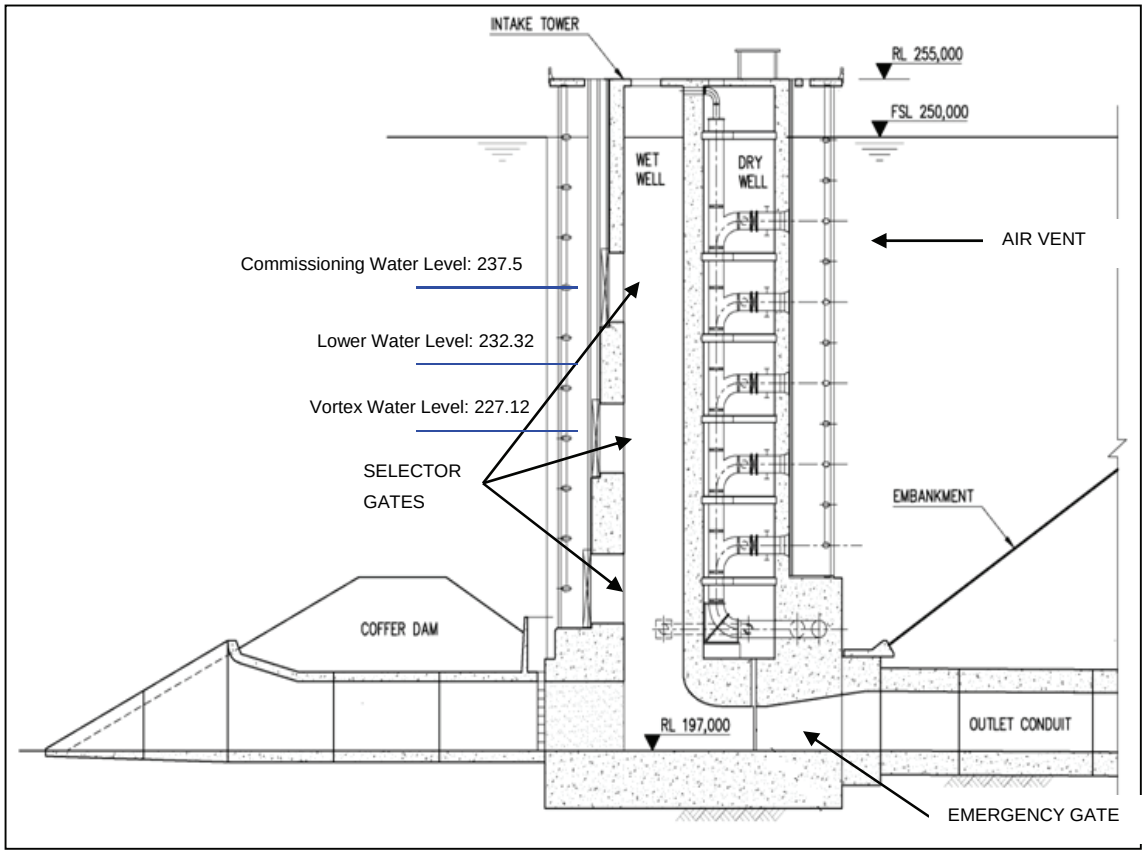

(a)

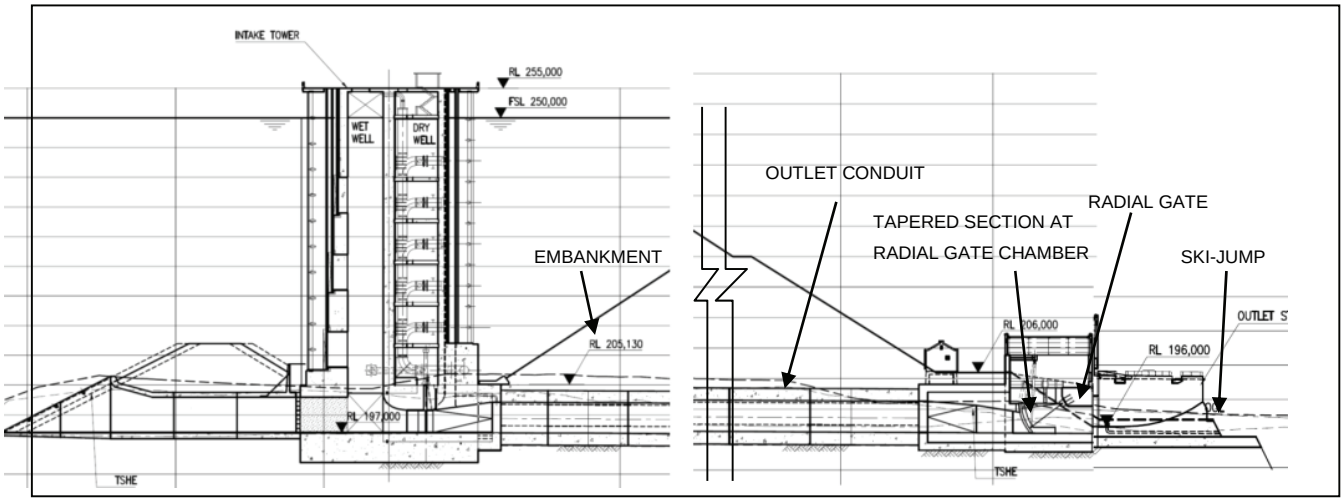

(b)

Figure 1-3: Cross-section of Berg River Dam intake tower (a) and outlet structure (b)

1.3 Background to the Project

A trial closure of the emergency gate of the Berg River Dam was undertaken by the TCTA on 12 June 2008. An air shaft was designed downstream of the emergency gate in order to introduce

air downstream of the gate to counteract the negative pressures that were expected in the conduit during emergency gate operations. Contrary to the theoretical design, the measured air shaft velocities indicated that, while the emergency gate was closing, very large volumes of air were continuously being released from the 1.8 m^2 air shaft, commencing when the gate was about 30% closed (i.e. 70% open), whereas it was designed that air should be drawn down the shaft (**Figure 1.4**) (refer to ***Annexure B*** for a report on the commissioning test on the Berg River Dam in June 2008).

The 1.8 m^2 Mentis grid cover on top of the shaft was blown off and lifted to a height of about 3 to 4 m, tipping the observer off the shaft top and against the upstream concrete wall.

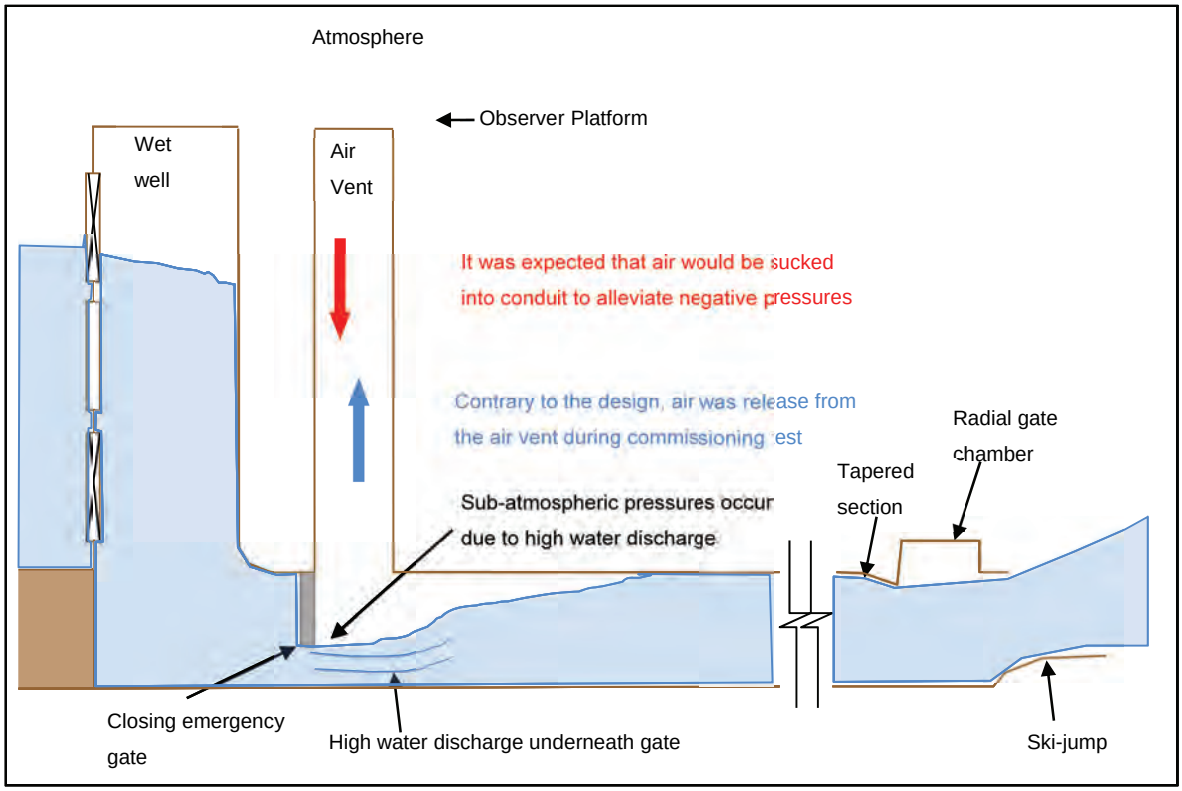

The full-scale structure under investigation is called the prototype (p), and a model (m) is a smaller version of the prototype. In 2003 a 1:18.966 scale model of the Berg River Dam was tested by Sinotech in Pretoria, and this test formed part of the detailed design process of the BWP. The study was specifically carried out to test the bottom outlet and concluded that air would be drawn down the shaft and that no visible vortex formed at the intake in the reservoir. Emergency gate operations

were not simulated, however, as it was accepted that air would be drawn into the air vent to alleviate the negative pressures that form downstream of the gate (Van Vuuren, 2003).

Guidelines for the design and operation of bottom outlet works with emergency gate closure were investigated, analysed and developed by the University of Stellenbosch in 2009. This project was commissioned by the South African Water Research Commission (WRC), who appointed the University of Stellenbosch to undertake the work. The University initially investigated the air vent operation by means of a physical 1:40 scale model (originally used for the 2003 detailed design of the outlet works) and a two-dimensional computational fluid dynamics (CFD) analysis. The study provided inconclusive results for the event where air was released from the air vent, as obtained during the June 2008 commissioning test. The study concluded that the flow of air through the air vent and the formation of vortices at the intake shaft on the physical model were not as proficient as they would be on the prototype and, hence, that the entrainment of air could not be analysed accurately on the 1:40 scale model, as the model was too small. It also concluded that a three-dimensional CFD analysis would be required for reliable computer simulation of the problem.

For the study covered by this report, a 1:14.066 (undistorted scale) physical model of the outlet works and air shaft of the Berg River Dam was constructed and 3 dimensional CFD model was created.

1.4 Report Outline

The physical modelling aspects of this study are covered in **Volume I**, and the computational modelling aspects are covered in **Volume II**.

The objective and scope of the physical and computational components of the study are given in Chapter 2 of Volume I and II respectively.

All the literature review is contained in **Volume I** (Chapter 3), while background to computational fluid dynamics (CFD) modelling of flows is given in Chapter 3 of **Volume II**.

Volume I further contains the physical model setup and measuring equipment (Chapter 4), the methodology used to analyse water and air flow conditions during gate closure (Chapter 5), the results (Chapter 6) and an evaluation thereof (Chapter 7), and conclusions from the physical model study (Chapter 8). The Volume ends with design guidelines and recommendations in Chapter 9.

The computational modelling part, covered in **Volume II,** consists of two consecutive studies or stages. Chapters 4 to 6 cover the first stage which involves simulation of static gate openings with steady-state solutions, and Chapters 7 to 11 cover the second stage in which the model was modified to simulate a continuously closing gate. Final conclusions and recommendations are made in Chapter 12.

2. OBJECTIVES AND SCOPE OF CFD STUDY

2.1 Objectives

The purpose of this study was to utilise numerical simulation methods (specifically computational fluid dynamics or CFD) and a three-dimensional model of the Berg River Dam outlet structure to investigate and study the flow behaviour which led to the unexpected air releases during the Berg River Dam commissioning tests. The study involved two stages.

2.1.1 Stage 1 Objectives

The objectives of the first stage of the study were to create a three-dimensional CFD model of the Berg River Dam outlet works, and monitor the fluid flow through the model for different **static emergency gate openings**. Together with the physical model study (See Volume I) this would establish whether there is an emergency gate opening for which the air vent is inadequate to provide the aeration demand behind the gate.

2.1.2 Stage 2 Objectives

After completion of Stage 1, the objectives of the second stage were to further develop the three-dimensional model of the Berg River Dam outlet works to run transient simulations of **continuous closure** of the emergency gate, and to validate the results against those of the physical model study.

2.2 Scope

The CFD modelling studies were performed on an as-built model of the Berg River Dam outlet works and do not consider any of the alterations included in the physical model study discussed in Volume I. Further, to enable direct comparison for validation purposes, the scale of the CFD model was set to be the same as the physical model (1:14.066 to the prototype) for the whole study.

In the first stage the scope of the simulations was limited to steady state solutions of gate openings of 20%, 30%, 40%, 50%, 60% and 70%. Steady-state simulations ignore time effects but allow for significantly shorter computation times than transient solutions.

In the second stage, due to limited computation time, only a single simulation of very rapid gate closure was completed and studied.

3. BACKGROUND TO CFD MODELLING

3.1 Introduction to CFD

Computational fluid dynamics (CFD) is a branch of fluid mechanics that uses numerical methods and algorithms to solve and analyze problems that involve fluid flows. It may also be defined as the analysis of systems involving fluid flow, heat transfer and other associated phenomena like chemical reactions by means of computer-based simulation. (Versteeg and Malalasekera, 2007).

Computational Fluid Dynamics is a design tool that has been developed over the past few decades and will be continually developed as the understanding of the physical and chemical phenomena underlying CFD theory improves.

Computers are used to perform the calculations required to simulate the interaction of liquids and gases with surfaces defined by boundary conditions. With high-speed supercomputers, better solutions can be achieved. On-going research, however, yields software that improves the accuracy and speed of complex simulation scenarios.

The goals of CFD are to be able to predict fluid flow accurately, heat transfer and chemical reactions in complex systems, which involve one or all of these phenomena. Presently, CFD is being increasingly employed by many industries either to reduce manufacturing design cycles or to provide an insight into existing technologies so that they may be analysed and improved. Examples of such industries include power generation, aerospace, process industries, automotive, chemical engineering and construction.

As a design tool in water resources applications, CFD presently is used together with experimental analysis where CFD does not produce absolute results. In order to provide validation and verification of CFD solutions, experimental methods are normally conducted in conjunction with numerical simulations to provide more realistic results. The reason for this is that the numerical methods, which govern the solutions in a CFD problem, rely on several modelling assumptions that may not have been validated to a satisfactory level.

The schematic below shows a rough sketch of how the problem relates to the analytical solution depending on which approach is chosen to determine the required solution.

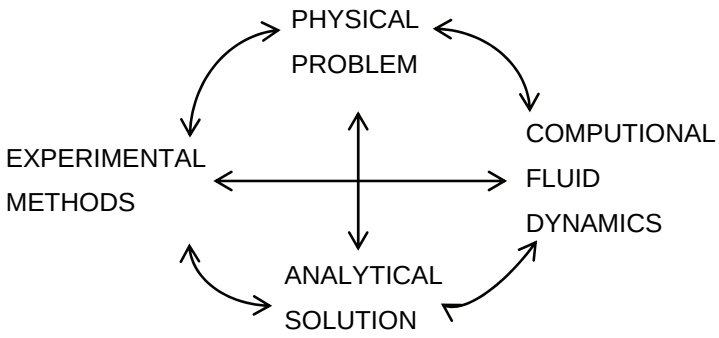

Figure 3-1: Schematic of approach to tackling engineering flow problems (Veersteg, 2007).

CFD presently offers itself as a powerful design tool and even more so in the future because:

(a) Dangerous or expensive trial and error experiments can be simulated and design parameters observed prior to any physical prototype being constructed;

(b) Computers are becoming more powerful and less expensive, thus allowing larger CFD simulations to be calculated, or more detailed simulations of present CFD problems;

(c) The numerical schemes and physical models that are the building blocks of CFD are being continually improved.

(d) If a CFD model can be established yielding accurate results on one particular design, then the model can be used as a tool of prediction for that design under many different operating conditions.

CFD modelling involves iteratively solving partial differential equations in time and/or space (which in this case describe the flow of fluids) to obtain a final numerical description of the total flow field under consideration. The computer program utilises the theory available on fluid flow dynamics to determine the solution for the problem at hand.

3.2 Methodology for Numerical Modelling

Computational Fluid Dynamics (CFD) codes are structured around numerical algorithms that can handle fluid flow. In order to provide easy access to their solving power, all commercial CFD packages include sophisticated user interfaces to input problem parameters and to examine the results. A three-dimensional model of the Berg River Dam bottom outlet structure was studied using the resources of the ANSYS GAMBIT and ANSYS FLUENT packages. The ANSYS processing package codes contain three main elements: (i) a pre-processor, (ii) a solver and (iii) a post processor.

3.2.1 Pre-Processing

This element consists of the input of a flow problem to a CFD program by means of an operator-friendly interface and the subsequent transformation of this input into a form that is suitable for use by the solver. The activities at the pre-processing stage involve constructing geometry and meshing.

Construction of Model Geometry

The first stage in any CFD model is to create a geometry which represents the object being modelled. This entails a definition of the geometry of the region of interest; the computational domain. Analysis begins with a mathematical model of a physical problem and conservation of mass, momentum and energy must be satisfied throughout the region of interest. Engineering assumptions are made to simulate the real process and modelling requires material properties and appropriate boundary and initial conditions. For this exercise the use of the AutoCAD package was employed to construct the model geometry. In order for the CAD drawings to be usable in any meshing tool application, they have to be exported in a format that is readable in the said application. The ANSYS GAMBIT application was used as the meshing tool before files were exported to ANSYS FLUENT for processing.

Meshing

Meshing entails breaking up or sub-division of the domain into a collection of smaller, non-overlapping sub-domains also called a grid (or mesh) of cells (or control volumes or elements). CFD then utilizes numerical/discretisation methods to develop algebraic equations that approximate the governing differential equations of fluid mechanics in the domain to be studied. The system of algebraic equations is solved numerically for the flow field variables in each computational cell.

Herewith, the properties of the fluid are defined and appropriate boundary conditions are specified at cells which coincide with the domain boundary. The solution to a flow problem (velocity, pressure, temperature, and so on) is defined at nodes inside each cell. The accuracy of a CFD solution is governed by the number of cells in the grid: the larger the number of cells, the better the solution accuracy. The accuracy of a solution and its cost in terms of necessary computer hardware and calculation time are dependent on the fineness of the grid. Optimal meshes are often non-uniform: finer in areas where large variations occur from point to point and coarser in regions with relatively little change. Over 50% of the time spent on a CFD project is devoted to the definition of the geometry and grid generation. Most CFD codes include their own

CAD (Computer Aided Design) style interface and/or facilities to import data from proprietary surface modellers and mesh generators. Most current pre-processors provide access to a library of material properties for common fluids and a facility to invoke special physical and chemical process models alongside the main fluid flow equations.

3.2.2 Processing

The solver employs the use of Computational Fluid Dynamics and most CFD codes are solely concerned with the finite volume method, a special finite difference formulation. In outline the numerical algorithm consists of the following steps:

- Integration of the governing equations of fluid flow over all the (finite) control volumes of the domain
- Discretisation, conversion of the resulting integral equations into a system of algebraic equations
- Solution of the algebraic equations by an iterative method

The control volume integration distinguishes the finite volume method from all other CFD techniques such as finite element and spectral methods. The resulting statements express the conservation of relevant properties for each finite size cell. The conservation of a general flow variable ϕ such as velocity within a finite volume can be expressed as a balance between the various processes tending to increase or decrease it. In words (Veersteg and Malalasekera, 2007):

$$\begin{bmatrix} Rate\ of\ change \\ of\ \phi\ in\ the \\ control\ volume \end{bmatrix} = \begin{bmatrix} Net\ rate \\ of\ increase \\ of\ \phi\ due\ to \\ convection \\ into\ the \\ control\ volume \end{bmatrix} + \begin{bmatrix} Net\ rate \\ of\ increase \\ of\ \phi\ due\ to \\ diffusion \\ into\ the \\ control\ volume \end{bmatrix} + \begin{bmatrix} Net\ rate \\ of\ creation \\ of\ \phi\ inside \\ the\ control \\ volume \end{bmatrix}$$

CFD codes contain discretisation techniques that are suitable for the treatment of the key transport phenomena, convection (transport due to fluid flow) and diffusion (transport due to variation of ϕ from point to point) as well as for the source terms (associated with the creation or destruction of ϕ) and the rate of change with respect to time. The underlying physical phenomena are complex and non-linear so an iterative solution approach is required. The following simulation in ANSYS FLUENT utilises the SIMPLE algorithm to ensure correct linkage between pressure and velocity.

3.2.3 Post processing

This involves the collection and analysis of the results from the simulation using the CFD code and analysis and verification and validation of the results. Using the solver's post-processing capabilities results can be displayed using versatile data visualisation tools such as;

- Domain geometry and grid display
- Vector plots
- 3D surface plots
- Path lines
- Tabulated results
- View manipulation (translation, rotation, scaling)
- Colour PostScript output

Results from the simulations have been displayed with some of the visualization tools mentioned above.

3.3 Errors and Uncertainty in CFD Modelling

The benefits of CFD, over time, have been recognised by large corporations, small and medium sized alike, and it is now used in design/development environments across a wide range of industries. This has focussed attention on 'value for money' and potential consequences of wrong decisions made on the basis of CFD results. The consequences of inaccurate CFD results are at best a waste of time, money and effort and at worst catastrophic failure of components, structures or machines. Moreover, the costs of a CFD capability may be quite substantial (Versteeg et al, 2007):

- Capital cost of computing equipment
- Direct operating cost: software licence(s) and salary of CFD specialist, if solicited
- Indirect operating cost: maintenance of computing equipment and provision of information resources to support CFD activity

The value of a modelling result is clear – time saving in design and product improvement through enhanced understanding of the engineering problem under consideration – but is rather difficult to quantify. The application of CFD modelling as an engineering tool can only be justified on the basis of its accuracy and the level of confidence in the results. With its roots in academic research, CFD development was initially focused on new functionality and improved understanding without the need to make very precise statements relating to confidence levels. Also, the engineering industry has a long tradition of making things work within the limitations of the current state of knowledge,

provided that the confidence limits are known. Assessment of uncertainty in experimental data is a well-established practice and the relevant techniques form part of every engineer's basic education. For this reason, extensive reviews of the factors influencing simulation results have been carried out and a systematic process developed to estimate uncertainty in experimental results for the quantitative assessment of confidence levels.

In the context of trust and confidence in CFD modelling, the following definitions of error and uncertainty have now been widely accepted:

3.3.1 Error

This may be defined as a recognisable deficiency in a CFD model that is not caused by lack of knowledge. Causes of errors defined in this way include numerical errors, coding errors and user errors (Malalasekera, 2007).

3.3.1.1 Numerical Errors

Computational Fluid Dynamics solves systems of non-linear partial differential equations in discretised form on meshes of finite time steps and finite control volumes that cover the region of interest and its boundaries. This gives rise to three recognised sources of numerical error, namely: round off errors, iterative convergence errors and discretisation errors.

Round off Errors

Round off errors is the result of representation of real numbers by means of a finite number of significant digits, which is termed the machinery accuracy. These types of errors contribute to the numerical error in a CFD result and can be generally controlled by careful arrangement of floating-point arithmetic operations to avoid subtraction of almost equal-sized large numbers or the addition of numbers with very large differences in magnitude. In CFD computations it is common practice to use gauge pressures relative to a specified base pressure, for example, in incompressible flow simulations a zero pressure value is set at an arbitrary location within the computational domain. This is a simple example of error control by good code design, since it ensures that the pressure values within the domain are always of the same order as the pressure difference that drives the flow. Thus, the calculation with floating-point arithmetic of pressure differences between adjacent mesh cells is not spoilt by loss of significant digits as would be the case if they were evaluated as the difference between comparatively large absolute pressures.

Iterative Convergence Errors

The numerical solution of a flow problem requires an iterative process and the final solution exactly satisfies the discretised flow equations in the interior of the domain and the specified conditions on its boundaries. If the iteration sequence is convergent the difference between the final solution of the coupled set of discretised flow equations and the current solution after *k* iterations reduces as the number of iterations increases. In practice, the available resources of computing power and time dictate that we truncate the iteration sequence when the solution is sufficiently close to the final solution. This truncation generates a contribution to the numerical error in the CFD solution. The most commonly constructed truncation criterion in CFD is one based on so-called residuals. The discretised equation for general flow variables, Ø, at mesh cell, *i*, can be written as follows:

$$(a_P \emptyset_P)_i = \left(\sum_{nb} a_{nb} \emptyset_{nb} \right)_i + b_i$$

where the subscript *i* indicates the control volume and a_P, a_{nb} *and* b_i are constants.

The final solution will satisfy the equation above exactly at all cells in the mesh but after *k* iterations there will be a difference between the left and right hand sides. The absolute value of this difference at the mesh cell *i* is termed as the local residual, $R_i^{\emptyset}$, whose sum over all control volumes within the computational domain gives an indication of the convergence behaviour across the whole flow field, also defined as the global residual, $\hat{R}^{\emptyset}$. This global residual is always equal to zero when the final solution is reached and it is a satisfactory average measure of the discrepancy between the final solution and the computed solution after *k* iterations. In commercial CFD codes, such as ANSYS FLUENT, the convergence test in the iterative sequences involves the specification of tolerances for the normalised global residuals for mass, momentum and energy. An iteration sequence is automatically truncated when all these residuals are smaller than their pre-set maximum values. Default values for the tolerances, which have been determined by systematic trials to give acceptable results for a wide range of flows, are supplied by the code vendors but for high accuracy work it may be necessary to reduce these values of tolerance from their default values to control and reduce the magnitude of the contribution to the numerical error due to early truncation of the iterative sequence.

Discretisation Errors

Temporal and spatial derivatives of the flow variable, which appear in the expressions for rates of change, fluxes, sources and sinks in governing equations are approximated in the finite

volume method on the chosen time and space mesh and this involves simplified profile assumptions for flow variable Ø, a practice that corresponds to the truncation of a Taylor series. This discretisation error is associated with the neglected contributions due to the higher-order terms, which give rise to errors in CFD results. Control of the magnitude and distribution of discretisation errors through careful mesh design is a major concern in high-quality CFD and in theory, the discretisation error can be made arbitrarily small by progressive reductions in the time step and space mesh size but this requires increasing amounts of memory and computing time. Thus, the ingenuity of the CFD user as well as resource constraints dictate the lowest achievable level of the contribution to the numerical error due to the simplified profile assumptions.

3.3.1.2 Coding Errors

This involves mistakes or 'bugs' in the software and is one of the most insidious forms of error.

3.3.1.3 User Errors

User errors are human errors through incorrect use of the software. Such errors may be reduced or eliminated to a large extent through adequate training and experience

3.3.2 Uncertainty

Uncertainty may be defined as a potential deficiency in a CFD model that is caused by lack of knowledge. The main sources of uncertainty are input uncertainty and physical model uncertainty (Veersteg and Malalasekera, 2007).

3.3.2.1 Input Uncertainty

Input uncertainty consists of inaccuracies due to limited information or approximate representation of geometry, boundary conditions, and material properties among others. It is associated with discrepancies between the real flow and the problem definition within a CFD model. There are three categories of input data that can lead to uncertainty in CFD:

Domain Geometry

The definition of domain geometry involves specification of the shape and size of the region of interest. In industrial applications this may come from a CAD model. It is impossible to manufacture the desired structure perfectly to the design specifications; manufacturing tolerances will lead to discrepancies between the design intent and a manufactured part.

Furthermore, the CAD model needs to be converted to be suitable within CFD and this conversion process could lead to discrepancies between the design intent and the geometry within CFD. Similar comments apply to the surface roughness. The boundary shape in CFD is a discrete representation of the real boundary. In summary, the macroscopic and microscopic geometry within the CFD model will be somewhat different from the real flow passage, which contributes to input uncertainty in the model results.

Boundary Conditions

Apart from the shape and surface state of solid boundaries, it is also necessary to specify the conditions on the surface for all other flow variables, such as velocity, temperature, species, and so on. It can be difficult to acquire this type of input to a high degree of accuracy. The choice of type and location of open boundaries through which flow enters and leaves the domain is a particular challenge in CFD modelling. Boundary conditions are chosen from a limited set of available boundary types for inlets and outlets. There must be compatibility between chosen open boundary condition type and the flow information available on the chosen surface location. In some cases, we only have partial information, such as average velocity and some indication of velocity distribution but no information on the turbulence parameters. Missing information must now be generated on the basis of past experience or inspired guesswork. In other cases, the assumed boundary condition may only be uniform on a fixed pressure boundary, but might actually be somewhat non-uniform. A contribution to the input uncertainty is associated with the inaccuracy of all assumptions involved in the process of defining the boundary conditions. The location of the open boundaries must be sufficiently far from the area of interest so that it does not affect the flow in this region. Solution economy on the other hand dictates that the domain should not be excessively large, so a compromise must be found, which may cause discrepancies between the real flow and the CFD model, resulting in a contribution to the input uncertainty.

Fluid Properties

All fluid properties like density, viscosity and the like depend to a greater or lesser extent on the local values of flow parameters, such as pressure. Often the assumption of a constant fluid property is acceptable provided that the spatial and temporal variations of the flow parameters influencing that property are small. The application of this assumption also benefits solution economy since CFD models converge more quickly if fluid properties remain constant; however, errors are introduced if the assumption of constant fluid properties is inaccurate. If the fluid properties are allowed to vary as functions of flow parameters we have to contend with errors due to experimental uncertainty in the relationships describing the fluid properties.

3.3.2.2 Physical Model Uncertainty

Physical model uncertainties are discrepancies between real flows and CFD due to inadequate representation of physical or chemical processes such as turbulence, or due to simplifying assumptions in the modelling process such as incompressible flow or steady state.

Lack of validity of sub-models

CFD modelling of complex flow phenomena such as turbulence, combustion, heat and mass transfer involves semi-empirical sub-models such as the turbulence models for Reynolds-averaged Navier-Stokes (RANS) equations. They encapsulate the best scientific understanding of complex physical and chemical processes. The sub-models invariably contain adjustable constants derived from high-quality measurements on a limited class of simple flows. In applying the sub-models to more complex flows we extrapolate beyond the range of these data. There are several reasons why the application of sub-models brings uncertainty in a CFD result:

A complex flow may involve entirely new and unexpected physical/chemical processes that are not accounted for in the original sub-model. In the absence of a better sub-model the user has no option but to work with less sophisticated description of the flow. In spite of the availability of a more comprehensive sub-model the user may also deliberately select a simpler sub-model with a less accurate account of physics/chemistry to save time in computation.

A complex flow may include the same mixture of physics/chemistry as the original simple flows but not exactly in the same blend, requiring adjustments of the sub-model constraints. The empirical constants within the sub-models represent a best fit of experimental data which will themselves have some uncertainty.

These sub-models contain adjustable constants that can only be used to capture exactly the class of flows that were used to calibrate their values and each sub-model will contain empirical constants that have limited validity. The empirical nature of the sub-models inside a CFD code, the experimental uncertainty of the values of the sub-model constants and the appropriateness of the chosen sub-model for the flow to be studied together determine the level of error in the CFD results due to physical model uncertainty.

Lack of Validity of Simplifying Assumptions

At the start of each CFD modelling exercise it is common practice to establish whether it is possible to apply one or more potential simplifications. Considerable simplification can be achieved if the flow can be treated as:

- Steady state vs. transient
- Two-dimensional, axisymmetric, symmetrical across one or more planes vs. fully three dimensional
- Incompressible vs. compressible
- Adiabatic vs. heat transfer across the boundaries
- Single species/phase vs. multi-component/phase

The simplification must be justifiable to good accuracy. Many flows exhibit geometrical symmetry about one or two planes. However, unless the inlet flow possesses the same symmetry, a model simplification based on geometrical symmetry will be inaccurate. For example, previous studies on the Berg River Dam outlet structure using a simplified 2-dimensional CFD model were inconclusive. The accuracy and appropriateness of all simplifying assumptions for a given flow determine the size of their contribution to physical model uncertainty.

3.4 Verification and Validation of CFD Models

Once it is recognised that errors and uncertainty are unavoidable aspects of CFD modelling, it becomes necessary to develop rigorous methods to quantify the level of confidence in its results.

3.4.1 Verification

This may be defined as the process of determining that model implementation accurately represents the developer's conceptual description of the model and the solution, as Roache (1998) puts it, 'solving the equations right'. The verification process involves quantification of the errors. Since computer coding and user errors are ignored, the round-off error, iterative convergence error and discretisation error need to be estimated.

- *Round-off error* can be assessed by comparing CFD results obtained using different levels of machine accuracy.
- *Iterative convergence error* can be quantified by investigating the effects of systematic variation of the truncation criteria for all residuals on target quantities of interest such as, the velocity at one or more locations of interest. Differences between the values of a target quantity at various levels of the truncation criteria provide a quantitative measure of the closeness to a fully converged solution.

- *Discretisation error* is quantified by systematic refinement of the space and time meshes. In high-quality CFD work we should aim to demonstrate monotonic reduction of the discretisation error for target quantities of interest and the flow field as a whole on two or three successive levels of mesh refinement.

Such methods merely estimate the numerical error of the code as it is and do not test whether the code itself accurately reflects the mathematical model of the flow envisaged by the code designer. Oberkampf and Truncano (2007), therefore, argued that a complete programme of verification activities should always include a stage of systematic comparison of CFD results with reliable benchmarks, that is, high accurate solutions of flow problems, such as analytical solutions or highly resolved numerical solutions.

3.4.2 Validation

This may be defined as the process of determining the degree to which a model is an accurate representation of the real world from the perspective of the intended uses of the model. Roache (1998) called this 'solving the right equations'. The process of validation involves quantification of the input uncertainty and physical model uncertainty.

- *Input uncertainty* can be estimated by means of sensitivity analysis or uncertainty analysis. This involves multiple test runs of the CFD model with different values of input data sampled from probability distributions based on their mean and expected variations. The observed variations of target quantities of interest can be used to produce upper and lower bounds for their expected range and hence are a useful measure of the input uncertainty. In sensitivity analysis the effects of variations in each item of input data are studied individually. Uncertainty analysis, on the other hand, considers possible interactions due to simultaneous variations of different pieces of input data and uses Monte Carlo techniques in the design of the programme of CFD test runs.

- Oberkampf and Truncano (2007) stated that quantitative assessment of the *physical modelling uncertainty* requires comparison of CFD results with high-quality experimental results. They also noted that meaningful validation is only possible in the presence of good quantitative estimates of (i) all numerical errors, (ii) input uncertainty, and (iii) uncertainty of the experimental data used in the comparison.

Thus, the ultimate test of a CFD model is a comparison between its output and experimental data. However, the way in which such a comparison should best be carried out is still a subject of discussion. The most common way of reporting the outcome of a validation exercise is to draw a graph of a target quantity on the *y*-axis and a flow parameter on the *x*-axis, and if the difference between computed and experimental values looks sufficiently small then the CFD model is considered to be validated. The latter judgement is rather subjective, and Coleman and Stern (1997) proposed a more rigorous basis for validation comparisons drawing on the practise of estimating uncertainty in experimental results involving several independent sources of uncertainty. They suggested that the errors should be combined statistically by calculating the sum of squares of estimates of numerical errors, input uncertainty and experimental uncertainty from an estimate of validation uncertainty. A simulation is considered to be validated if the difference between experimental data and CFD model results is smaller than the validation uncertainty. The level of confidence in the CFD model is indicated by the magnitude of the validation uncertainty.

Oberkampf and Truncano (2007) pointed out that this approach would have the slightly paradoxical implication that it is easier to validate a CFD result with poor-quality experimental results containing a large amount of scatter. They suggested an alternative validation metric, which includes a statistical contribution, the influence of which decreases as the variance of the experimental data decreases with increase in the number of repeat experiments. Thus, the metric indicates increased levels of confidence in a validated CFD code if (i) the difference between the experimental data and CFD results is small, and (ii) the experimental uncertainty is small.

Since it is now clear that the accuracy of CFD results cannot be taken for granted, verification and validation are mission-critical elements of the confidence-building process. For this reason, we require experimental data with:

i.) Comprehensive documentation of problem geometry and boundary conditions.
ii.) Detailed measurements of distributions of flow properties, such as velocity components, static or total pressure and so on.
iii.) Complementary overall measurements such as mass flow rate.

Naturally, we should limit ourselves to information from trusted sources to generate a sufficiently credible validation. If suitable experimental results for a comprehensive validation are not available it will be necessary to identify a dataset for a closely related problem. If the problem chosen for validation is sufficiently close to the actual problem to be studied, we should be able

to apply roughly the same CFD approach in both cases. It should be noted that a sufficient level of confidence in CFD simulations can only be achieved through rigorous verification and validation. If the search for validation data draws a complete blank then it is essential that a reasonable programme of experimentation be undertaken alongside CFD to provide solid foundations for design recommendations.

3.5 Theoretical Information

3.5.1 Governing Equations of Fluid Flow

The governing equations of fluid flow represent mathematical statements of the conservation laws of physics, namely:

i.) The mass of a fluid is conserved

ii.) The rate of change of momentum equals the sum of the forces on a fluid particle (Newton's second law)

iii.) The rate of change of energy is equal to the sum of the rate of heat addition to and the rate of work done on a fluid particle (first law of thermodynamics)

The fluid will be regarded as a continuum. For the analysis of fluid flows at macroscopic length the molecular structure of matter and molecular motions may be ignored. The behaviour of the fluid is described in terms of macroscopic properties, such as velocity, pressure, and density and their time and space derivatives.

For all flows, ANSYS FLUENT solves the conservation equations for mass and momentum. Additional transport equations are also solved when the flow is turbulent.

A flow is incompressible when changes in density are negligible, both with respect to time and space. Below are the governing equations for an incompressible Newtonian fluid.

Table 3-1: Governing Equations for an Incompressible Newtonian Fluid

Continuity	$div(\rho \boldsymbol{u}) = 0$
x-momentum	$div(\rho u \mathbf{u}) = -\frac{\partial p}{\partial x} + div(\mu grad\, u) + S_{Mx}$
y-momentum	$div(\rho v \mathbf{u}) = -\frac{\partial p}{\partial y} + div(\mu grad\, v) + S_{My}$
z-momentum	$div(\rho w \mathbf{u}) = -\frac{\partial p}{\partial z} + div(\mu grad\, w) + S_{Mz}$

Where,

μ – Constant

ρ – Density (kg/m^3)

x,y,z – coordinate system

S – Constant (Source term)

u,v,w – velocity variables in the x, y and z direction respectively

p – Pressure

The continuity equation, the momentum equations, and an energy equation are often collectively referred to as the Navier-Stokes equations.

3.5.2 Turbulence Modelling

It is a fact of nature that for sufficiently large Reynolds numbers flows show rapid apparently random fluctuations, even when the controlling factors of the flow, such as body geometry and upstream conditions, are stationary. Such flows are called turbulent. One of the main characteristics of turbulent flow is fluctuating velocity fields. These fluctuations cause mixing of transported quantities like momentum, energy and species concentration and also fluctuations in the transported quantities. Because of the small scales and high frequencies of the fluctuations they are too computationally expensive to simulate directly in practical engineering situations. Instead, the instantaneous governing equations are time-averaged to ignore the small scale fluctuations and the result is a set of less expensive equations containing additional unknown variables. These unknown (turbulence) variables are determined in terms of modelled variables in turbulence models. This process of time-averaging is called Reynolds averaging. When this is done the solution variables in the instantaneous Navier-Stokes equations are decomposed into the mean (time-averaged) and fluctuation components (Reynolds decomposition). Since turbulence is governed by the Navier-Stokes equations, turbulent flow can be computed from first principles by solving the Navier-Stokes equations.

A number of different models are available for modelling turbulence, but no single one of these is everywhere accepted as superior. The choice of a turbulence model depends on a number of factors including the types of flow and the established practice in a certain field (ANSYS Inc., 2009). For the simulation of the bounded two-phase flow in this project the **RNG k-ε model** was used.

The standard k-ε model has long been one of the most popular models due to its economy, robustness and reasonable accuracy for a wide variety of flows. In this model two equations are solved separately for the turbulence kinetic energy (k) and its dissipation rate (ε). In FLUENT the standard k-ε model is available as well as two improved models: the RNG, and the Realisable k-ε models. The RNG model, based on a statistical technique called renormalisation group theory (RNG) improves the standard k-ε model by including an extra term in the ε equation for better accuracy and by accounting for the effect of swirl on turbulence. It is therefore more reliable and accurate for a wider variety of flow types. The Realisable k-ε model is still relatively new and it is not yet known where it provides consistently better results than the RNG model (ANSYS Inc., 2009).

3.5.3 Volume of Fluid (VOF) Solver

The VOF model is a surface tracking technique applied to a fixed mesh. It is designed for two or more immiscible fluids where the position of the interface between the fluids is of interest. In the VOF model, a single set of momentum equations is shared by the fluids, and the volume fraction of each of the fluids in each computational cell is tracked throughout the domain. Applications of the VOF model include stratified flows, free-surface flows, filling, sloshing, motion of liquid after a dam break, the prediction of jet breakup (surface tension), and the steady or transient tracking of a liquid-gas interface.

Among the various models that FLUENT uses to solve the equations of the appropriate properties and variables in any simulation, the VOF model is chosen as the most appropriate for the simulation in question. The VOF formulation relies on the fact that two or more fluids (or phases) are not interpenetrating. For each additional phase that is added to the model, a variable is introduced, namely: the volume fraction of the phase in the computational cell. In each control volume, the volume fractions of all phases sum up to unity. The fields for all variables and properties are shared by the phases and represent volume-averaged values, as long as the volume fraction of each of the phases is known at each location. Thus the variables and properties in any given cell are either purely representative of one of the phases, or

representative of a mixture of the phases, depending upon the volume fraction values. In other words, if the *q*th fluid's volume fraction in the cell is denoted as α_q, then the following three conditions are possible (ANSYS Fluent User's Manual, 2009):

- $\alpha_q = 0$: the cell is empty (of the *q*th fluid)
- $\alpha_q = 1$: the cell is full (of the *q*th fluid)
- $0 < \alpha_q < 1$: the cell contains the interface between the *q*th fluid and one or more other fluids.

Based on the local value of α_q the appropriate properties and variables will be assigned to each control volume within the domain.

STAGE 1: FIXED GATE OPENING SIMULATIONS

4. MODEL SET-UP FOR FIXED GATE OPENINGS STUDY

4.1 Computational Domain

From the available two-dimensional AutoCAD drawings that were prepared for the design and used for the construction of the prototype of the Berg River Dam bottom outlet structure a three-dimensional model domain was developed to create the domain for the numerical model. The numerical model was built to the same scale as the 1:14.066 physical model that was constructed and tested in the Stellenbosch University Hydraulics Laboratory to allow direct comparison for validation and verification of the numerical model.

The report on the commissioning of the outlet works at the Berg River Dam only provides details for the velocity of air released during the closure of the emergency gate over a certain period of time, until the occurrence of the said incident. Such little detail made it inadequate to effectively compare the results from the numerical model to those for the prototype, for instance, issues regarding pressures in the conduit structure that could have contributed to the sudden air release.

The 3-dimensional CFD model used to investigate the sudden air release problem was run for steady state simulations with static emergency gate openings and the water level in the reservoir maintained at the commissioning water level. This was to determine whether there was a static gate opening for which the aeration demand could not be satisfied by the air vent. This also helped to establish some of the conditions favourable for further CFD research regarding the problem in question.

Hydraulic properties for Perspex were used in the simulation runs for the CFD numerical model, as this was the material from which the physical model was constructed.

Figure 4.1-1 below shows a sketch of the generated model.

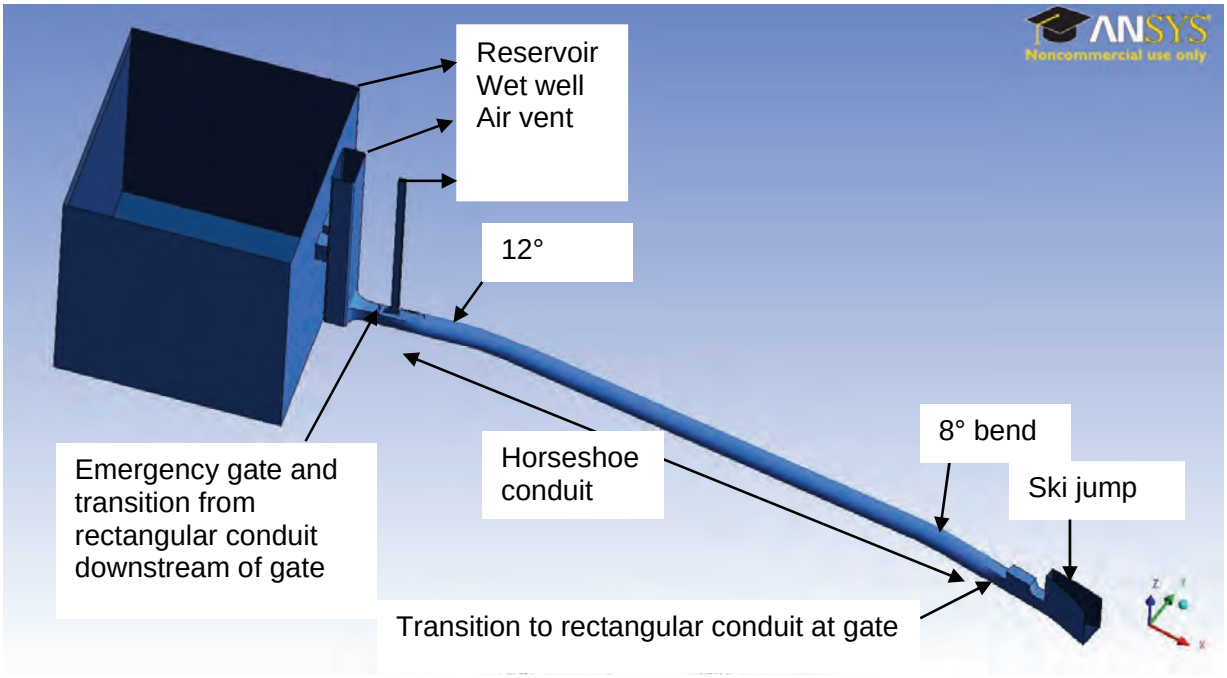

Figure 4-1: Set-up of the 3-dimensional model domain

As seen in the Figure 4-1 above, the model domain was constructed with an assumed rectangular reservoir as in the physical model.

The gate structure was constructed with a 60 degree gate lip modification as shown in Figure 4-2 below. The figure also shows the transition from the rectangular section at the emergency gate to the horseshoe shaped section of the conduit.

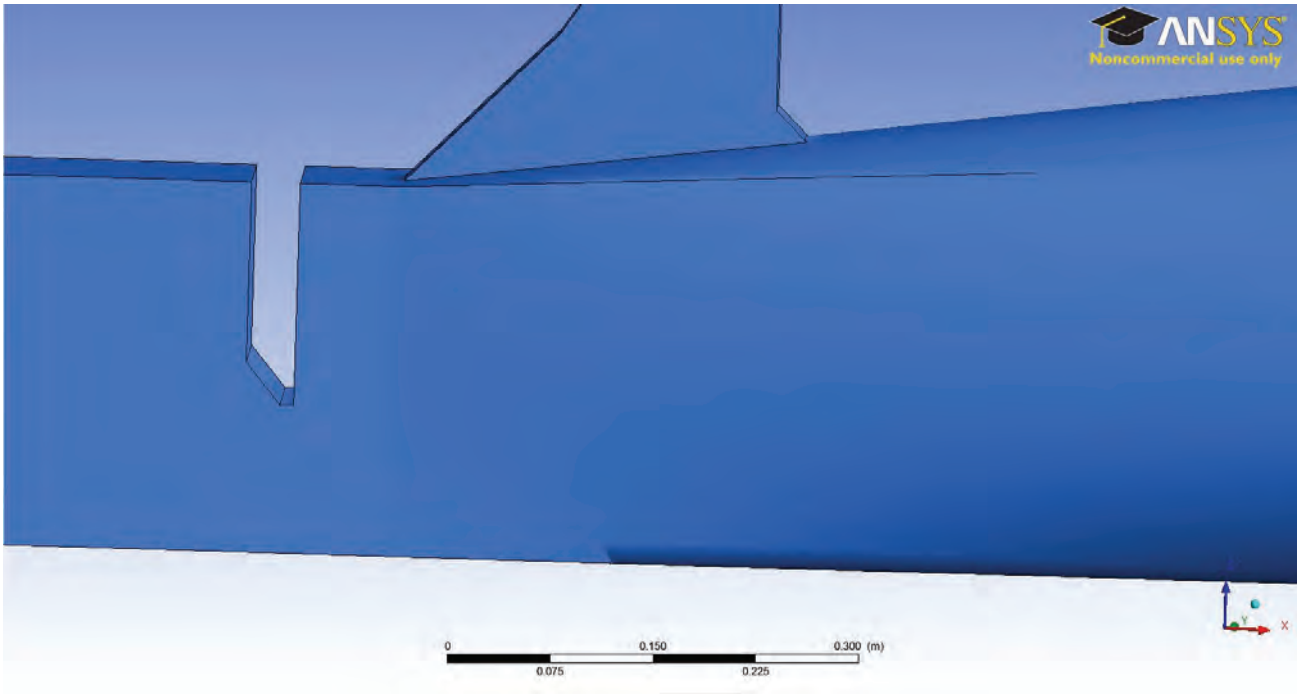

Figure 4-2: Set-up of the 3-dimensional model domain

4.2 Meshing the model domain

Meshing, also known as grid generation, involves the sub-division of the domain into a number of smaller, non-overlapping sub-domains thus forming a grid (or mesh) of cells (or elements, or control volumes) at which solutions are calculated. Refinement and meshing of the domain was done using the ANSYS GAMBIT tool.

Due to the complexity of the geometry, it was difficult to generate a uniform mesh without skewed elements across the whole domain. A mesh with a lot of skew elements affects the final solution, so this drawback was alleviated through the decomposition of the domain into smaller volumes that could be easily meshed. Different mesh sizes were used for different sections of the geometry but conformity of the meshes at the connections was ensured. The mesh for the domain was created with the TGrid function, which means that the grid is composed primarily of tetrahedral mesh elements but may include hexahedral, pyramidal, and wedge elements where appropriate.

The reservoir was meshed with a size of 60 mm, the intake tower and the rectangular section of the conduit including the emergency gate and the air vent had a 10-20 mm mesh. A 40 mm mesh was adapted for the horseshoe shaped conveyance conduit all the way to the ski jump. The finer mesh was adopted in the critical sections of the domain for purposes of accuracy in simulation results and

quick convergence but this required more processing time. Overall, approximately 2.5 million elements were generated for the whole domain.

The Figure 4-3 below shows a screen shot of the meshed model, ready for processing in ANSYS FLUENT.

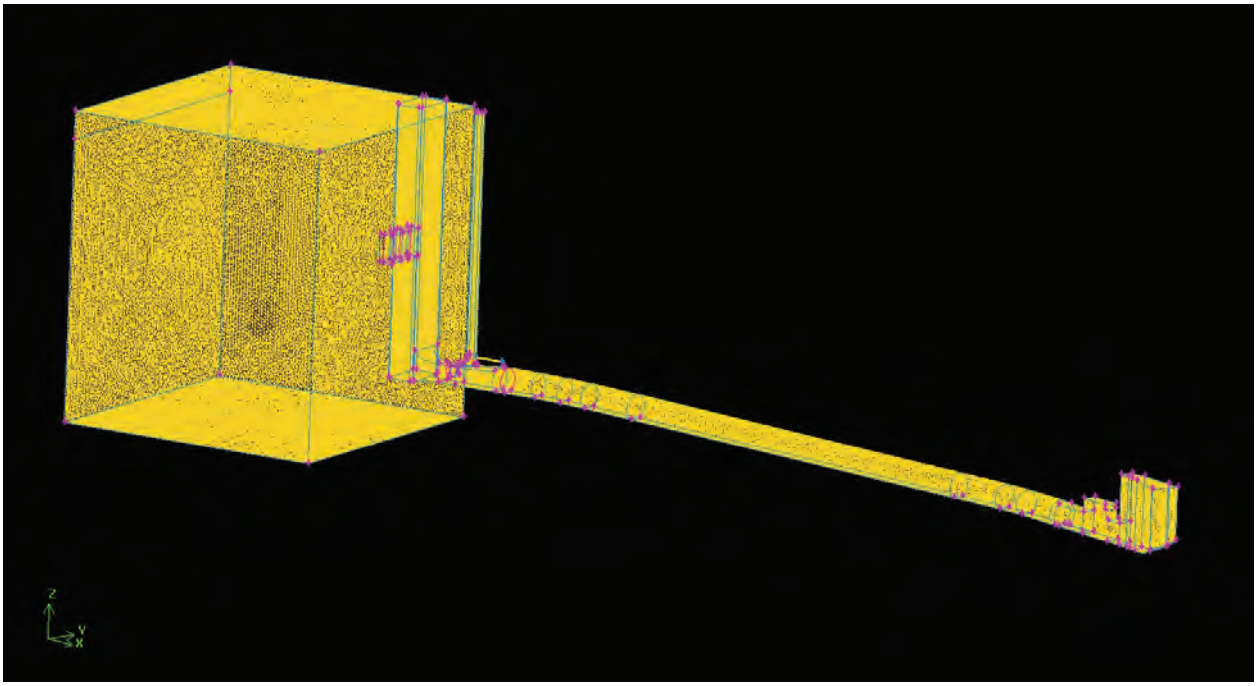

Figure 4-3: Schematic of the meshed geometry

4.3 Initial and Boundary conditions

All CFD problems are defined in terms of initial and boundary conditions. Therefore it is important to specify these correctly and understand their role in the numerical algorithm because it is these conditions that affect the nature of the result. The choice of type and location of open boundaries through which flow enters and leaves the domain is a particular challenge in CFD modelling. Boundary conditions are chosen from a limited set of available boundary types and there must be compatibility between the chosen open boundary condition type and the flow information available for the chosen surface location. In some cases information is partial and as such missing information must be generated on the basis of past experience or assumptions. In other cases, the assumed boundary condition may only be approximately true.

For the BRD model the following boundary conditions were applied:

- In order to reduce the calculation time needed to run the simulations, part of the domain was initially patched with water as shown in Figure 4-4 below.

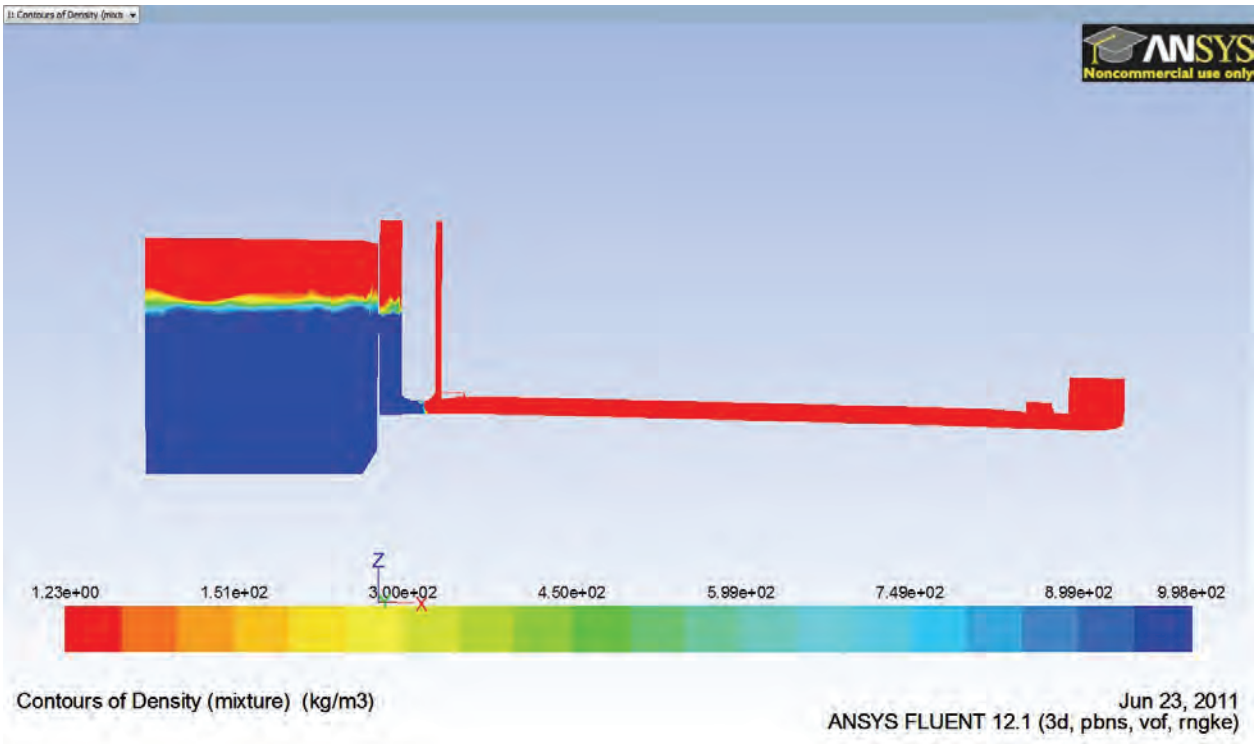

Figure 4-4: Initially patched domain

- The water level in the reservoir (shown in blue) was maintained at the required level by allowing excess to spill out of the domain through a face at the front of the reservoir. The red colour represents air.
- The reservoir was allowed to gradually fill up from the bottom because this prevented disturbance of the flow as it entered the wet well. Another option would be to model an extremely large reservoir that filled up from the side allowing the water to gradually flow towards the intake tower. However, this would call for more calculation time and storage space due to the increased domain.
- Flow into the wet well was allowed by means of the two middle selector gates ignoring the top and bottom paired selector gates with the assumption that these were closed and that there was no contribution of flow into the wet well from them as was the case during the commissioning of the bottom outlet structure.
- The surface of the reservoir was assumed to be open to the atmosphere and the pressure there was set to atmospheric pressure. An opening was also left on the side of the reservoir to allow spillage so as to maintain the water level as required.

- No boundary condition was applied to the intake selector gates since they were directly connected to the reservoir and the water could freely flow into the intake tower.
- The top of the wet well was left open to the atmosphere. This provided another possible source of aeration to the flow from the reservoir.
- The top of the air vent was set to allow aeration from the atmosphere which would be required to balance out the negative pressure that would develop behind the emergency gate.
- The vertical face and top face at the end of the ski jump were set as openings to the atmosphere with an outflow boundary condition, implying that unless the fluid escaped through any other opening, this was the only outlet to the domain.
- The radial gate just before the ski jump was ignored in this simulation because it was fully open at all times during the commissioning,
- The rest of the domain was taken as the wall structure containing the conveyed fluid and no-slip conditions were applied to this wall structure.
- The conveyed fluid was an air-water mixture. The reservoir filled up from the bottom at an assumed rate of 0.03 m/s. Higher fill-up rates caused divergence of the solutions.
- Figure 4-5 below shows the boundary conditions graphically.

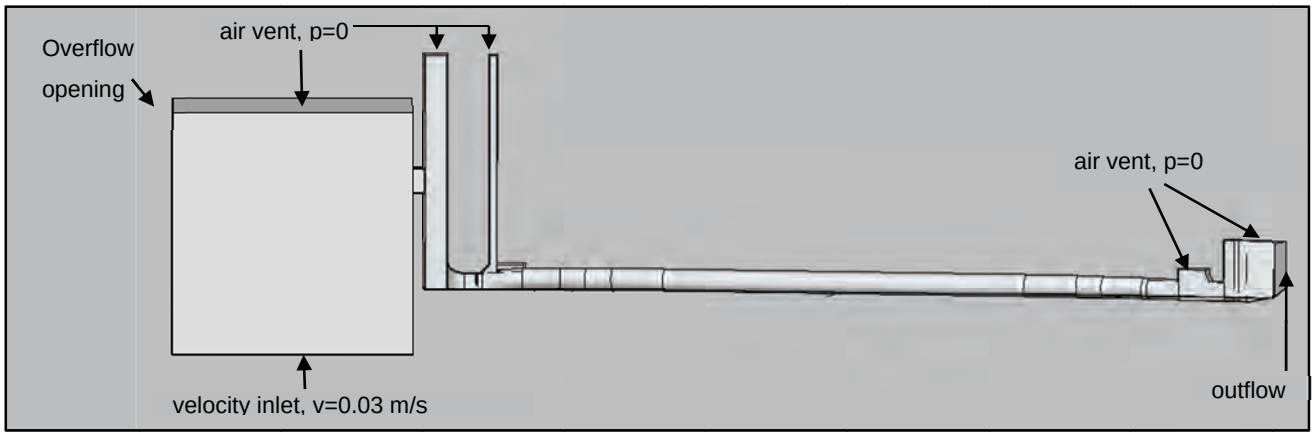

Figure 4-5: Boundary conditions for the steady-state approach

4.4 Model Settings

Various parameters in the solver have to be set before the simulations can be started. Scaling and unit setting is done in the solver but there is no provision for unit conversion so all such requirements have to be satisfied before importing the mesh into the solver. The quality of the mesh can be checked in the solver but before the mesh is exported to the solver such conditions as hydraulic boundary surfaces and the hydraulic diameter of such surfaces must be specified.

The hydraulic diameter is defined by the equation,

$$D_h = \frac{4A}{P}$$

Where A is the area of surface (m^2) and P is the wetted perimeter of the said surface (m).

Table 4-1 below shows the dimensions of the boundary surfaces used in the calculation of the solution for the BRD model.

Table 4-1: Hydraulic diameters for the different boundary surfaces

Boundary Surface	Hydraulic Diameter (m)
Reservoir inlet (Bottom)	4.266
Reservoir Surface (Top)	4.266
Reservoir Spillage (Side)	0.775
Wet Well Surface	0.573
Air vent Surface	0.092
Ski jump Surface (Top)	0.565
Ski jump Surface (Side)	0.500

Other initial parameters that need to be defined include: the turbulence models to be used in the solution calculation (see 3.5.2), the materials and phases in the domain, details of the boundary conditions and cell zone conditions, solution methods, solution controls (relaxation factors), monitors, initialization of the solution, and calculation activities. A gauge pressure of 0 Pa was used.

Table 4-2 below summarises other parameters that were defined for the running of the simulations.

Table 4-2: Other parameters adopted in the simulations

General conditions	Pressure based solver	Water-Air surface tension coefficient (n/m)		0.0728
	Absolute velocity formulation	Operating pressure (Pa)		101325
	Steady state calculations	Viscocity	Air (kg/m.s)	1.79E-06
	Gravity enabled (9.81 m/s^2)		Water(kg/m.s)	0.001003
Models	Viscous model (RNG k-epsilon model)	Density	Air (kg/m^3)	1.225
	Standard wall functions		Water (kg/m^3)	998.2
	Multi phase model - Volume of Fluid (VOF)	Under-relaxation controls		0.5-0.8
	Implicit volume fraction parameters	Material (Perspex) Hydraulic roughness (mm)		0.003
	Two eulerian fluids (air and water)	Phases	Water	
	Implicit body force formulation		Air	

4.5 Limitations of Numerical Model

Like any other experimental, physical or computational procedures, a few problems were encountered in the running of the simulations.

- Getting the model to stabilise and converge was a major task because there were many varying parameters that had to be adjusted specific to the said simulation. This required experience with the use of the software.
- Processing is time consuming given the various tasks that the program has to process for every given element. There is no assurance in the behaviour at the beginning of the simulation (whether there will be divergence later in the simulation process or not) so one has to wait until it has run to completion to determine whether the results are realistic and usable or not. If not, then the whole set up has to be redone, parameters readjusted, and the simulation rerun until usable results are obtained.
- If the given parameters need to be monitored against a time variance then the simulations must be run as transient and it should be noted that the simulation time is not the same as the real time. Transient simulations take a lot more time to run although they give results similar to steady state simulations.
- The software requires that there is constant connection to the network server for the licence to be usable otherwise simulations get interrupted.
- With experience comes the skill to use the software, otherwise divergence of the solution will occur if specified parameters such as relaxation factors are not correctly used. Expert use of the package requires repeated use as parameters vary from one model to another, whether 2 dimensional or 3 dimensional.
- Depending on the amount of information that needs to be processed, a considerable memory is required to construct, mesh and run simulations. Over 2 million elements had to be processed and files with over 500 gigabytes needed to be stored for each model set up.
- Assumptions must be made of what happens outside the model since one cannot visibly or numerically monitor what goes on beyond the limits of the domain. For this reason, whatever water is not held up in the reservoir beyond the required level is spilled in order to simulate the reservoir water level during the commissioning test.
- It was necessary to compromise between storage and simulation data. With the data files so large, it was demanding to have to save data very frequently.
- Animations of the simulation could only be created at the end of the whole simulation process and all case and data files generated during the simulation had to be kept in order to create the animation. This required more storage space.

5. RESULTS OF FIXED GATE OPENINGS STUDY

All simulations carried out on the 3-dimensional model were steady state for fixed gate openings. The reservoir was filled at a constant rate of 0.03 m/s and any inflows excess of the releases overflowed the front side of the reservoir. The open surface flow through the selector gates into the wet well was simulated as well as the pressurised flow underneath the emergency gate. The CFD simulations of the flow underneath the emergency gate showed higher velocities than those measured in the physical model. These CFD simulations are compared with the physical model results (discussed in Volume I, Section 6) in Section 5.2 below. (Note that the physical model results have not been converted to prototype values as they have in the results section of Volume I)

Depending on the emergency gate opening, steady state was achieved after approximately 5000 iterations. Simulation results were only extracted from files for which equilibrium was established. Turbulence upstream of the emergency gate was attributed to the circulation of flow as it dropped down into the intake tower and that downstream of the emergency gate was attributed to the occurrence of highly aerated flow in the conduit.

The layout of this chapter shows the pictorial results of the CFD modelling which provides a visual representation of the simulation output. Then results for discharge, velocity and pressure are also compared with the calculated results and the results of the physical modelling study (See Volume I).

5.1 Pictorial Representation of Results

5.1.1 Density Contours

The density contours aided in the visualisation of the flow pattern in the domain. The flow pattern exhibited by the numerical model was quite similar to that observed in the physical model for all gate openings save for the 70% gate opening for which the emergency gate was fully submerged.
Figures 5-1A to 5-6A below show contours of density in the domain for emergency gate openings of 20%, 30%, 40%, 50%, 60%, and 70%.

A study by Nafaji et al. (2010) on flow patterns in gated tunnels showed that the flow pattern in transition tunnels could exhibit rooster tail (cross) wave formation. The study attributed such behaviour to flow conditions and geometry of the tunnel. This flow pattern is observed in the CFD numerical solutions downstream of the 12° bend as the flow progresses from pressurised to free surface flow.

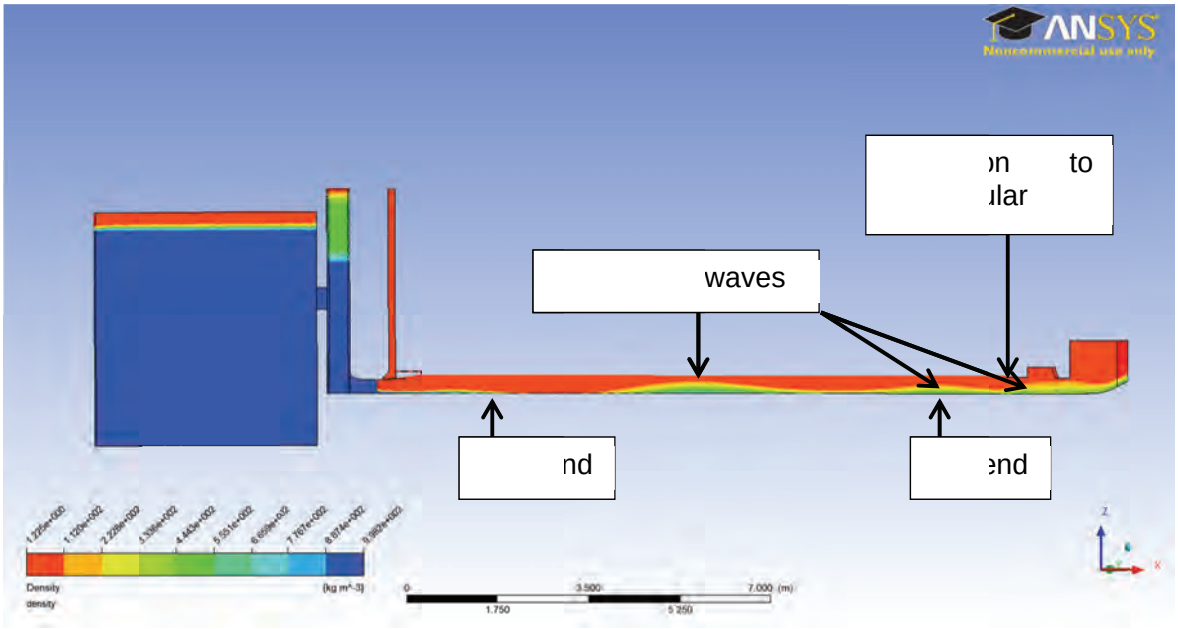

Figure 5-1 A: Density contours for 20% emergency gate opening

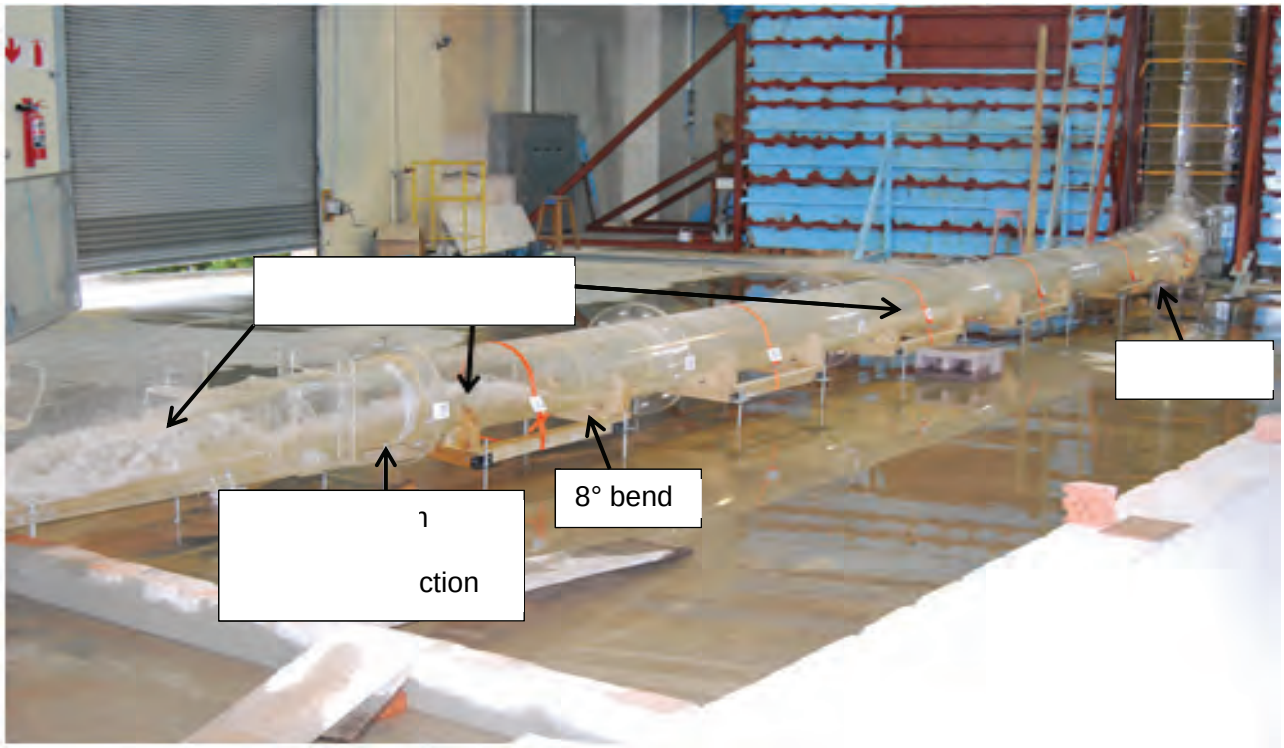

Figure 5-1 B: Flow patterns in physical model for 20% emergency gate opening

Figure 5-1A shows the following:

- Water (shown in dark blue) with a density of 998.2 kg/m^3 occurs in the reservoir and wet well upstream of the emergency gate.

- Air (shown in red) with a density of 1.225 kg/m^3 is drawn down the air vent and downstream in the conduit.
- The jet under the gate becomes more aerated with densities varying between 200 kg/m^3 and 400 kg/m^3 (shown in colours orange, yellow and green).

Figure 5-1B shows the flow pattern in the conduit section of the physical model for 20% emergency gate opening. As similar flow pattern is observed as in the CFD numerical model with the formation of rooster tail waves in the conduit.

Figure 5-2A shows the following:

- The jet issuing underneath the emergency gate is less aerated than that for the 20% gate opening.
- The fluid in the conduit has densities ranging between 200 kg/m^3 (shown in orange) and 550 kg/m^3 (shown in light green).
- The cross waves appear deeper than in the 20% emergency gate setting. This may be attributed due to the increased discharge.

Figure 5-2B shows a section of the conduit upstream of the 8 degree bend, on the physical model at 30% emergency gate opening.

As in the CFD numerical model, the aerated flow exhibits rooster tail wave formation in the conduit due to reduced flow velocities. In Nafaji's study, rooster tail wave formation in tunnels caused the blockage of air passages above free surface flows and therefore prevented the circulation of air from the tunnel outlet.

In Figures 5-2A and 5-3A, the flow in the conduit increases with increasing emergency gate opening, and aeration is adequately provided by the air vent. Air is allowed to flow downstream from the air vent into the conduit but the formation of cross waves at the transition from the horseshoe to the rectangular section of the radial gate block up-flow of air into the conduit.

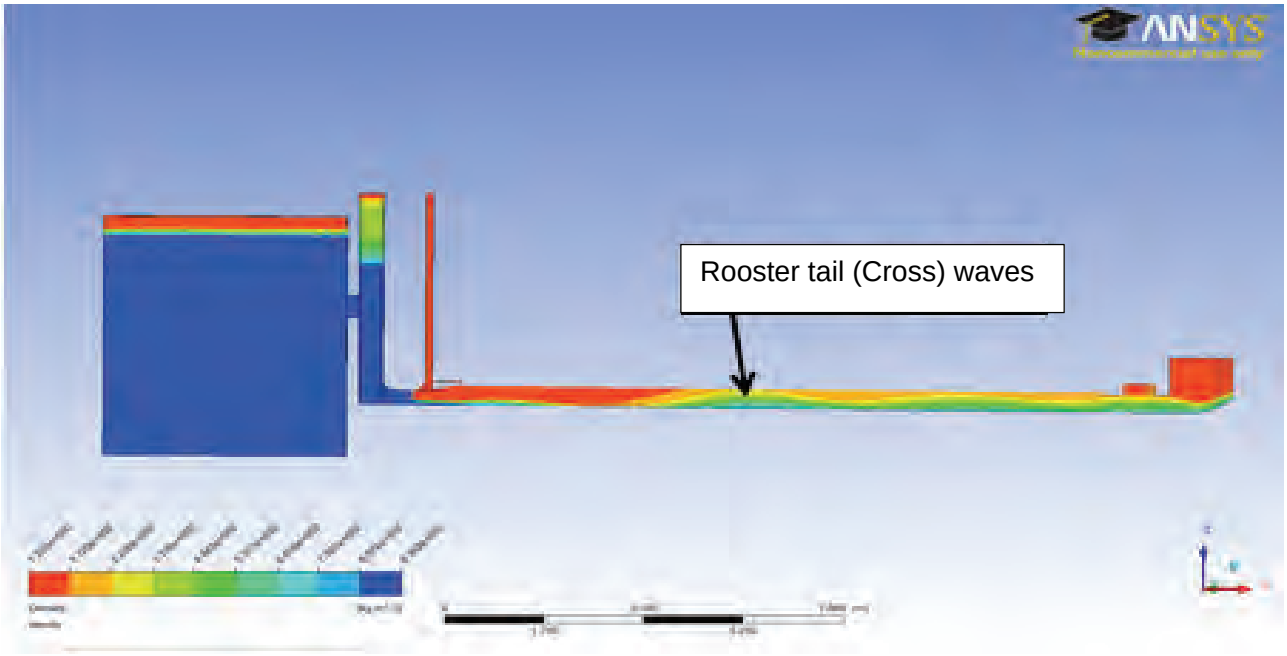

Figure 5-2A: Density contours for 30% emergency gate opening (Numerical)

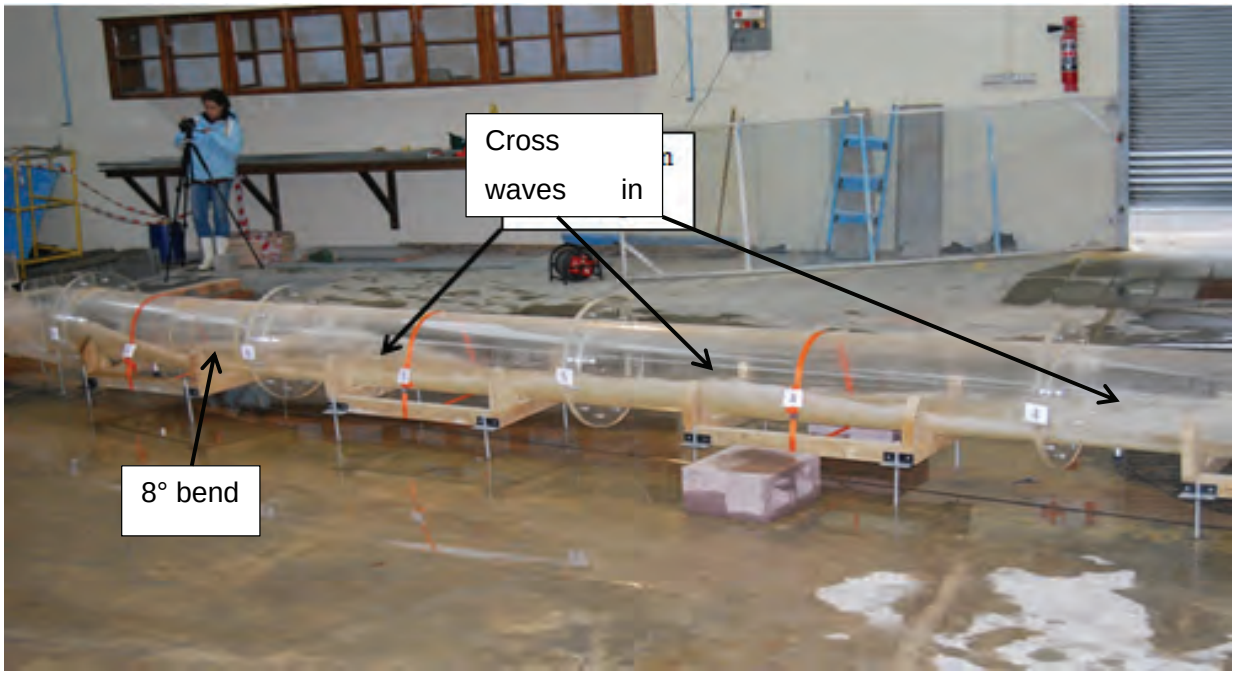

Figure 5-2 B: Flow pattern in physical model for 30% emergency gate opening

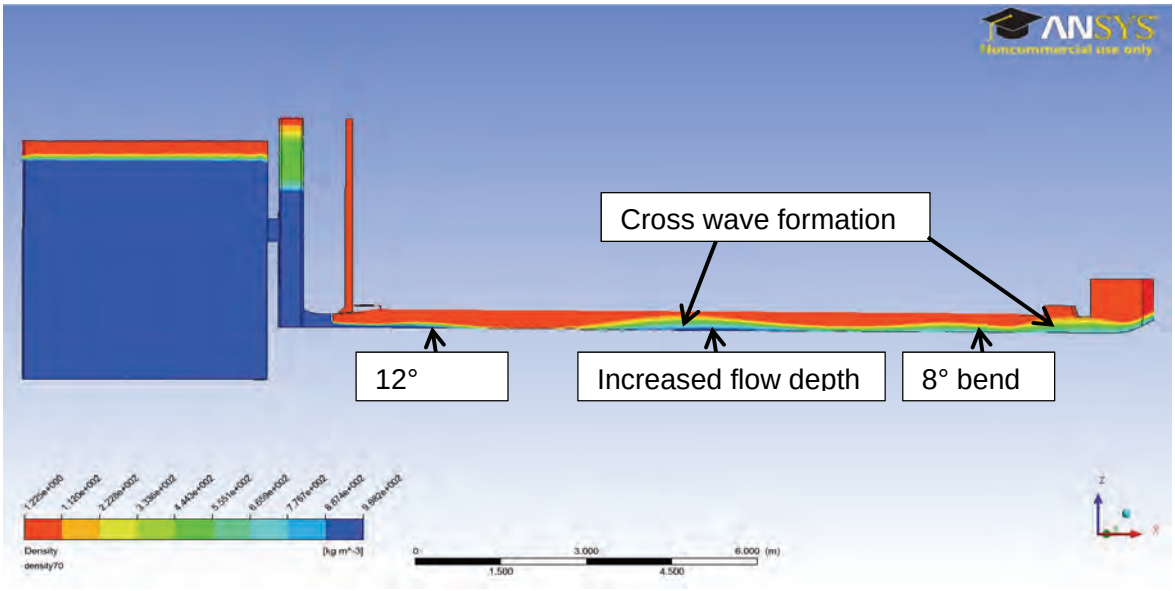

Figure 5-3A: Density contours for 40% emergency gate opening

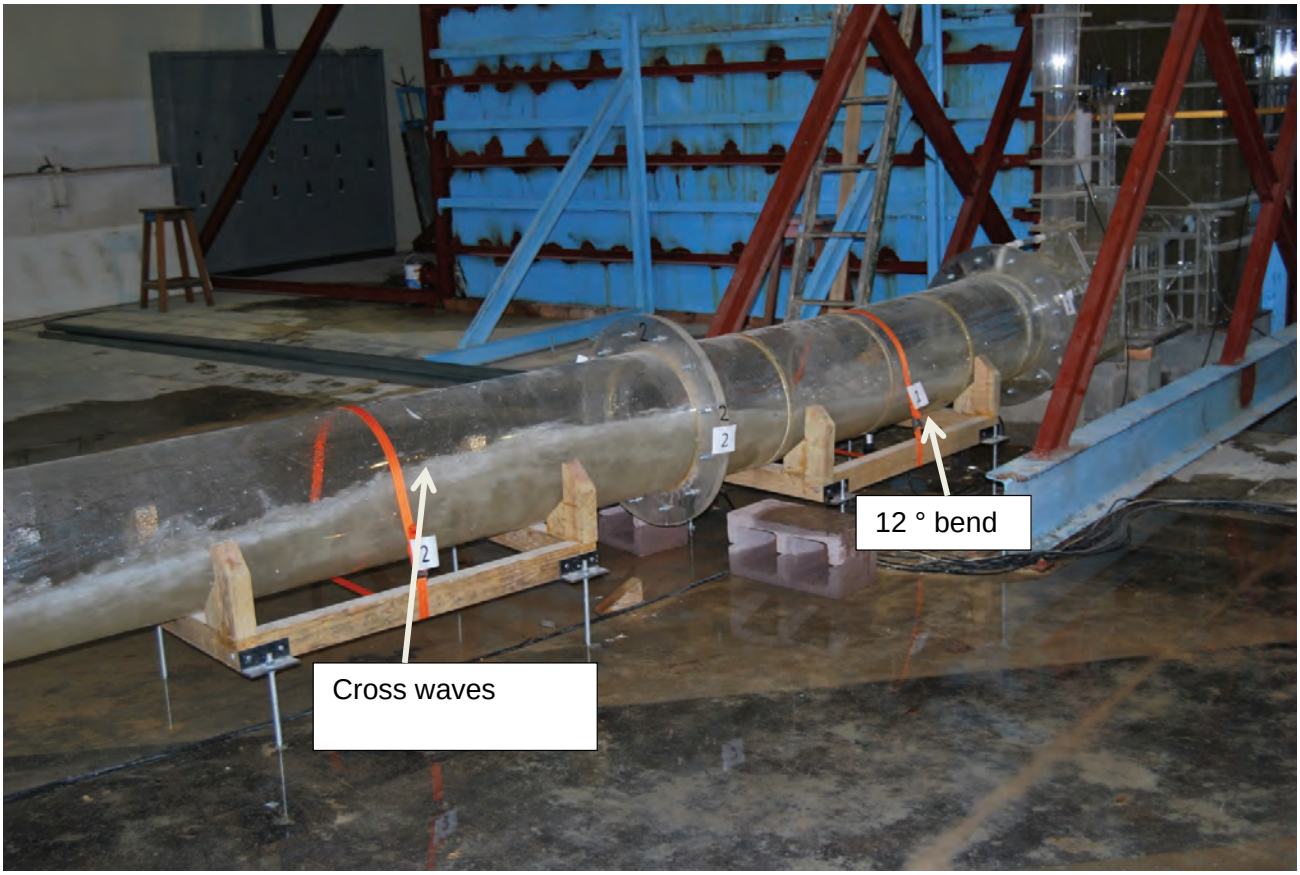

Figure 5-3 B: Flow pattern in physical model for 40% emergency gate opening

For the 40% emergency gate opening, Figure 5-3A indicates that:

- Upstream of the emergency gate the flow is aerated by the open surfaces of the wet well and the reservoir.
- The jet underneath the gate is less aerated than that for the 20% and 30% emergency gate opening with densities ranging from 300 kg/m^3 (shown in yellow) and 998.2 kg/m^3 (shown in dark blue).
- The amount of air entrained in the flow throughout the conduit due to the formation of cross waves reduces.
- The increased depth of flow downstream of the emergency gate is evident and this aerated flow appears to fill the conduit upstream of the ski jump at the constriction where the conduit area reduces.

Figure 5-3B shows a section of the conduit from the physical model at 40% emergency gate opening.

The flow pattern exhibited in the physical model is similar to that of the CFD numerical model. Air is entrained in the surface of the flow as it moves downstream in the conduit. The increase in water depth further downstream in the conduit appears to result from reduced velocities on account of friction losses with some evidence that cross waves may occur.
In Figure 5-4A the following is observed:

- The jet issuing underneath the gate begins to fill up the conduit with densities of the fluid ranging from 200 kg/m^3 (shown in orange in the air pockets) and 998.2 kg/m^3 (shown in dark blue).
- Air pockets begin to form downstream of the 12 degree bend where the flow is almost full.
- At the position of the radial gate the conduit appears to be blocked by the flow, preventing free air release downstream as the flow enters the ski jump.

Figure 5-4B shows a section of the conduit from the physical model at 50% emergency gate opening. The flow pattern is similar to that from the CFD numerical model in Figure 5-4A.

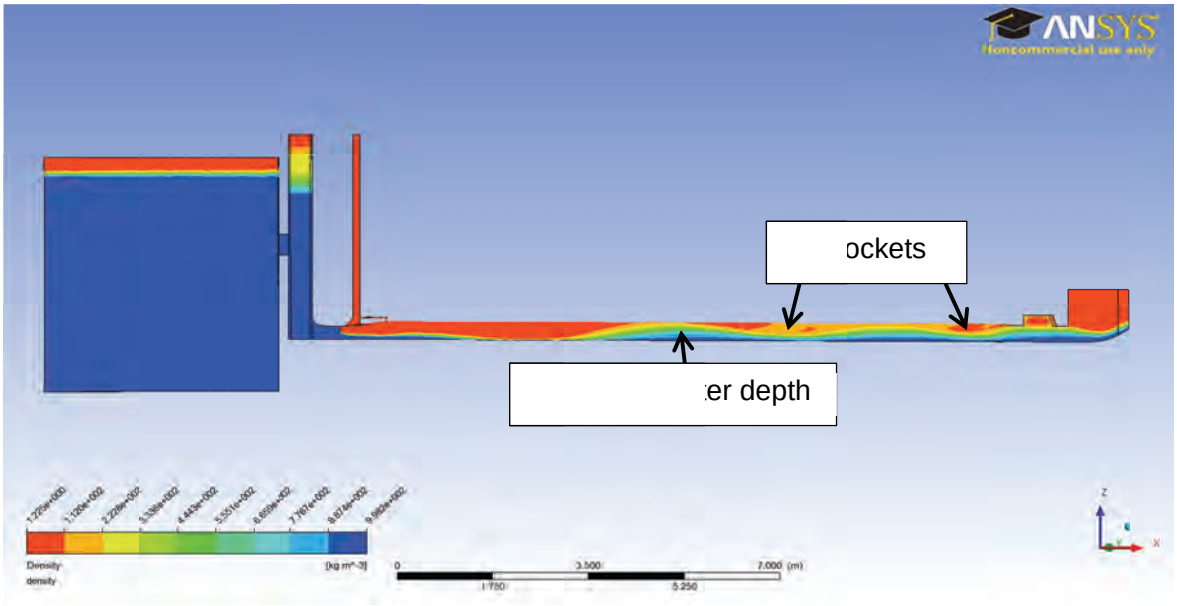

Figure 5-4A: Density contours for 50% emergency gate opening (Numerical)

Figure 5-4 B: Flow pattern in physical model for 50% emergency gate opening

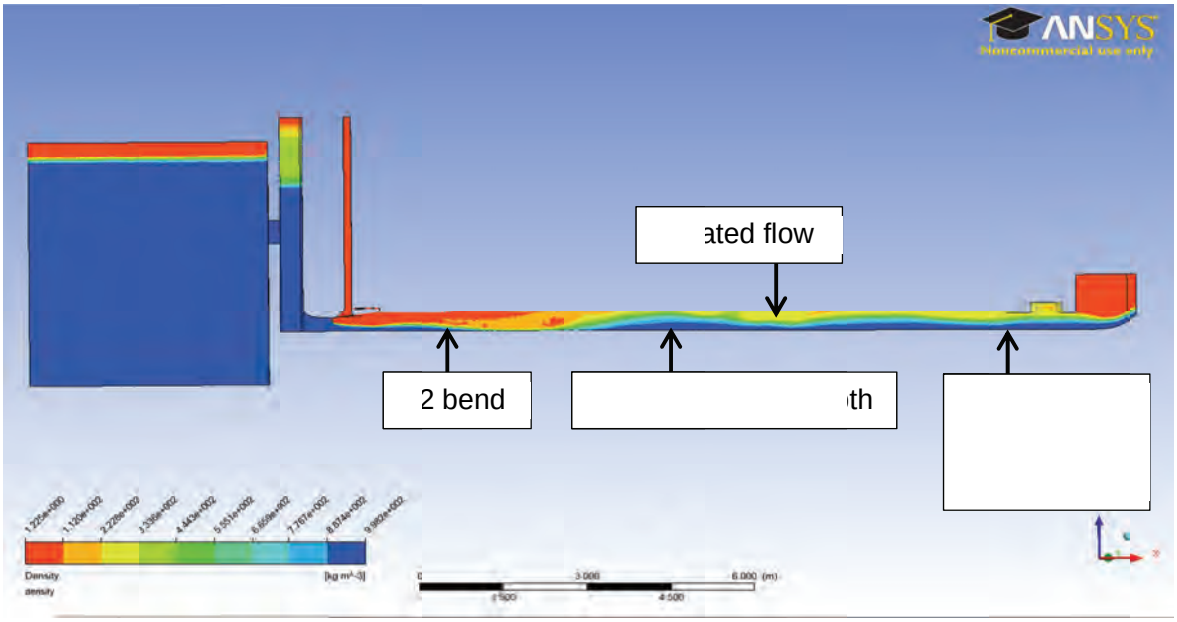

Figure 5-5A: Density contours for 60% emergency gate opening

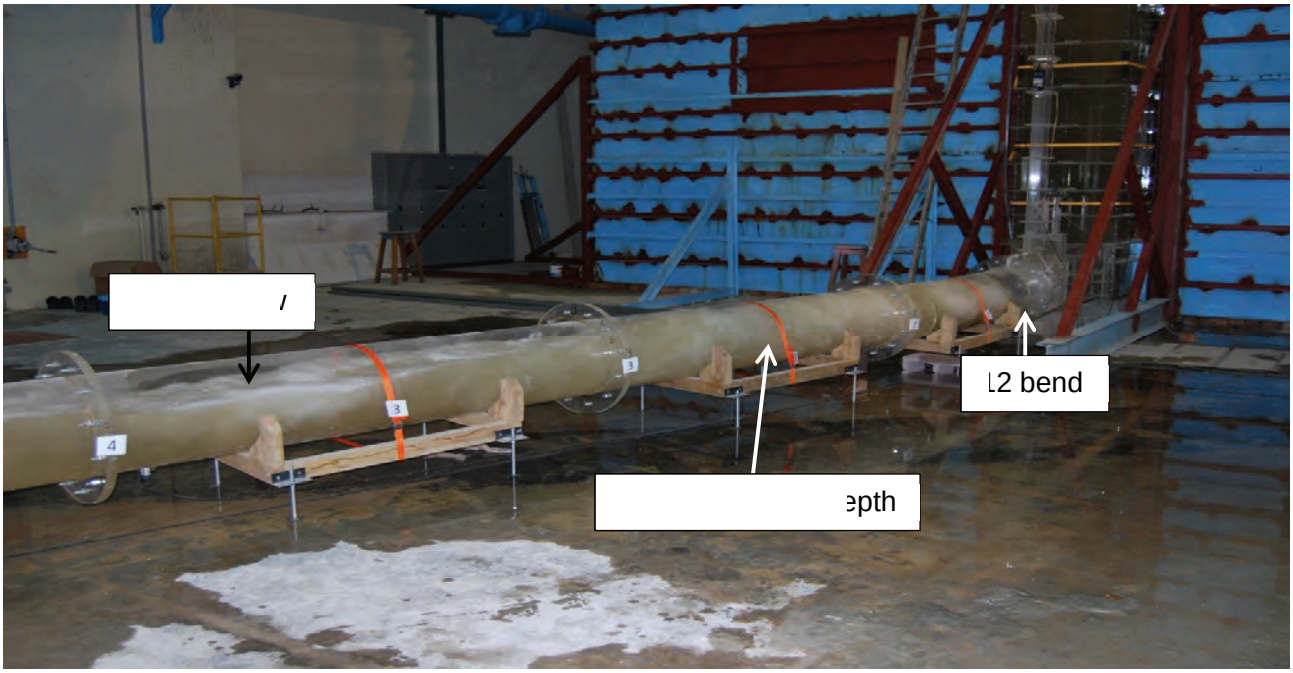

Figure 5-5 B: Flow pattern in physical model for 60% emergency gate opening

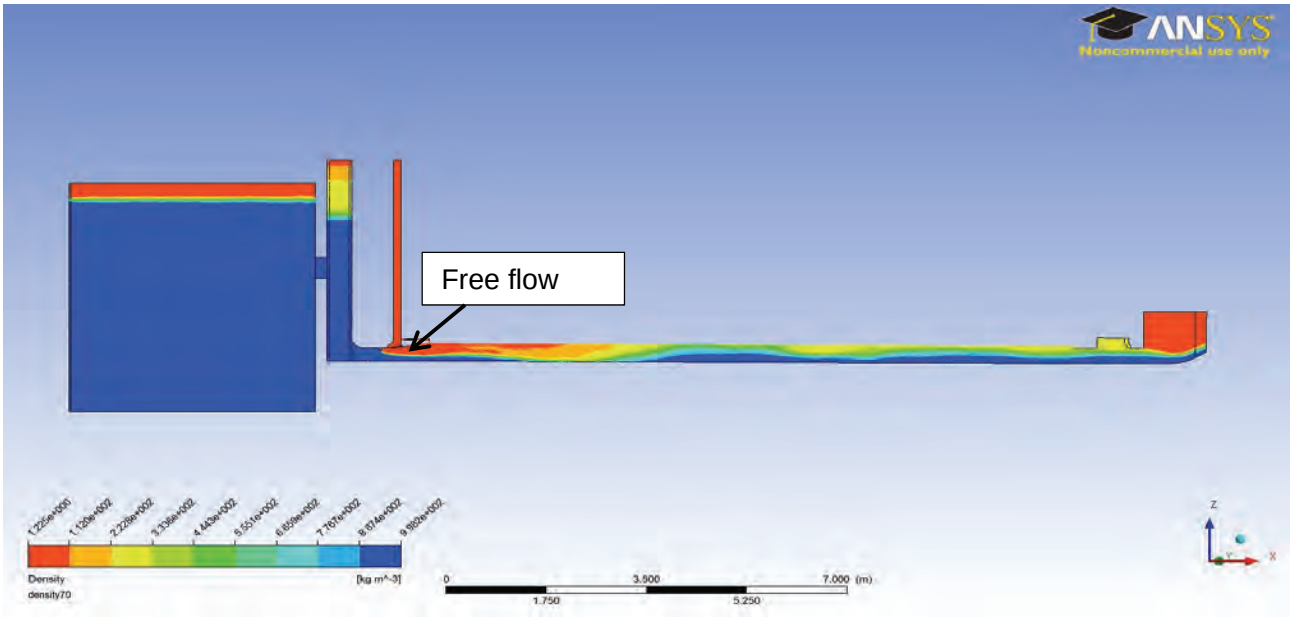

Figure 5-6 A: Density contours for 70% emergency gate opening

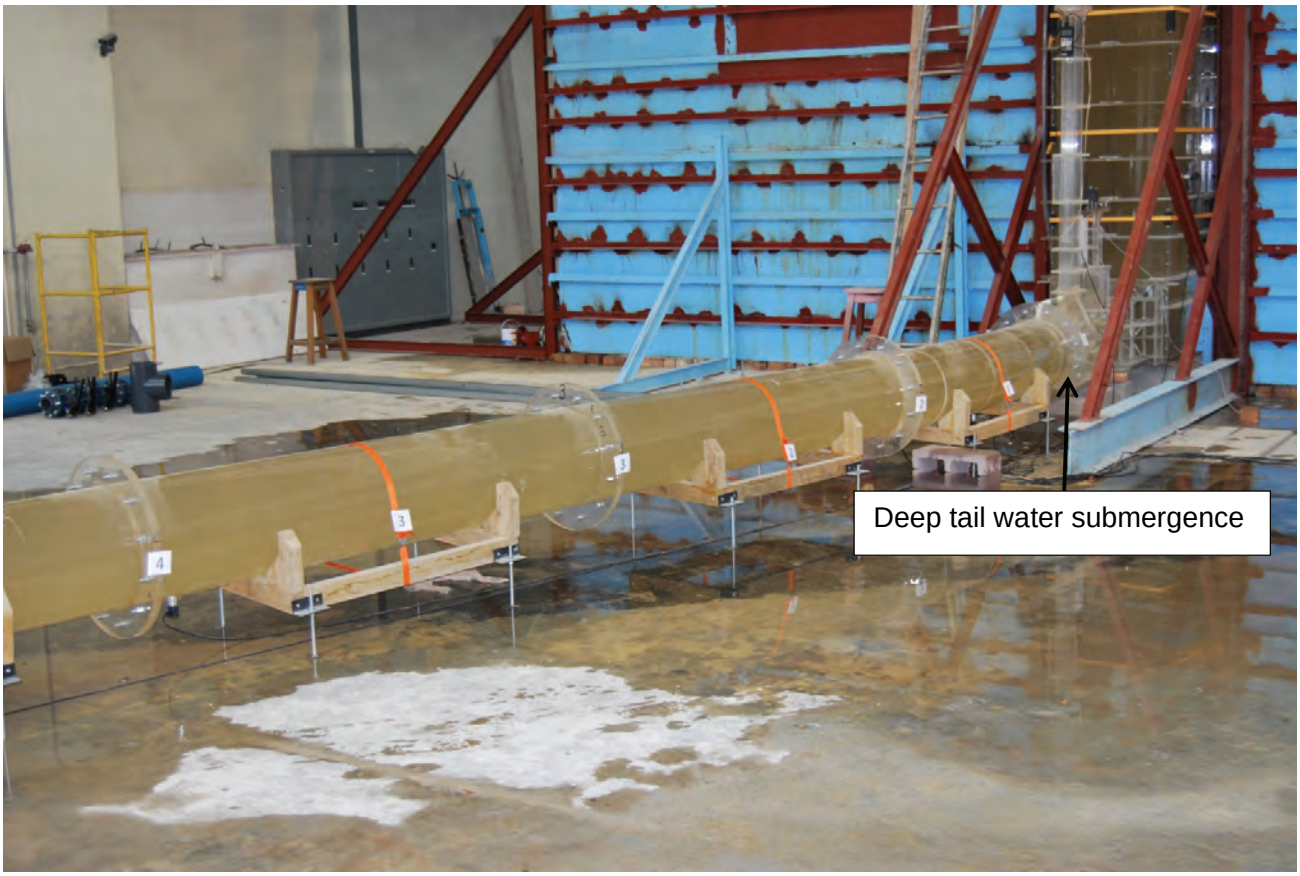

Figure 5-6 B: Flow pattern in physical model for 70% emergency gate opening

At 60% emergency gate opening, Figure 5-5A and Figure 5-5B below the following:

- The conduit is flowing full after the 12 degree bend and the flow density ranges between 200 kg/m^3 (shown in orange) and 998.2 kg/m^3 (shown in dark blue).
- The sudden increase in water depth after the 12 degree bend may imply the formation of a hydraulic jump but after determining the Froude number at various sections along the conduit, it was established that the flow was supercritical throughout. With the flow being supercritical and still entraining air in the air pockets formed at the top of the conduit, the air vent should be able to provide enough aeration to satisfy the entrainment.
- There is circulation of air from the air vent immediately downstream of the emergency gate above the issuing jet, which causes aeration for the flow.
- The top of the wet well and the reservoir provide aeration for the flow upstream of the emergency gate.

Figure 5-6A shows the following:

- The flow in the conduit downstream of the emergency gate is full and the density of the fluid varies between 300 kg/m^3 (shown in green and 998.2kg/m^3 (shown in dark blue).
- There is no submergence of emergency gate as was experienced in the hydraulic model (Figure 5-6B).
- There are no air pockets formed on the surface of the flow in the conduit.

The conduit flowed partially full for gate openings of 20%, 30% and 40%. At 50%, 60% and 70% the conduit started to flow full, with an air-water mixture at the surface as shown in Figure 5-6A and 6B.

Continuous damming of the flow upstream of the ski jump was observed at the position of the radial gate. When this damming blocked air from being pushed out of the domain it led to oscillation of the flow in the conduit.

Both the numerical and physical model results for all tested emergency gate openings provided no release of air up the air vent as in the prototype commissioning test.

5.1.2 Velocity Vectors in the Wet Well Tower

The figures below show the velocity vectors, coloured by density of the flow into the wet well tower for emergency gate openings of 20%, 30%, 40%, 50%, 60% and 70%. As for the contours above, red represents air and blue represents water.

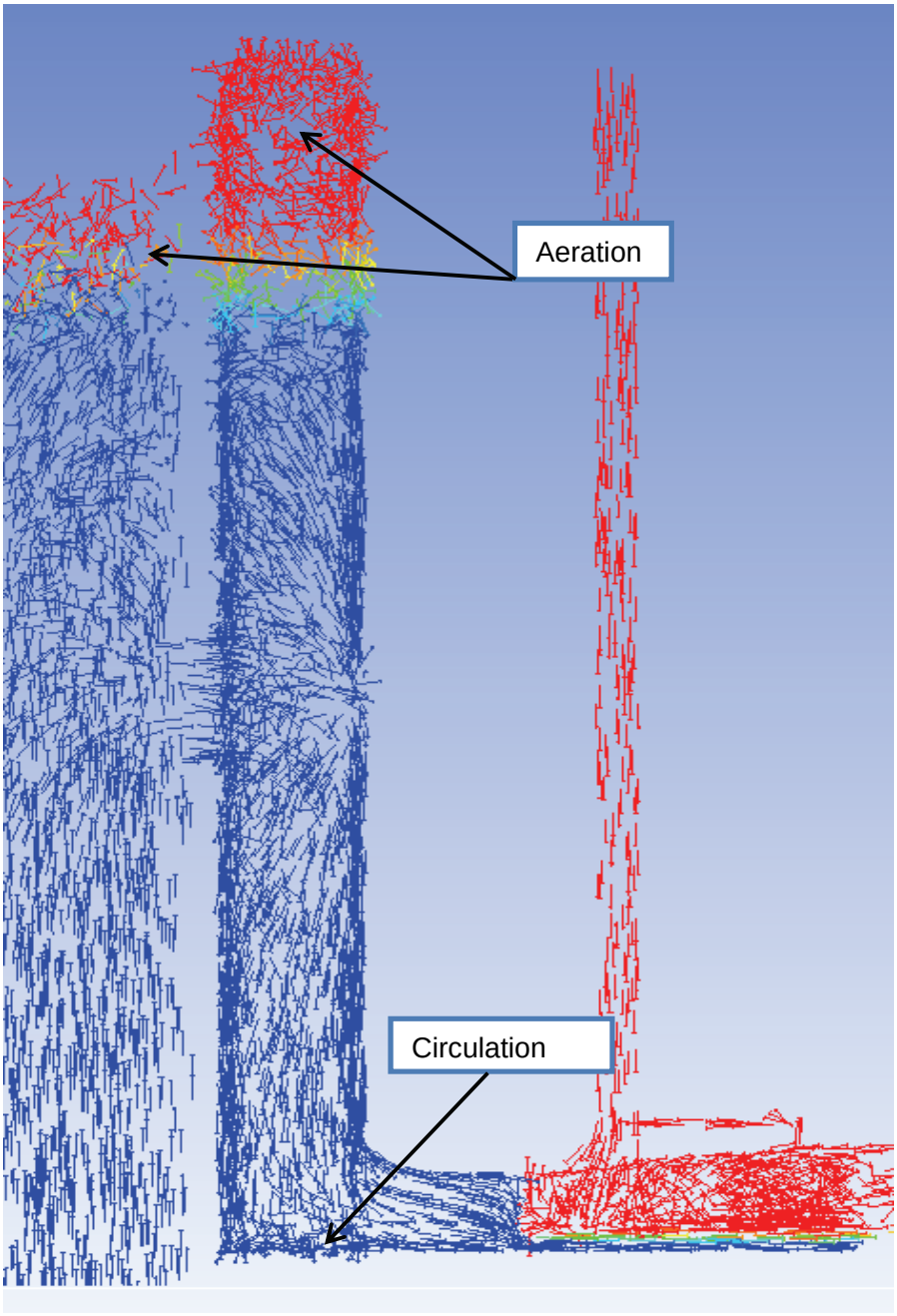

Figure 5-7: Wet well velocity vectors for 20% emergency gate opening

Figure 5-7 shows the following:

- As the flow leaves the reservoir into the wet well tower, the main potential sources of aeration are the top of the wet well upstream of the emergency gate and the air vent at the outlet downstream of the emergency gate.
- There appears to be rotational flow at the bottom of the wet well tower. As the wet well fills up, the flow area is constricted at the emergency gate and there appears to be a contra flow at the top of the conduit immediately upstream of the gate.

- Air is drawn down the air vent to the downstream of the emergency gate and there is air circulating above the issuing jet.

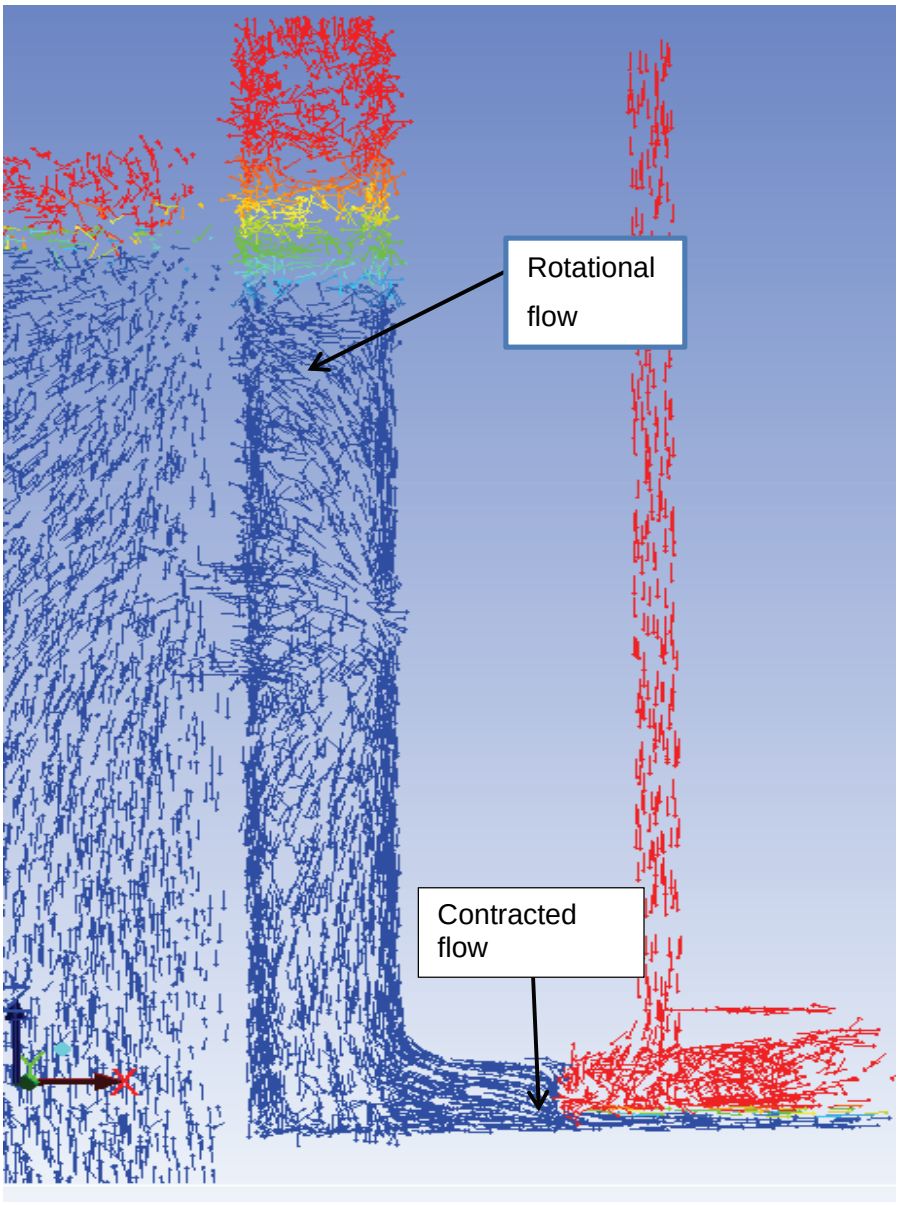

Figure 5-8: Wet well velocity vectors for 30% emergency gate opening

From the 30% gate opening (Figure 5-8) and onwards, horizontal rotational flow is observed on the surface of the water in the wet well tower, above the selector gates. Such rotational flow was also observed in the wet well in the physical model. This could lead to the formation of vortices that entrap air upstream of the emergency gate (Sharma, 1976) but no vortices were observed in the numerical model.

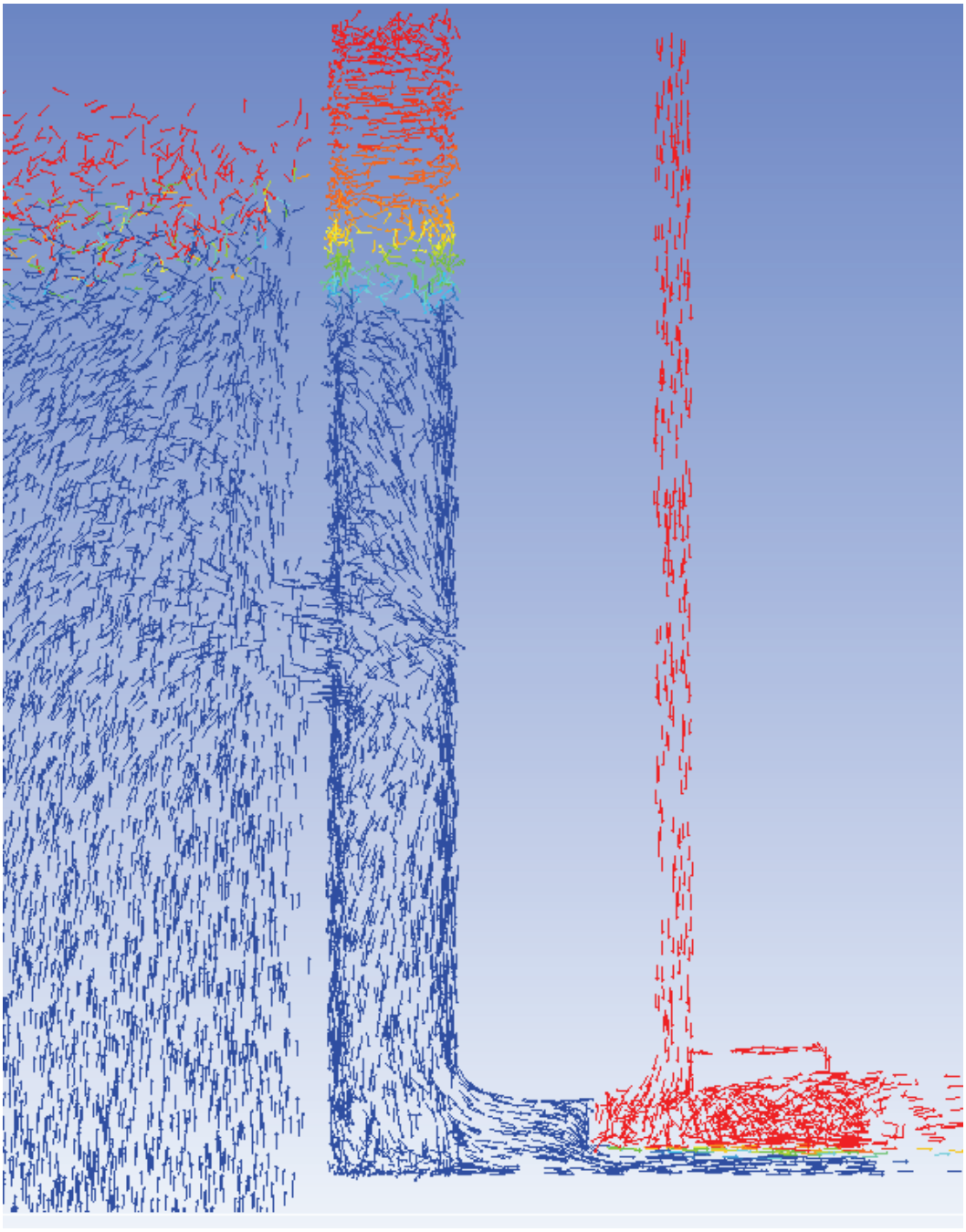

Figure 5-9: Wet well velocity vectors for 40% emergency gate opening

The fluid at the surface of the tower (Figure 5-9 to Figure 5-12), above the intake gates, appears to be entrapped with air; aeration being provided by the top of the wet well. The air, however, does not appear to go down further into the wet well and therefore is not considered a source of air downstream of the emergency gate. This phenomenon was not evident in the physical model.

The rotational flow at the surface of the water in the wet well tower is expected due to the horizontal flow into the wet well the intake gates.

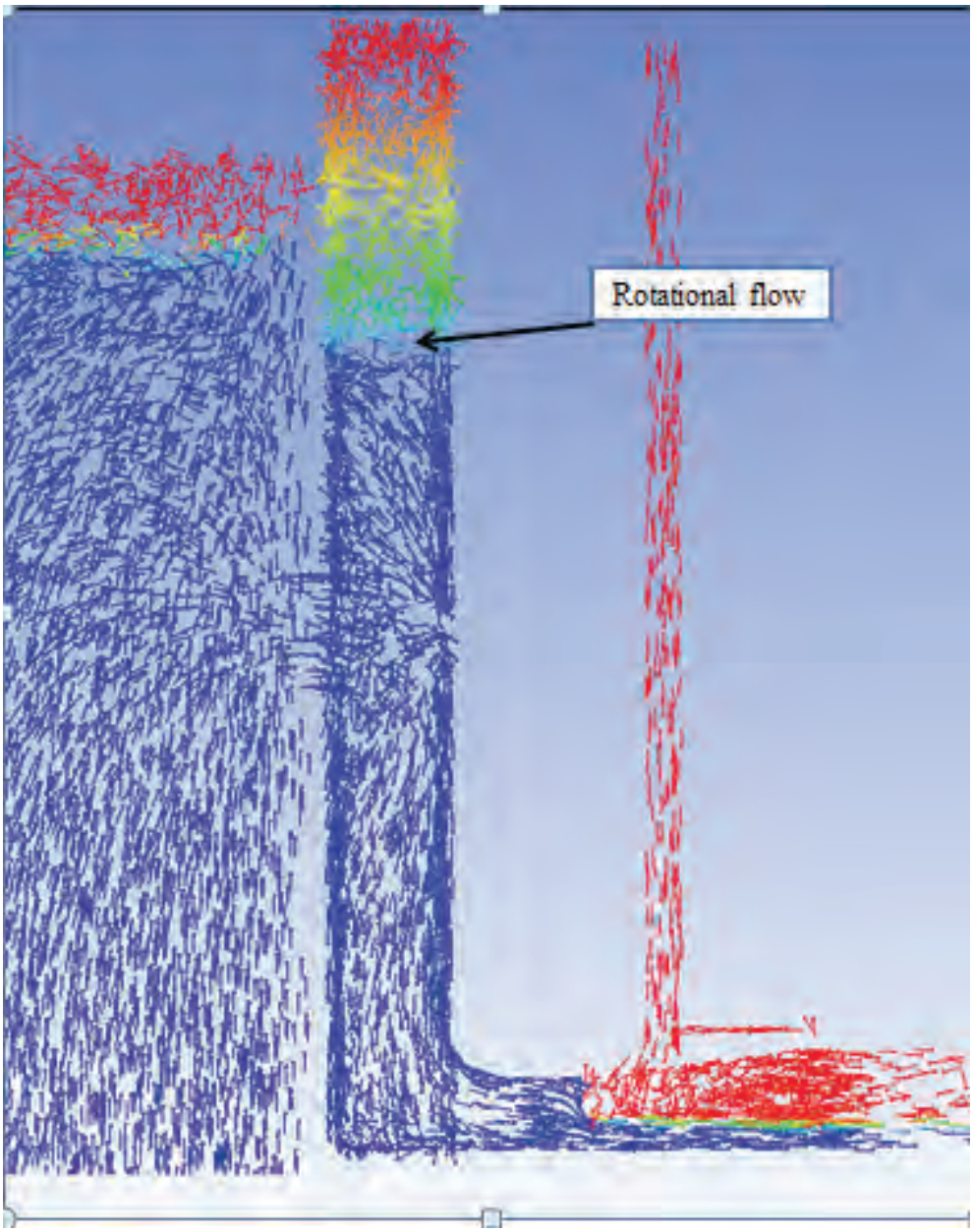

Figure 5-10: Wet well velocity vectors for 50% emergency gate opening

For the 50% emergency gate opening shown in the Figure 5-10 above and the 60% emergency gate opening shown in the Figure 5-11 below, there is not as much circulation observed in the wet well tower as in previous settings. As the flow area at the emergency gate increases, the velocity of flow decreases. However, the discharge through the emergency gate also increases.

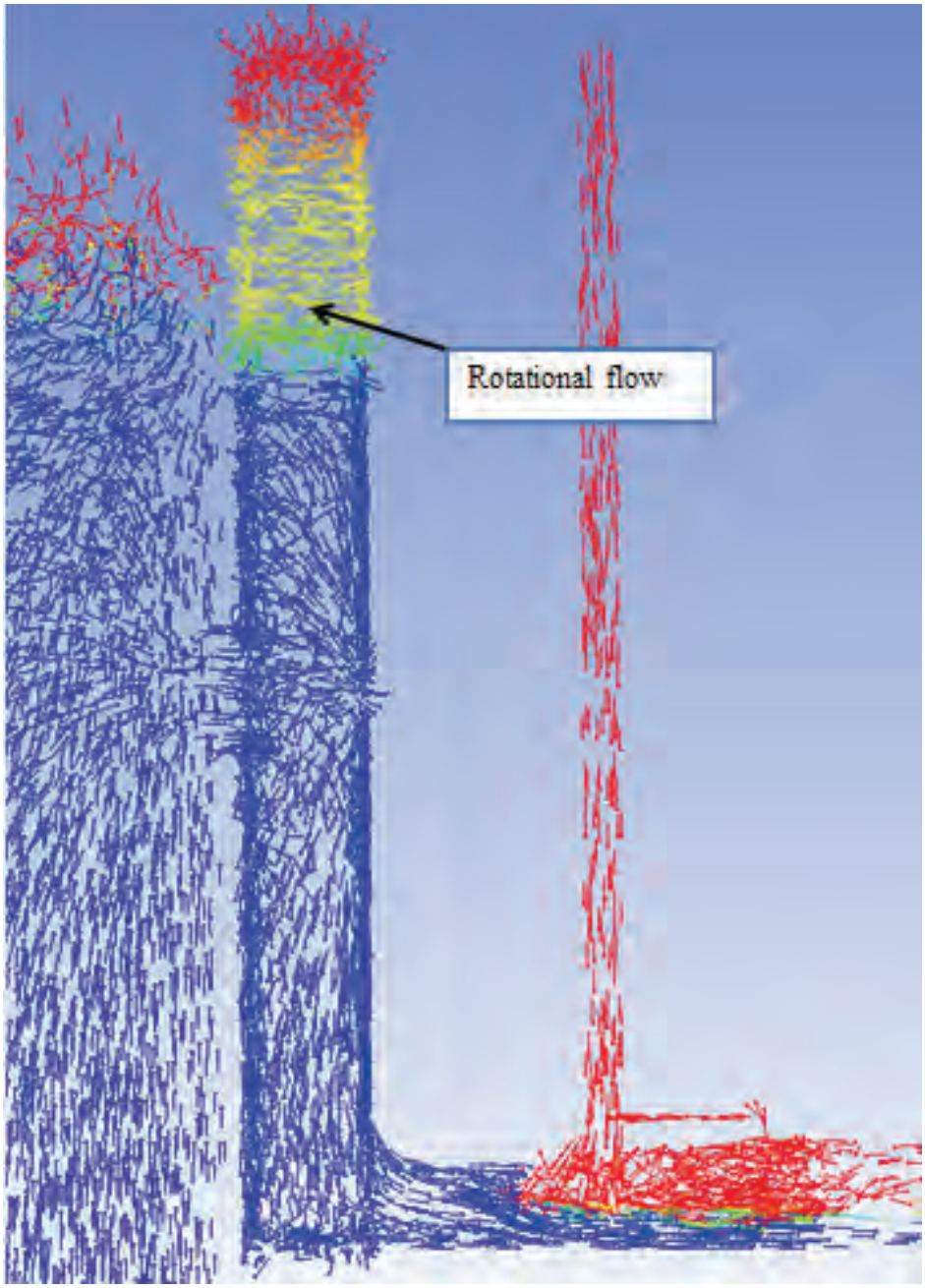

Figure 5-11: Wet well velocity vectors for 60% emergency gate opening

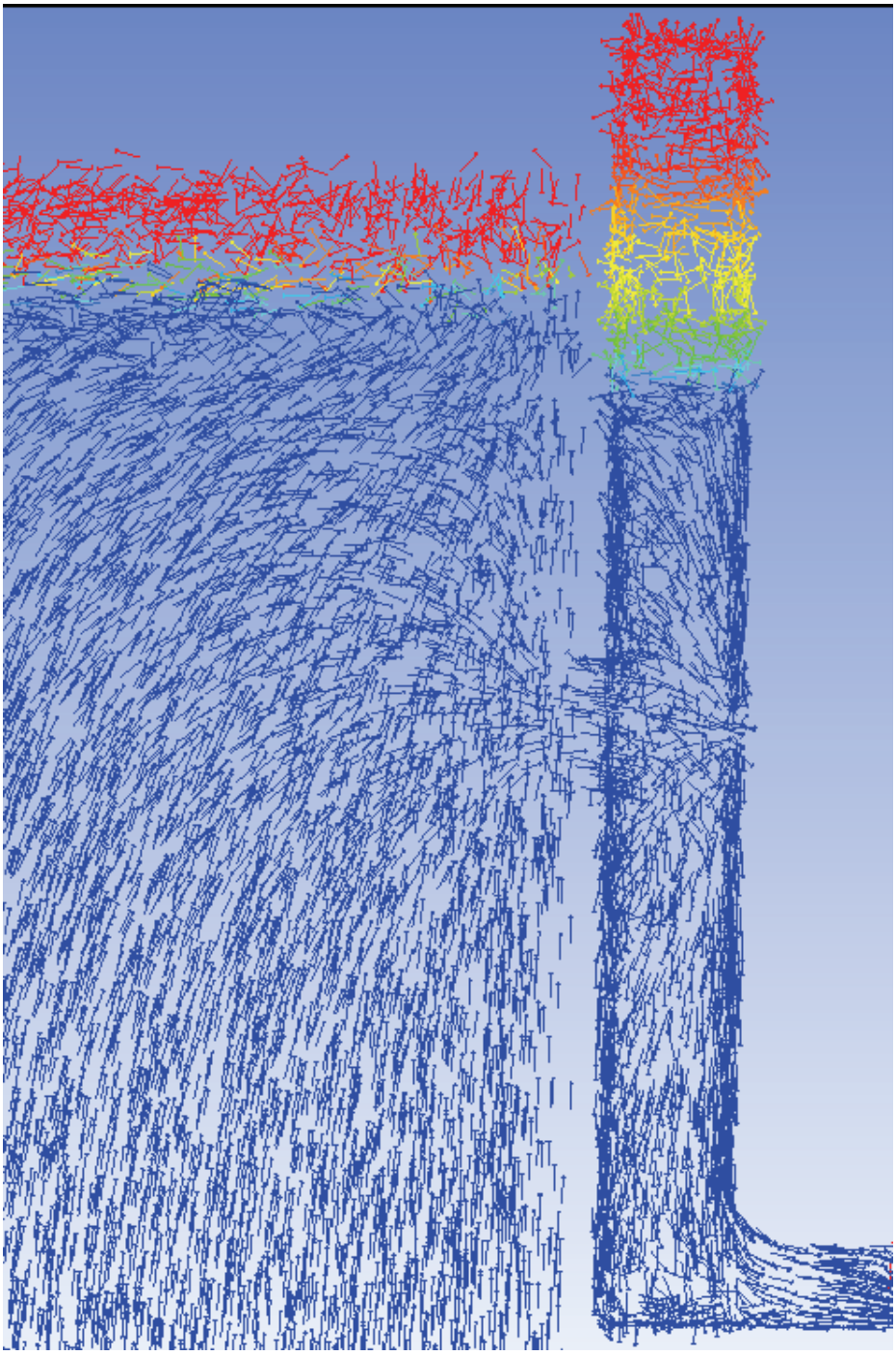

Figure 5-12: Wet well velocity vectors for 70% emergency gate opening

For all scenarios where rotational flow in the wet well tower was observed, it is possible that such flow could entrain large amounts of air. However, it was not established whether aeration at the top of the wet well contributed to the air downstream of the emergency gate.

5.1.3 Velocity Vectors in Gate and Air Vent Region

The figures below show the velocity vectors of the flow, coloured by density (Blue representing water and red representing air), as it approaches the emergency gate and proceeds into the conduit, for emergency gate openings of 20%, 30%, 40%, 50%, 60% and 70%.

The mesh at the gate was set up as in the physical model with modifications made to the gate lip but the side grooves for the gate were not incorporated in the numerical model geometry. The exclusion of the side grooves should not affect the results of the simulation and their introduction would mean extra unnecessary cells.

Because of the highly pressurized flow upstream of the emergency gate (Figure 5-13 A) and the small flow area of the gate, the water issues from the gate in the form of a spray jet and the water depth of highly aerated flow increases further downstream in the conduit.

The 20% emergency gate opening setting results in the greatest aeration to the flow on account of the highly pressurised jet issuing from underneath the gate. There is high circulation of air just below the air vent, immediately downstream of the emergency gate, as the vent provides the required aeration demand.

Figure 5-13 B shows the similarity of the flow patterns for the numerical and physical models. Air is continuously sucked into the model through the air vent.

The discharge underneath the gate increases with increasing gate opening and for 30% and 40% gate openings as seen in Figures 5-14 A/B and 5-15 A/B below, the jet issuing is free flow. No submergence of the emergency gate is observed but continued aeration is provided by the air vent.

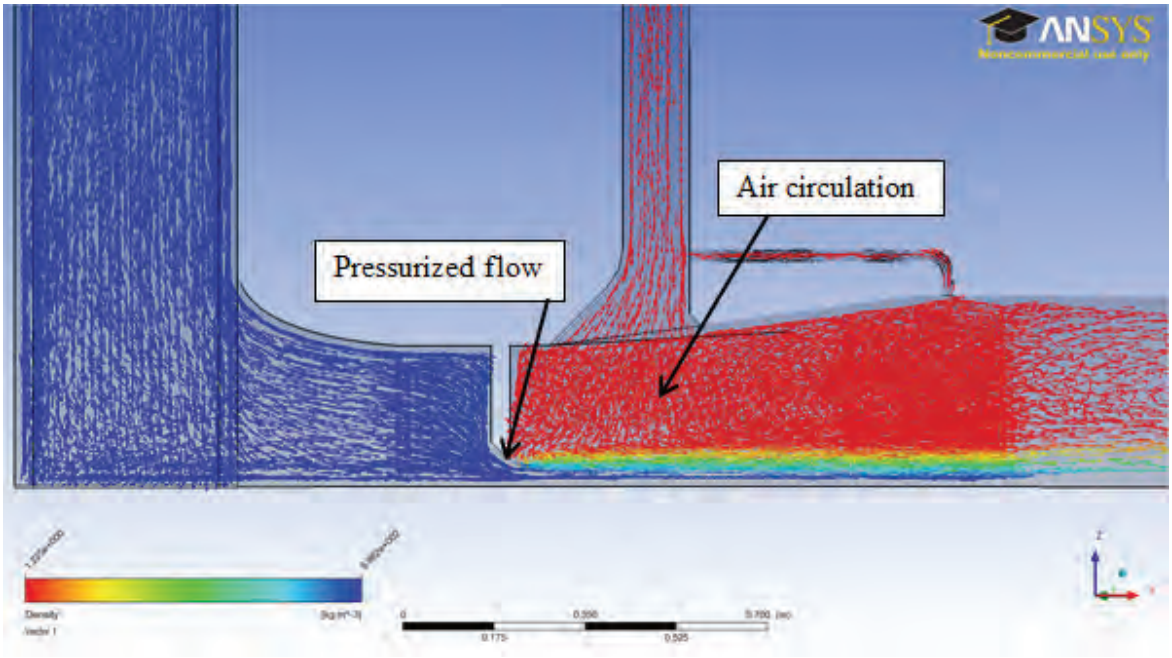

Figure 5-13 A: Velocity vectors in emergency gate and air vent region for 20% emergency gate opening

Figure 5-13 B: Flow pattern in emergency gate and air vent region for 20% emergency gate opening (Physical)

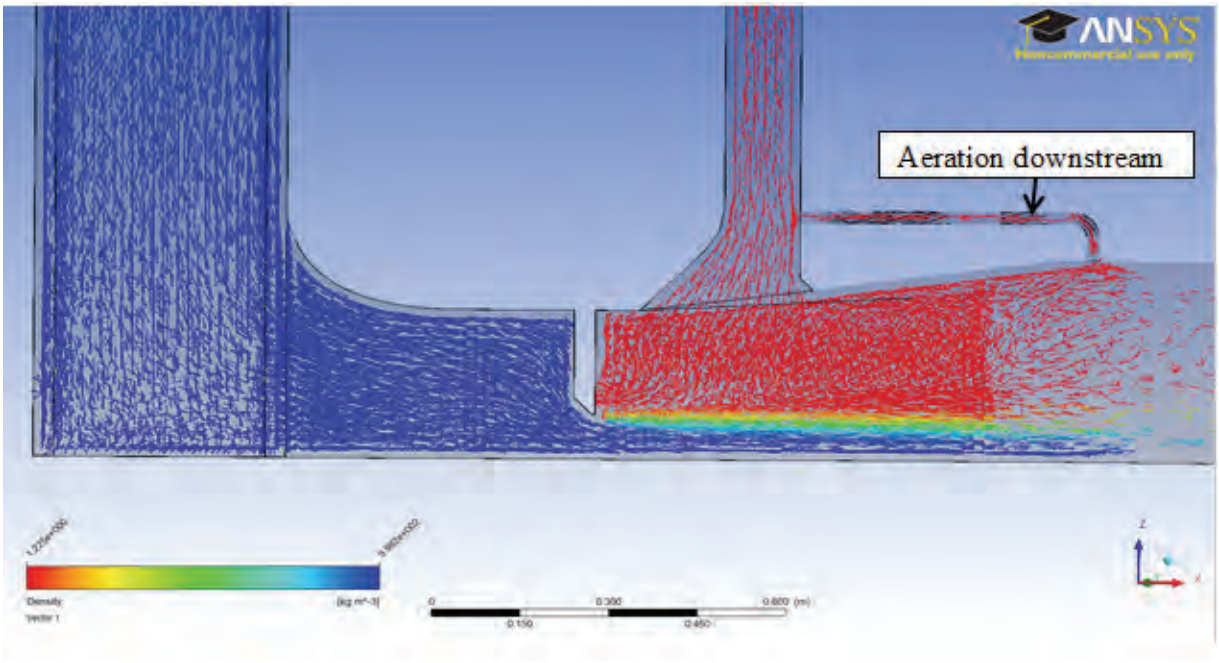

Figure 5-14 A: Velocity vectors in emergency gate and air vent region for 30% emergency gate opening

Figure 5.14 B: Flow pattern in emergency gate and air vent region for 30% emergency gate opening (Physical)

Figure 5-14 A above shows the small pipe attached to the air vent providing aeration downstream of the emergency gate, at the beginning of the conduit.

On account of a short coming of the software used for post processing, it was not possible to develop uniform vectors across the whole domain. This was because of the complexity of the geometry and because during the meshing, the domain had to be partitioned into smaller components that had different mesh sizes. Smaller mesh sizes were used in the critical sections of the model such as the gate lip and the air vent region. Therefore, the density of the plotted vectors in the various sections of the domain has no relation to nature of the result. This is a post processing drawback.

Figure 5-14 B shows the flow pattern at emergency gate and air vent region for 30% emergency gate opening in the physical model. Considering the shape of the gate lip structure as shown in Section 4.1 above and the velocities at which the flow emerges through the gate, the flow does not contract greatly. For the 40% emergency gate opening shown in Figure 5-15 A and 5-15 B for the CFD and physical model, the upstream angle on the gate lip allows the flow to be directed smoothly underneath the gate and also reduces the pressure on the upstream side of the emergency gate.

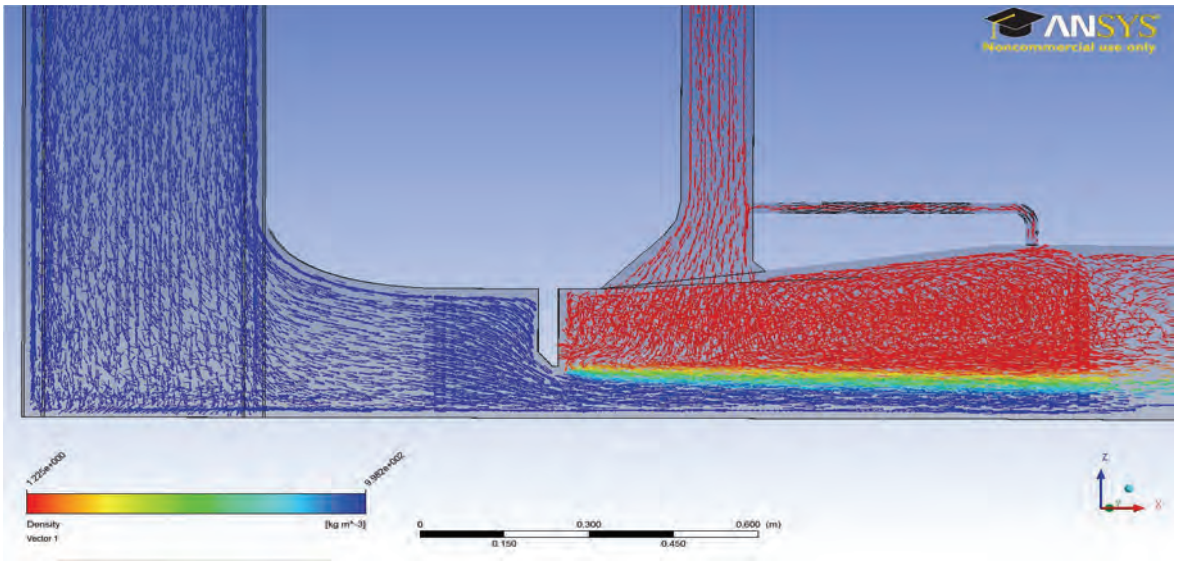

Figure 5-15 A: Velocity vectors in emergency gate and air vent region for 40% emergency gate opening

Figure 5.15 B: Flow pattern in emergency gate and air vent region for 40% emergency gate opening (Physical)

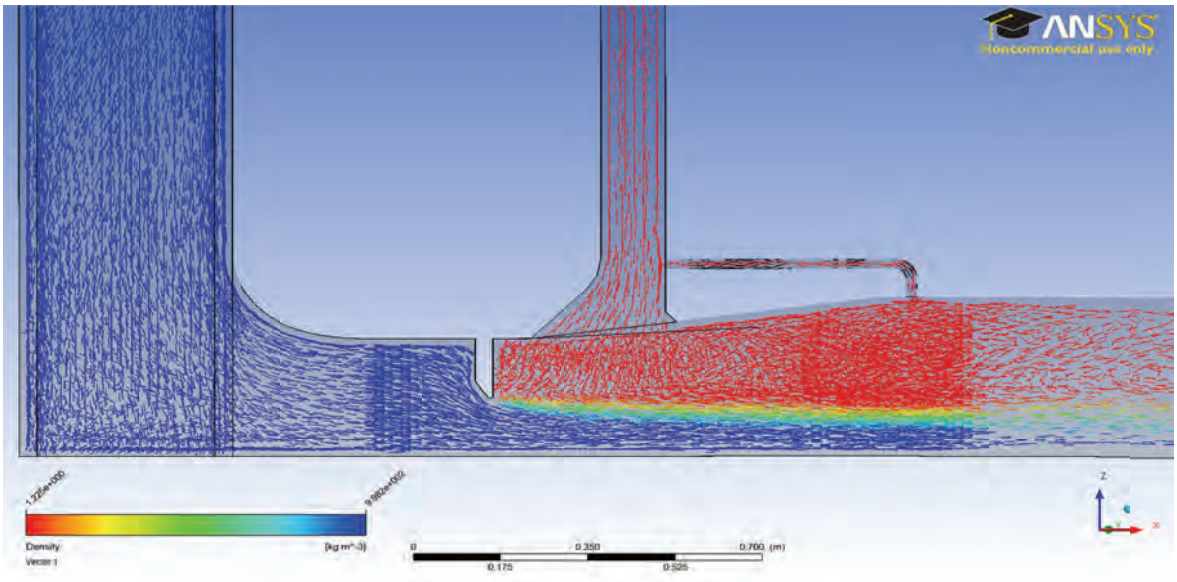

Figure 5-16 A: Velocity vectors in emergency gate and air vent region for 50% emergency gate opening

Figure 5-16 B: Flow pattern in emergency gate and air vent region for 50% emergency gate opening (Physical)

For the 50% emergency gate opening shown in the Figure 5-16 A and the 60% emergency gate opening as shown in the Figure 5-17 A there is minimal rotational flow upstream of the emergency gate, at the bottom of the wet well. The rotation reduces as the flow area at the emergency gate increases.

There is no deep tail-water submergence in the numerical and physical models as free flow occurs downstream of the emergency gate. The conduit flows partially full downstream of the emergency gate and further downstream the conduit begins to flow full as discussed in Section 5.1.1 with aeration being efficiently provided by the air vent.

Except for the 60% and 70% gate openings, the flow pattern immediately downstream of the emergency gate for all other simulated gate openings was similar to that of the physical model. At the 60% and 70% emergency gate openings, the physical model exhibited deep tail-water submergence of the flow immediately downstream of the emergency gate (Figures 5-17 B and 5-18 B) where there was increased water depth. The flow appeared fully pressurized with the conduit

flowing full all the way from the emergency gate down to the ski jump whereas the CFD model showed aerated flow.

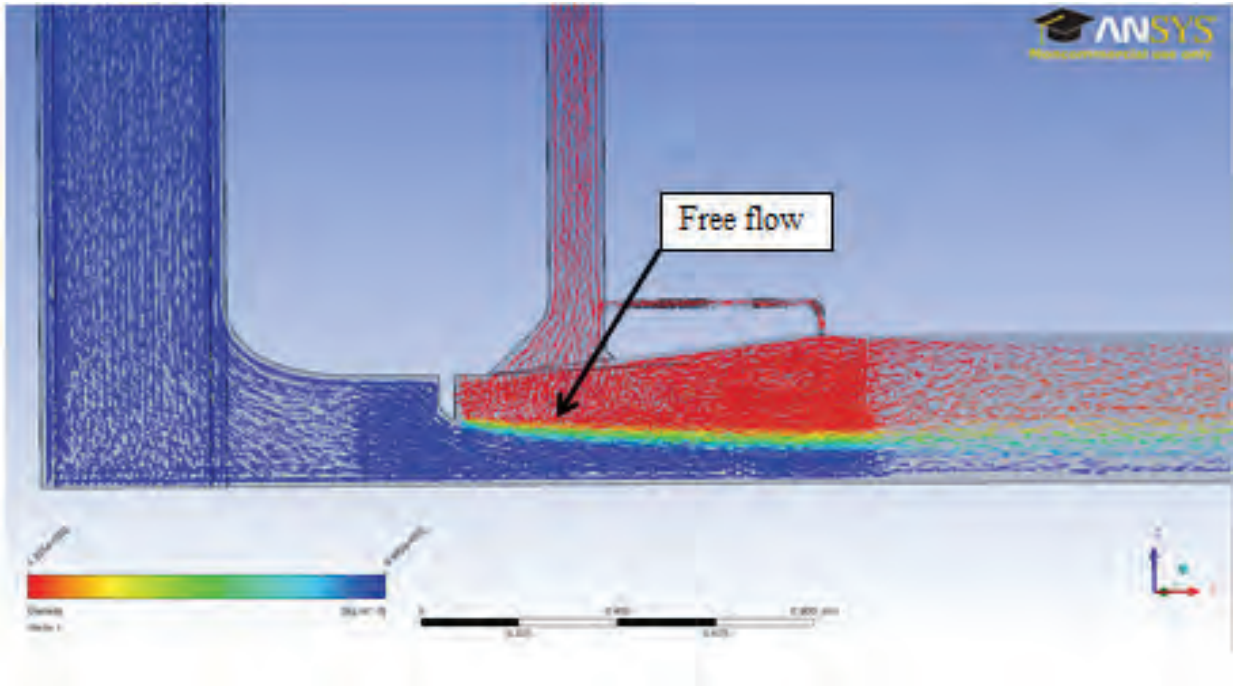

Figure 5-17 A: Velocity vectors in emergency gate and air vent region for 60% emergency gate opening

Figure 5-17 B: Flow pattern in emergency gate and air vent region for 60% emergency gate opening (Physical)

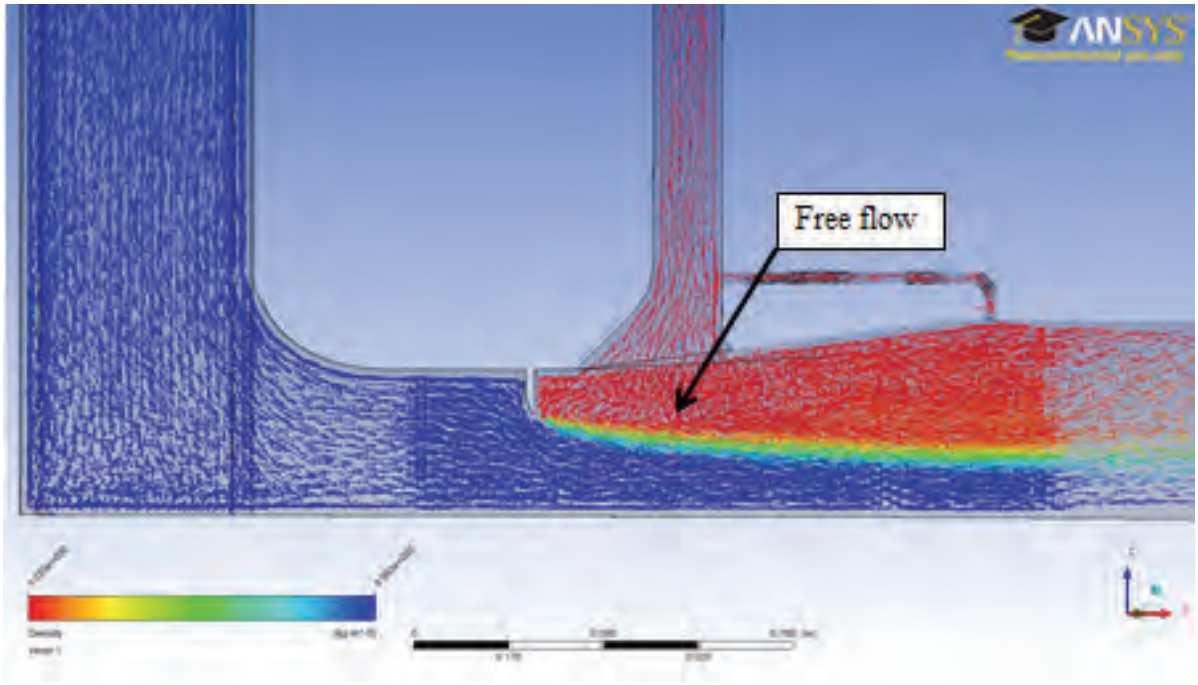

Figure 5-18 A: Velocity vectors in emergency gate and air vent region for 70% emergency gate opening

Figure 5-18 B: Emergency gate region on physical model for 70% emergency gate opening

5.1.4 Velocity Vectors at the End Box and Ski Jump

The flow pattern at the ski jump was monitored as well to determine its possible influence on the occurrence of full flow which resembles a hydraulic jump. Blue represents water, red represents air and colours in between (such as orange, yellow and green) represent aerated flow.

The following figures display the flow pattern at the ski jump in the form of velocity vectors coloured by density for emergency gate openings of 20%, 30%, 40%, 50%, 60% and 70%.

For the 20% emergency gate opening (Figure 5-19 A and 5-19 B) there is formation of cross waves upstream of the ski jump. The conduit flows partially full and the density of the flow is low with a lot of air entrained. There is circulation of air above the flow especially in the area of the 8 degree bend where the conduit begins to constrict and at the end box where the radial gate is located.
For the 30% opening, Figure 5-20 A indicates that the flow has air entrained in it with the density ranging between 300 kg/m^3 and 600kg/m^3.

Figure 5-20 B shows the flow pattern in the physical model for the 30% gate opening.
At 40% as seen in Figure 5-21 A/B, there is damming of flow upstream from the ski jump and the density of the water still varies between 400 kg/m^3 and 800 kg/m^3 meaning that there is still a significant amount of air entrapped in the flow. This damming is not a hydraulic jump since the flow was found to be supercritical throughout the conduit. The pressurized flow issues from the emergency gate at high velocities and the velocities decrease due to friction losses as the flow goes down the conduit with increased flow area. At the end of the horseshoe conduit, the conduit area reduces causing the flow depth to increase before the flow is discharged at the ski jump. This situation causes damming upstream of the ski jump.

For gate openings of 30% and for larger openings, there is minimal circulation of air at the 8 degree (second) bend however there is some circulation above the ski jump. For larger openings the conduit flows fuller and less air is entrained in the flow.

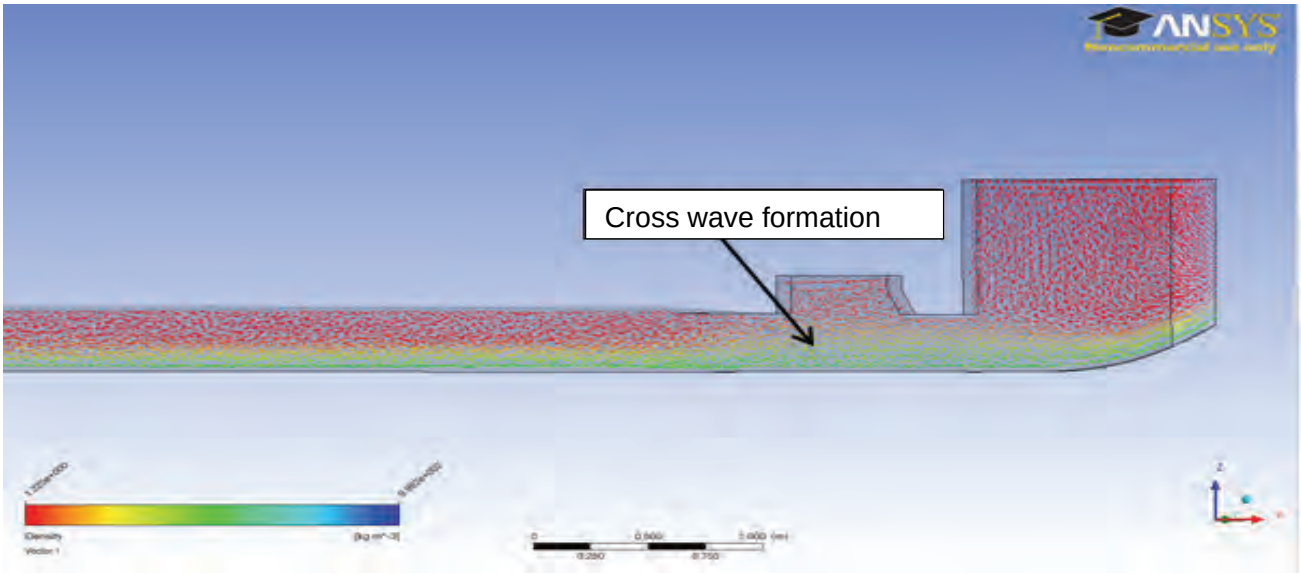

Figure 5-19 A: Velocity vectors at the ski jump for 20% emergency gate opening

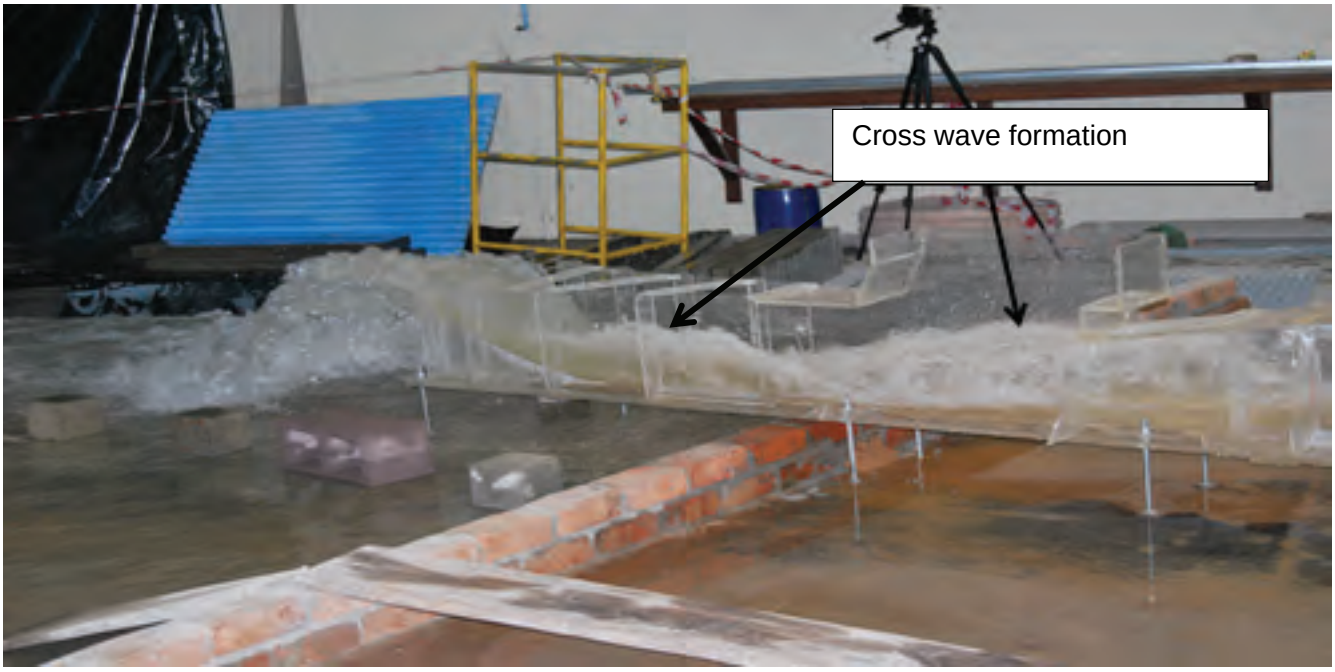

Figure 5-19 B: Flow pattern at ski jump and end box for 20% emergency gate opening

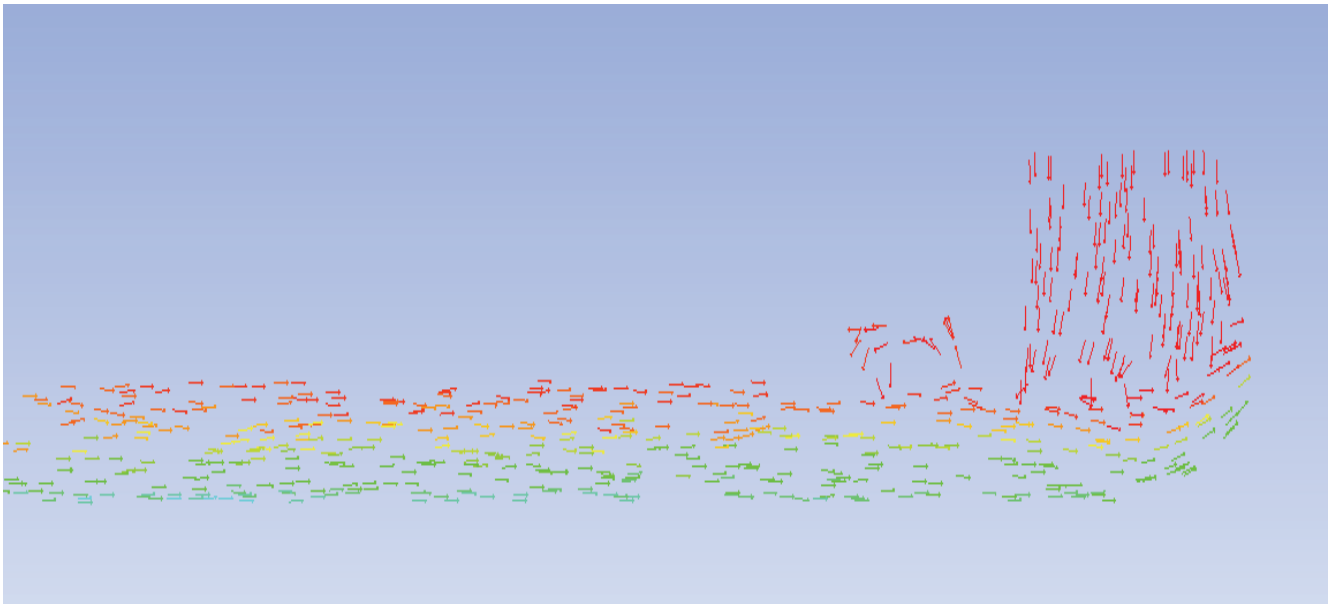

Figure 5-20 A: Velocity vectors at the ski jump for 30% emergency gate opening

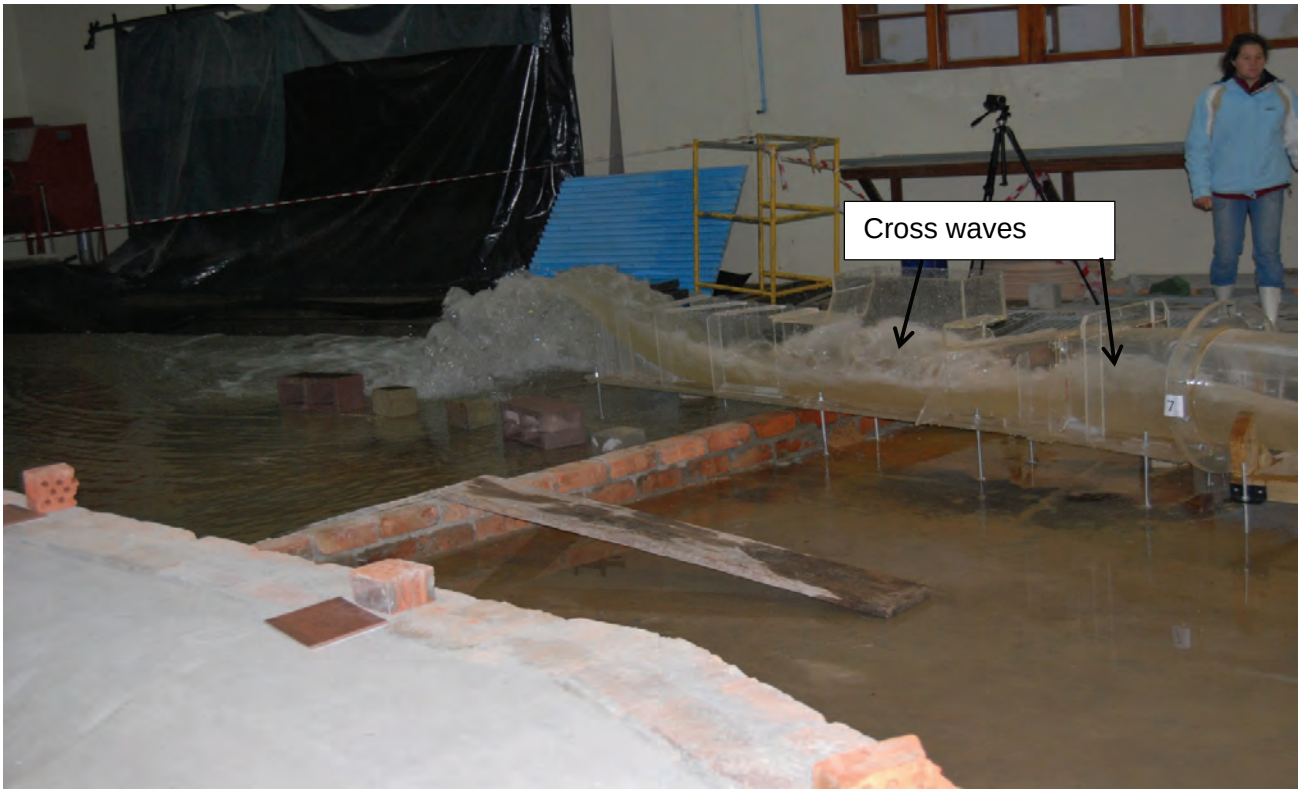

Figure 5-20 B: Flow pattern at ski jump and end box for 30% emergency gate opening

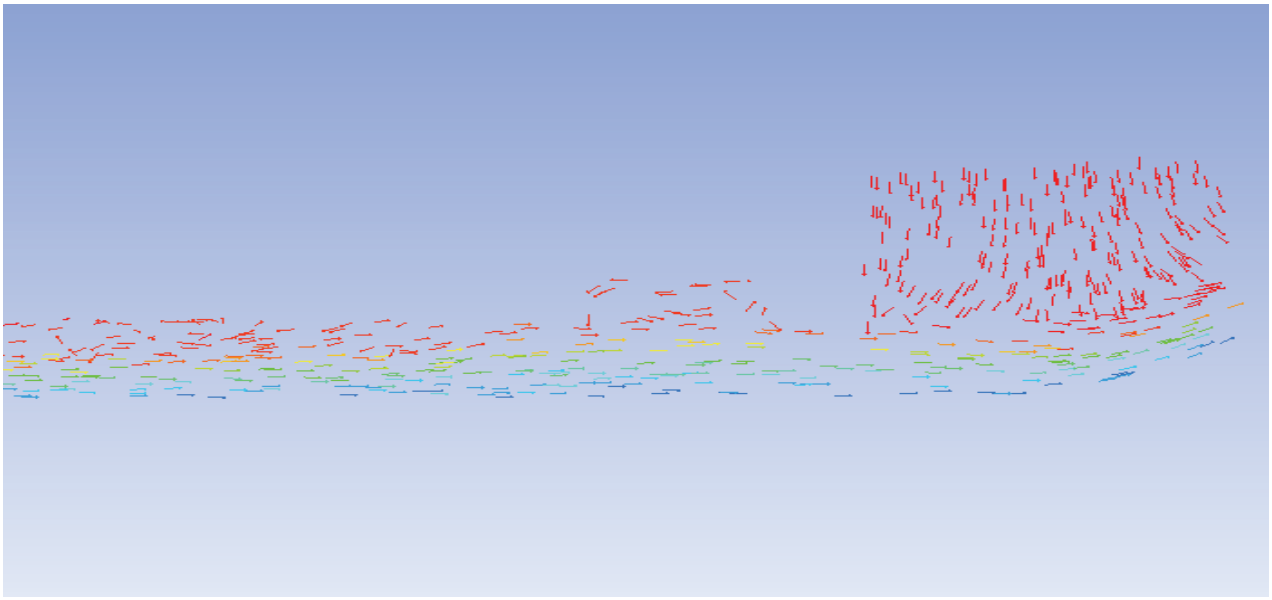

Figure 5-21 A: Velocity vectors at the ski jump for 40% emergency gate opening

Figure 5-21 B: Flow pattern at ski jump and end box for 40% emergency gate opening

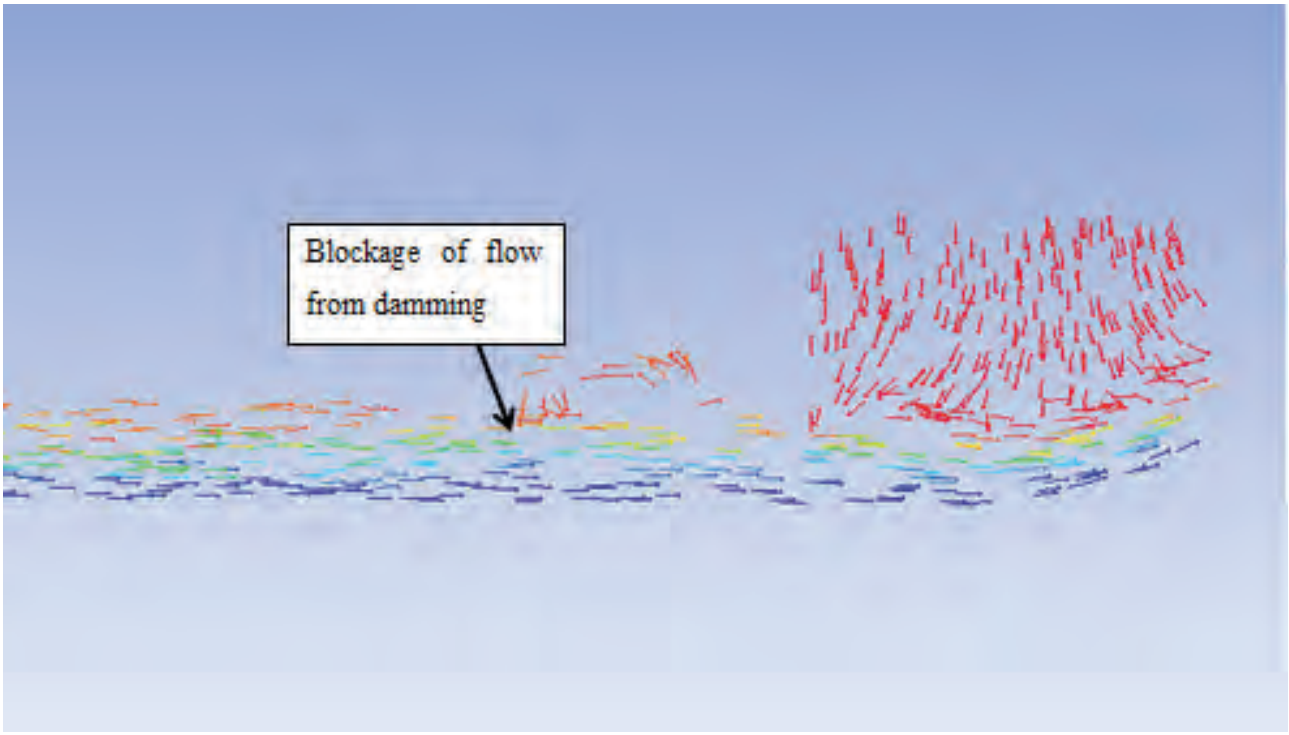

Figure 5-22 A: Velocity vectors at the ski jump for 50% emergency gate opening

Figure 5-22 B: The ski jump for 50% emergency gate opening (Physical)

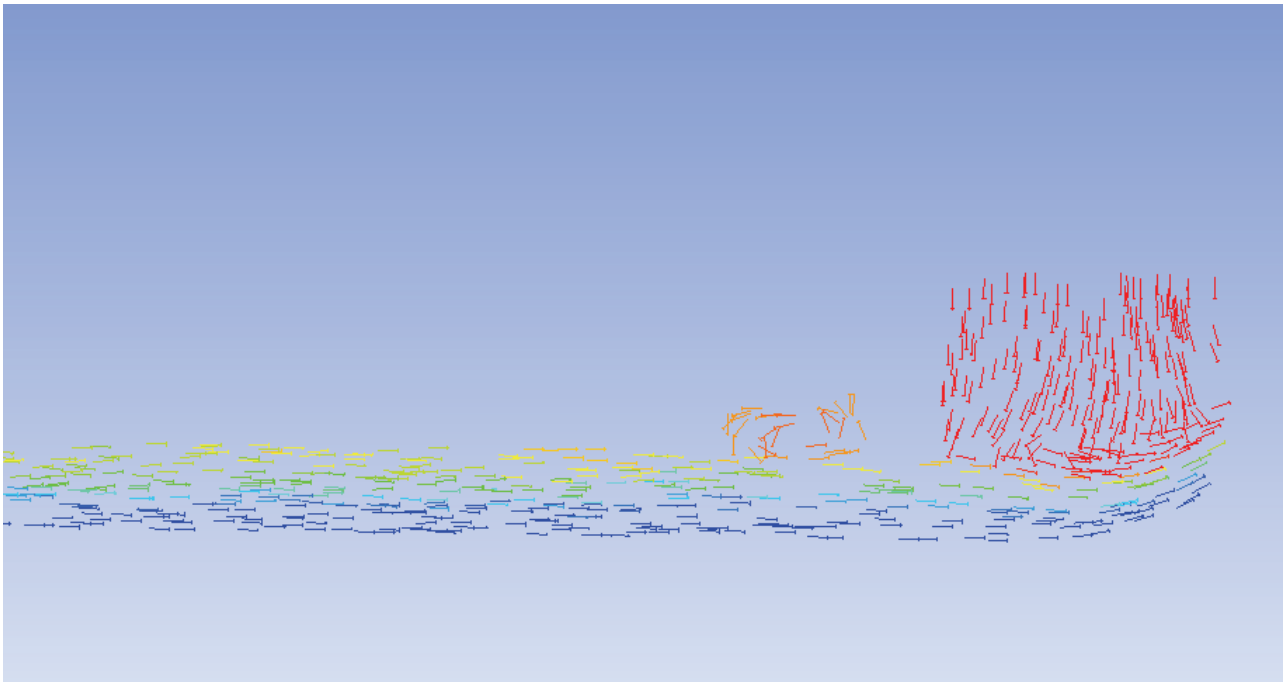

Figure 5-23 A: Velocity vectors at the ski jump for 60% emergency gate opening (numerical)

Figure 5-23 B: The ski jump for 60% emergency gate opening (Physical)

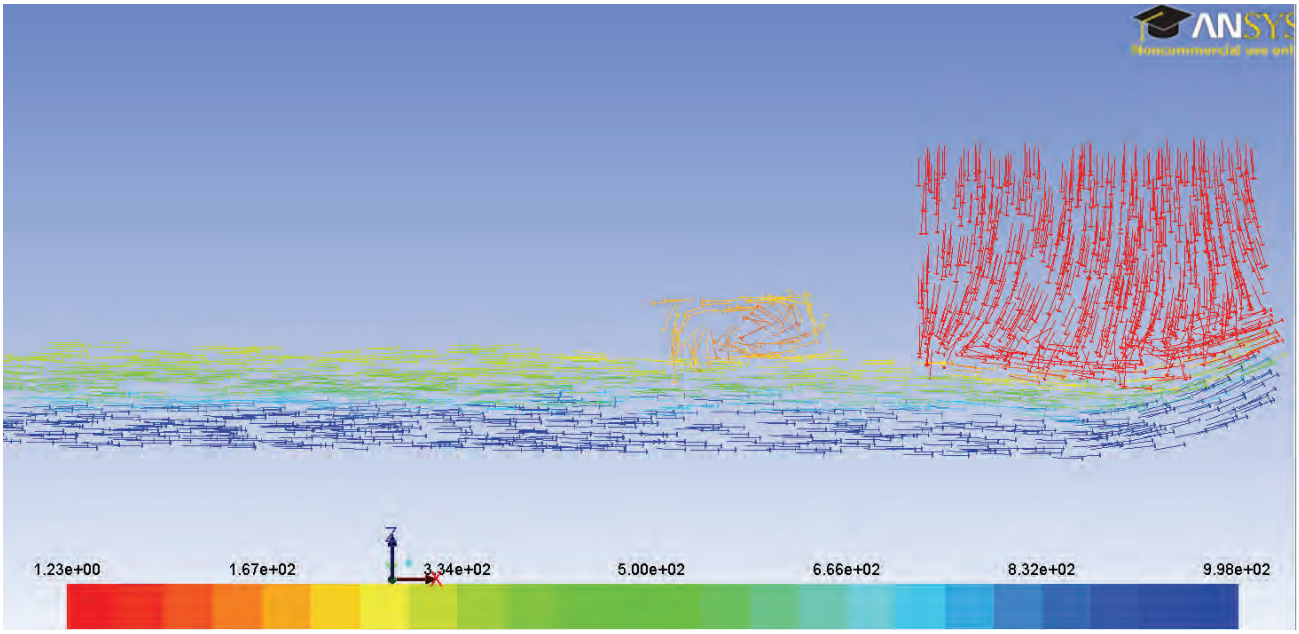

Figure 5-24 A: Velocity vectors at the ski jump for 70% emergency gate opening

Figure 5-24 B: The ski jump for 70% emergency gate opening (Physical)

Visually, from the colour coding, for the 50% gate opening (Figure 5-22 A) and onwards, the flow appears to have less air entrained in it and the pipe still appears to be flowing partially full with the most air trapped at the surface of the flow. The flow seems to block the smaller cross-section after

the last bend and upstream of the ski jump, at the beginning of the end box due to the narrowing of the pipe (Figure 5-22 A/B) which causes a contraction to the flow of air and water.

For 60% and 70% emergency gate openings (Figure 5-23 A and 5-24 A), the pipe appears to be flowing full downstream of the emergency gate, with densities ranging from 500 kg/m^3 to 998.2 kg/m^3. There is, however, still air entrained in the flow as can be seen from the varying densities (yellow and green representing the air-water mix and blue representing water). The conduit is flowing full and there is circulation of air above the flow on the ski jump.

5.1.5 Pressure Contours in Domain

Figure 5-25 below shows the contours of pressures developed in the domain for the 20% emergency gate opening. Other figures for the different gate openings have not been included because they look exactly the same as the one below but the differences are in the values of the results generated.

The pressure varies from 4 m of water at the bottom of the reservoir (represented by red) and 0.2 m of water at the top of the reservoir (represented by light green).

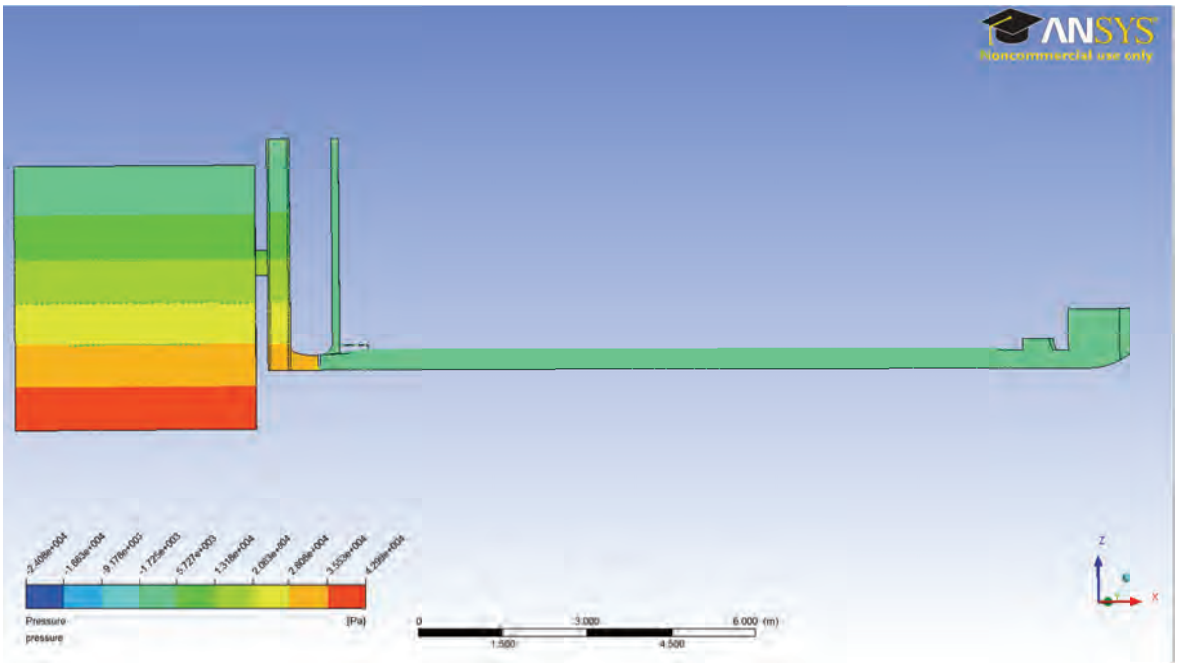

Figure 5-25: Static pressure contours for 20% emergency gate opening

These very coarse pressure contours (Figure 5-25) indicate that the pressures in the reservoir and the wet well are the same, the highest pressure being experienced at the bottom of the reservoir. However, as the flow issued underneath the emergency gate, the pressures began to vary further on in the conduit although this is not evident in the caption because the contours are too coarse.

At 20% emergency gate opening, downstream of the emergency gate, along the length of the conduit, pressures vary between 0.176 m below and 1.346 m above gauge pressure (numerical model values). Since the initial condition for pressure in the model was set to atmospheric pressure, values of pressure below zero were taken as being below atmospheric pressure.

At 30% emergency gate opening, the pressures in the conduit vary between 0.517 m below and 1.116 m above gauge pressure (numerical model values), with the negative pressures being experienced mainly downstream of the emergency gate and at the floor of the ski jump.

At 40% emergency gate opening, negative pressures in the order of 0.26 m below gauge pressure (numerical model values) were modelled downstream of the emergency gate and 1.059 m above gauge pressure (numerical model values) further on in the conduit up to the ski jump for the given conditions.

At 50% emergency gate opening the pressures downstream on the floor of the conduit vary between 0.38 m below and 0.976 above gauge pressure (numerical values). Negative pressures are also shown on the floor of the ski jump which is surprising as this is a concave surface.

For the 60% emergency gate opening the pressures on the floor of the conduit vary between 0.328 m below and 1.01 m above gauge pressure(numerical model values) and for the 70% emergency gate opening the pressures vary between 0.325 m below and 2 m above atmospheric pressure (numerical model values).

5.1.6 Pressure Contours at the Emergency Gate and Air Vent Region

The following figures display the pressure contours in the region of the emergency gate at the base of the air vent where connects to the conduit for gate openings of 20%, 30%, 40%, 50%, 60% and 70%. It should be noted that the colour scales for the pressures shown in Figures 5-26 to 5-31 below are not consistent.

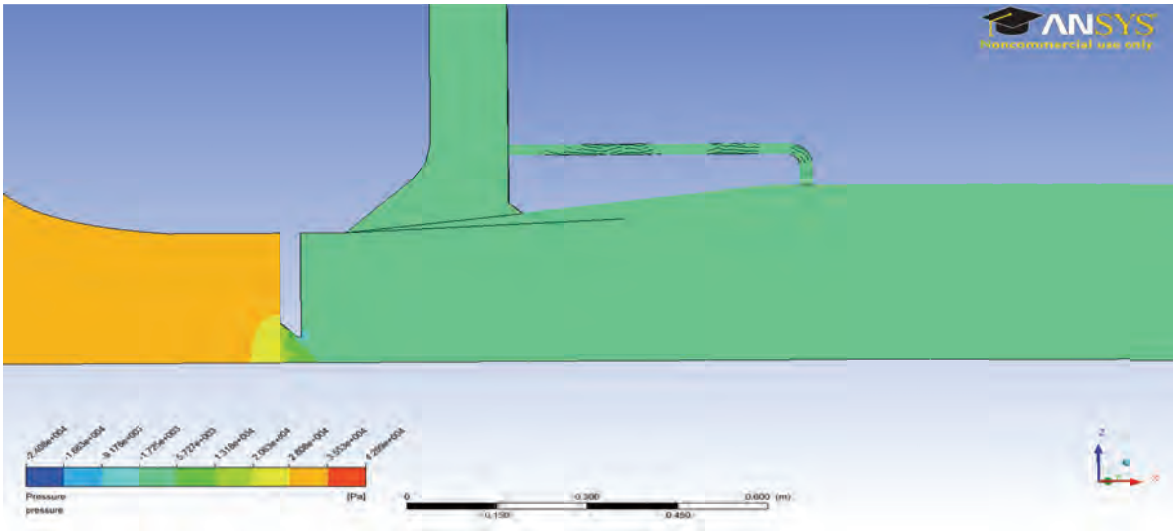

Figure 5-26: Static pressure contours at emergency gate and air vent region for 20% emergency gate opening

The numerical results of the simulation showed that negative pressures develop at the downstream side of the gate lip.

For the 20% emergency gate opening, shown in Figure 5-26, pressures of up to 0.176 m below gauge pressure (numerical model values) were observed on the gate lip.

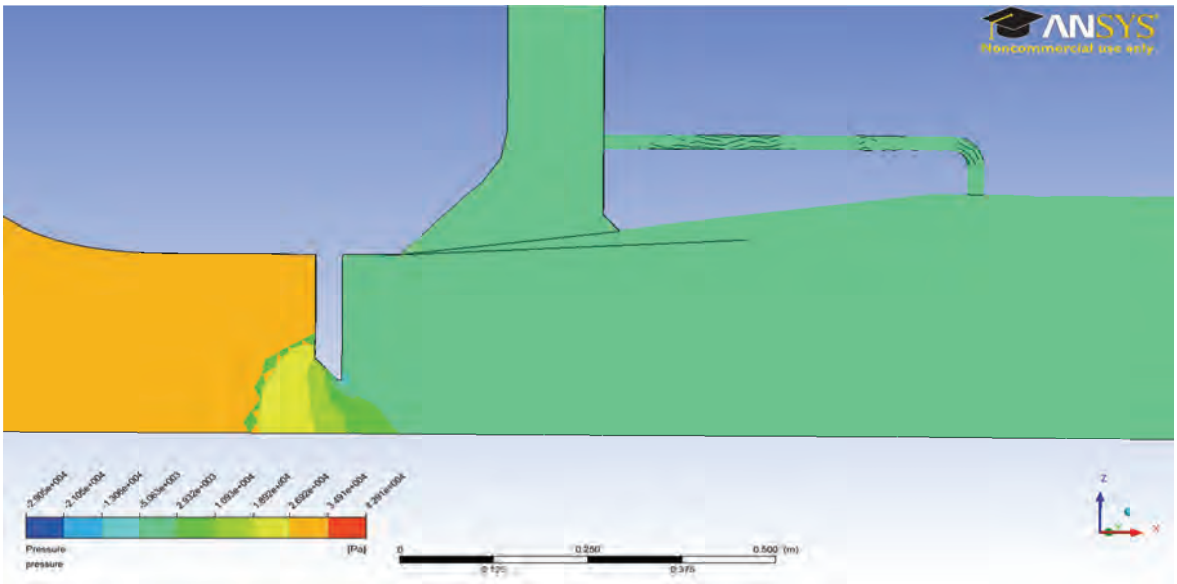

Figure 5-27: Static pressure contours at emergency gate and air vent region for 30% emergency gate opening

At 30% emergency gate opening, shown in Figure 5-27, there were no negative pressures shown upstream of the emergency gate but pressures of up to 0.52 m below gauge pressure were shown on the downstream side of the gate lip.

At 40% emergency gate opening, as seen in Figure 5-28 below, pressures of up to 0.267 m below gauge pressure were shown on the downstream side of the gate lip.

At 50% emergency gate opening, as seen in Figure 5-29 below, pressures of up to 0.38 m below gauge pressure were observed on the downstream side of the gate lip.

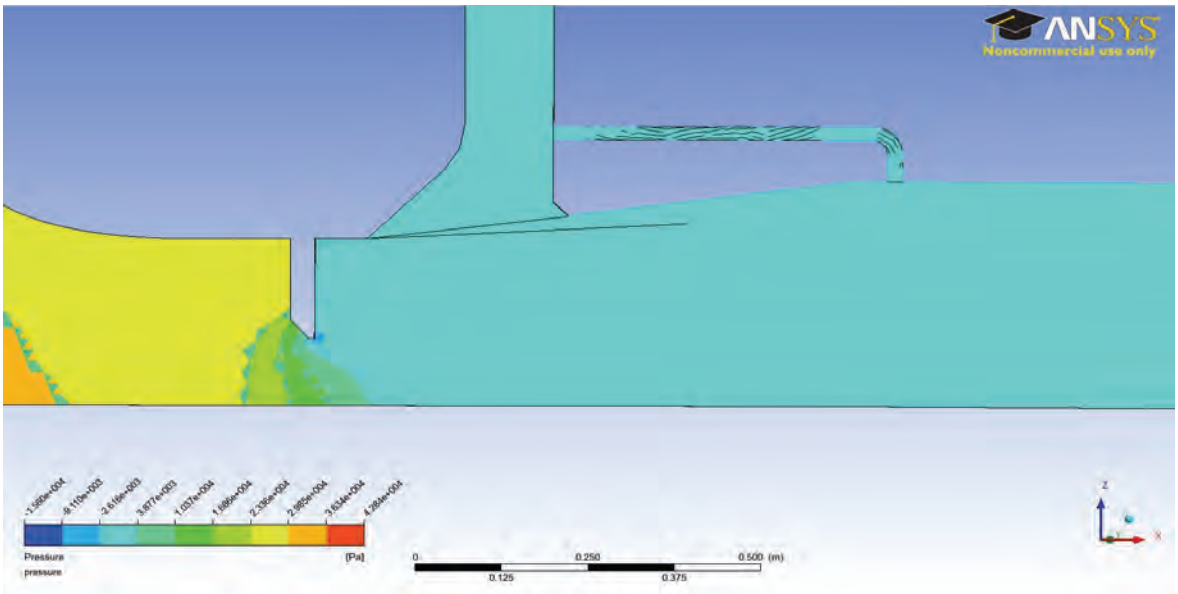

Figure 5-28: Static pressure contours at emergency gate and air vent region for 40% emergency gate opening

The pressure contours shown in Figure 5.26 to 5-31 show how the pressures reduce from the upstream to the downstream of the emergency gate.

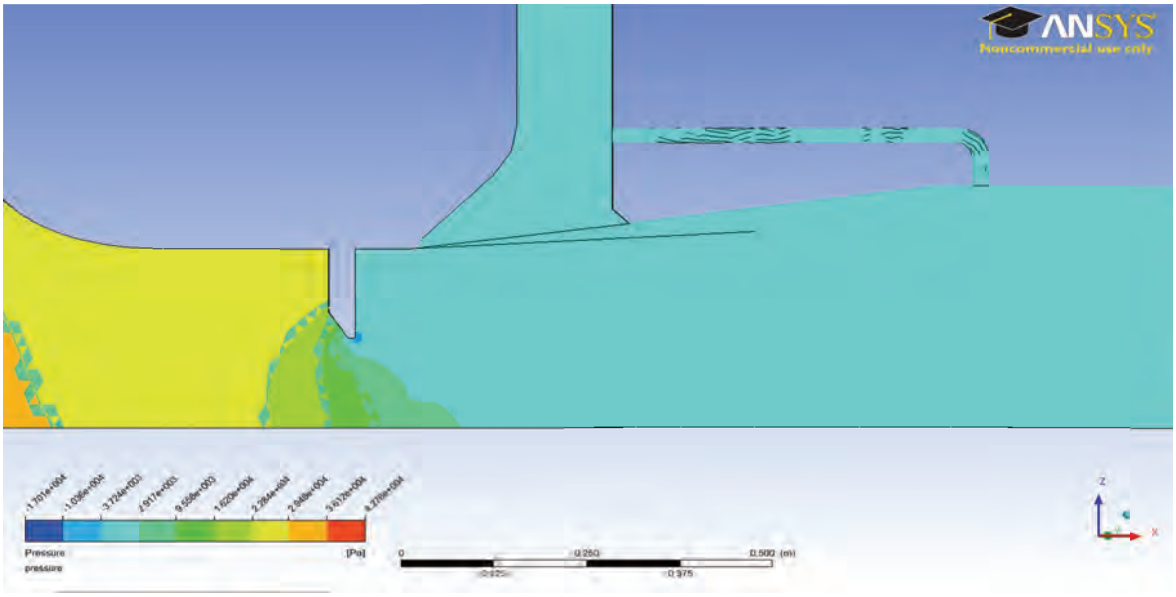

Figure 5-29: Static pressure contours at emergency gate and air vent region for 50% emergency gate opening

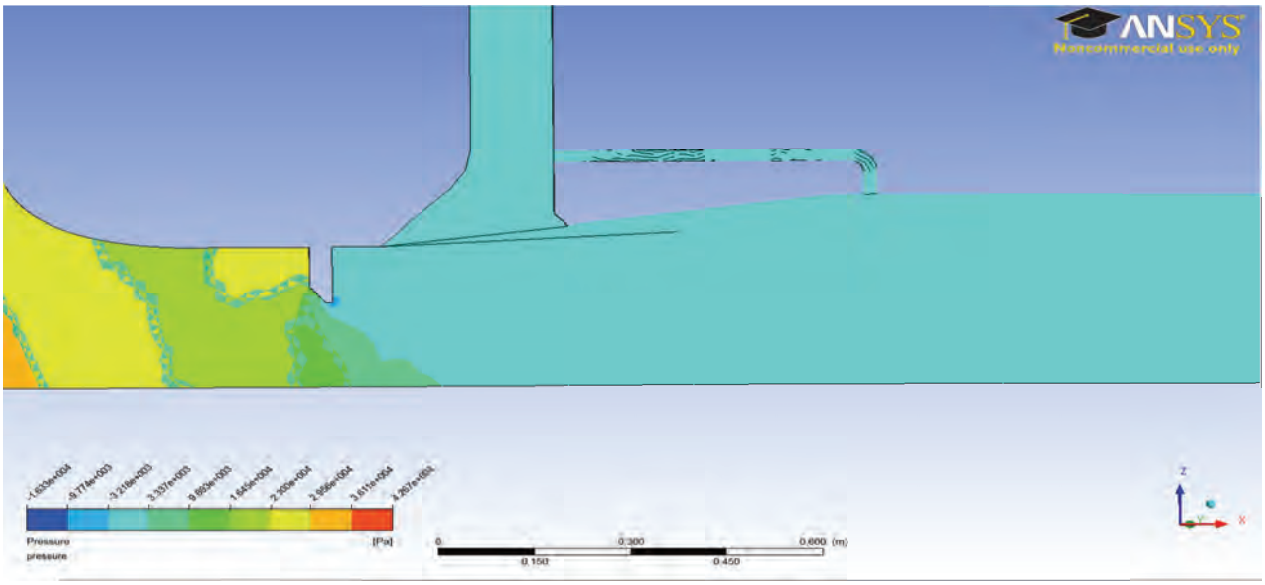

Figure 5-30: Static pressure contours at emergency gate and air vent region for 60% emergency gate opening

At 60% emergency gate opening, as seen Figure 5-30 above, pressures of 0.33 m below gauge pressure were shown on the downstream side of the gate lip and as mentioned in Section 5.1.5, negative pressures were shown to occur further downstream in the conduit.

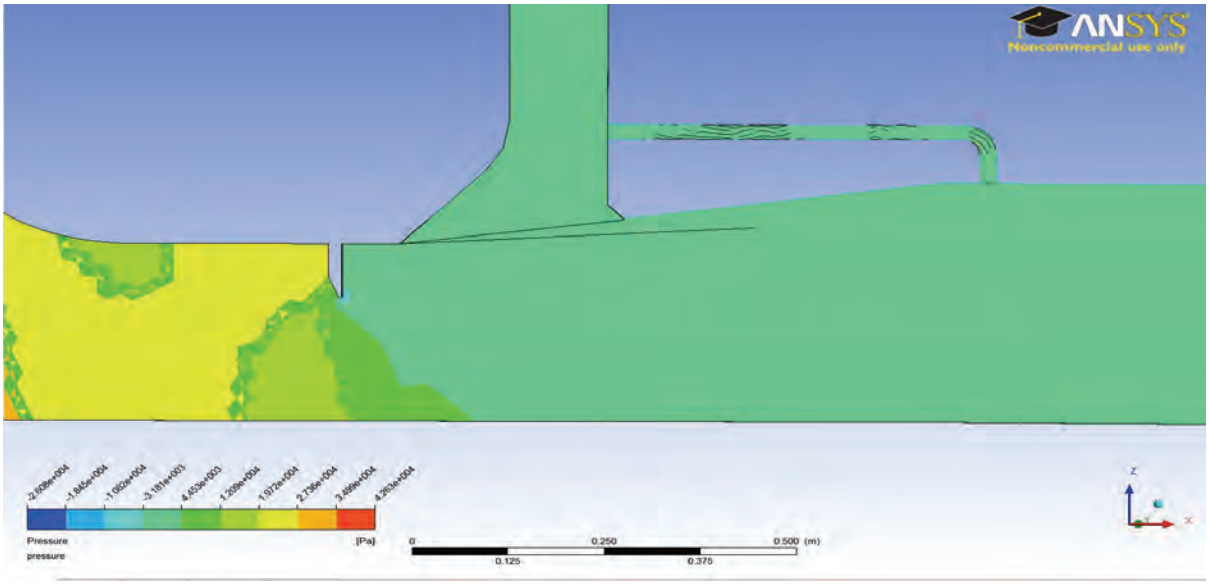

Figure 5-31: Static pressure contours at emergency gate and air vent region for 70% emergency gate opening

At 70% emergency gate opening, negative pressures up to 0.325 m below atmospheric pressure (numerical values) were determined at the downstream end of the gate lip although these are not shown on Figure 5-31.

Table 5-1 below summarises the gate lip pressures determined for the various emergency gate openings.

Table 5-1: Simulated negative pressures at the emergency gate lip

Emergency gate opening (%)	Pressure at gate lip (m)
20	-0.176
30	-0.520
40	-0.467
50	-0.380
60	-0.330
70	-0.325

Figure 5-32 below graphs the negative pressures for the various gate openings.

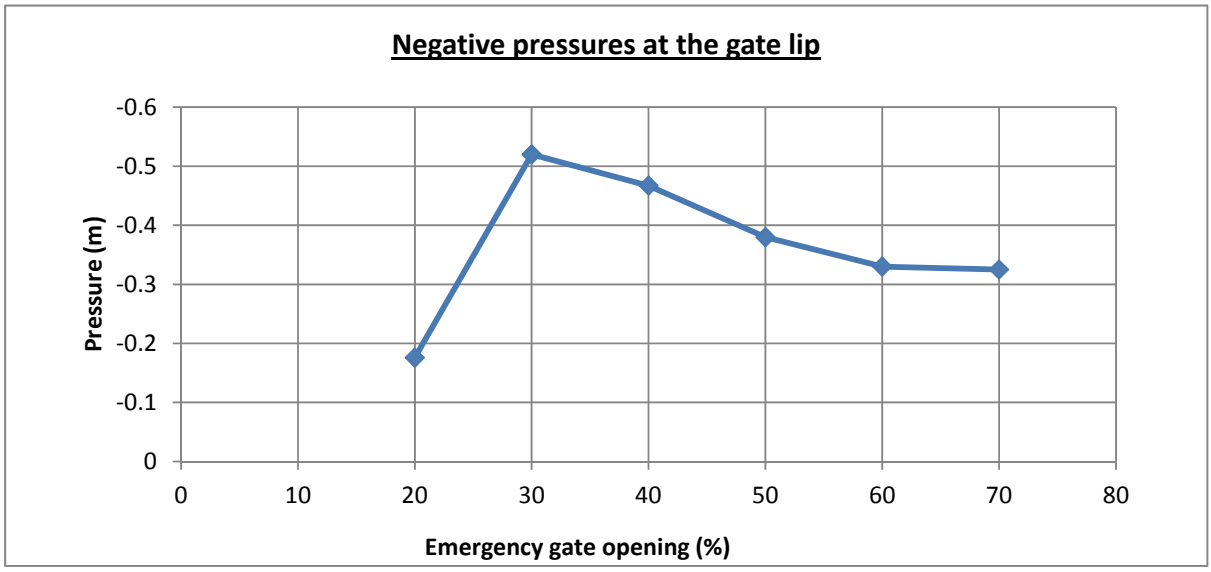

Figure 5-32: Plot of negative pressures at the emergency gate lip for different gate openings (Note: Magnitude of negative pressures is considered)

Borodina (1969) suggests that negative pressures lips reduce with increasing gate opening since the amount of air entrained in the water decreases as the discharge increases. The conduit begins to flow full. Figure 5-32 above, indicates that this is the case but however, the negative pressure for the 20% emergency gate opening is not consistent with Borodina's hypothesis. There is no explanation for the inconsistent pressure for the 20% emergency gate opening but it might be safe to conclude that emergency gate openings below 30% are critical. Such pressures at the gate lip might cause adverse cavitation effects if they are less than atmospheric pressure, however, this would not be the case for the prototype.

Gate openings less than 20% could not be tested on the physical model for fear of damage to the model, as had been experienced before in previous tests of the model.

5.1.7 Streamlines

The following figures display the velocity streamlines for static gate openings of 20%, 30%, 40%, 50%, 60% and 70%. The streamlines show the progression of the flow in the domain.

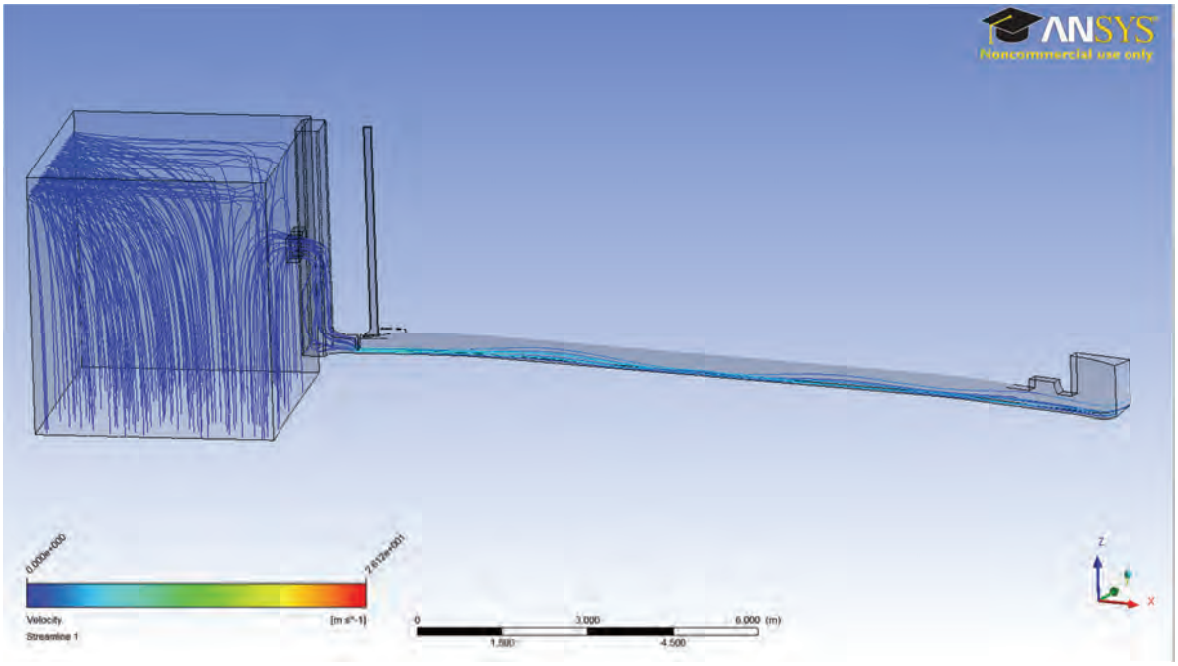

Figure 5-33: Velocity streamlines for 20% emergency gate opening

The streamlines originating from the bottom of the reservoir upward show how the reservoir fills up from the bottom.

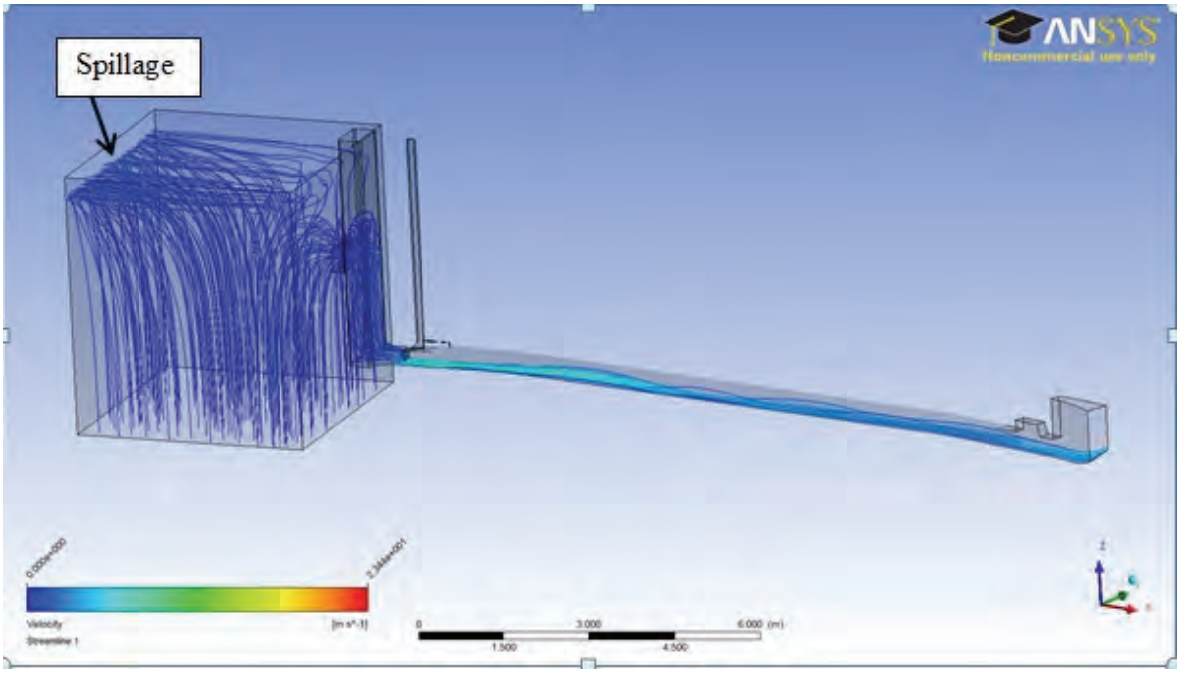

Figure 5-34: Velocity streamlines for 30% emergency gate opening

As expected (Figures 5-33 to 5-38), the number of streamlines increases with increasing emergency gate openings due to the increase in discharge. Also, there is increased swirling flow as the flow fills up in the wet well tower due to the increase in flow through the selector gates.

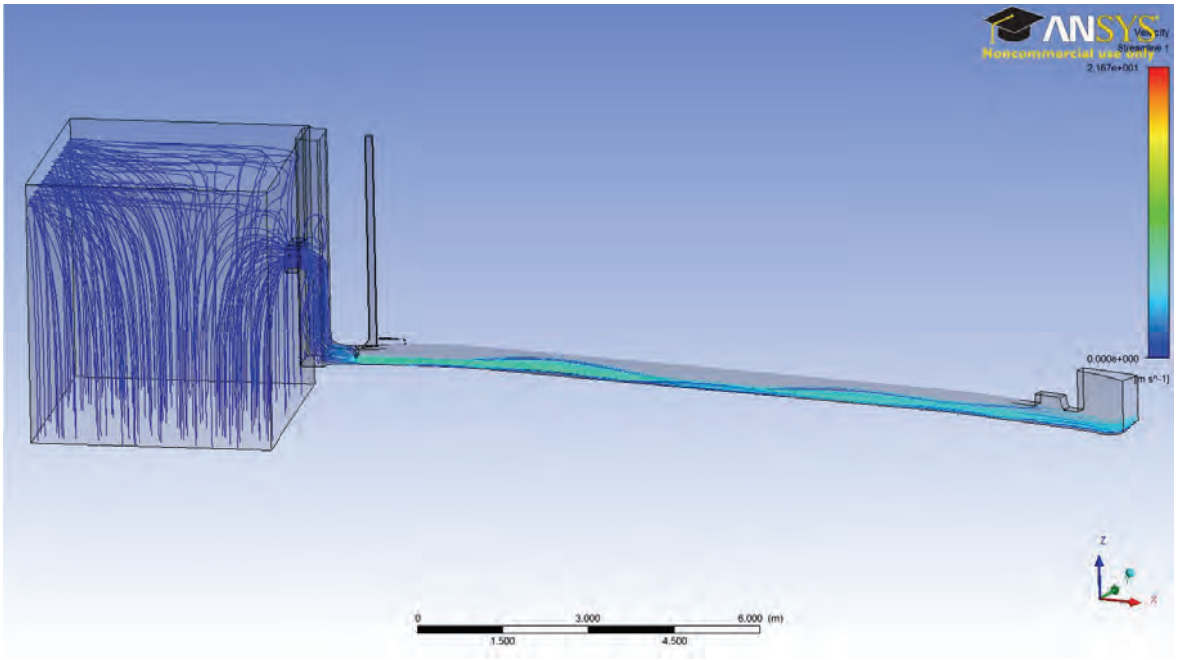

Figure 5-35: Velocity streamlines for 40% emergency gate opening

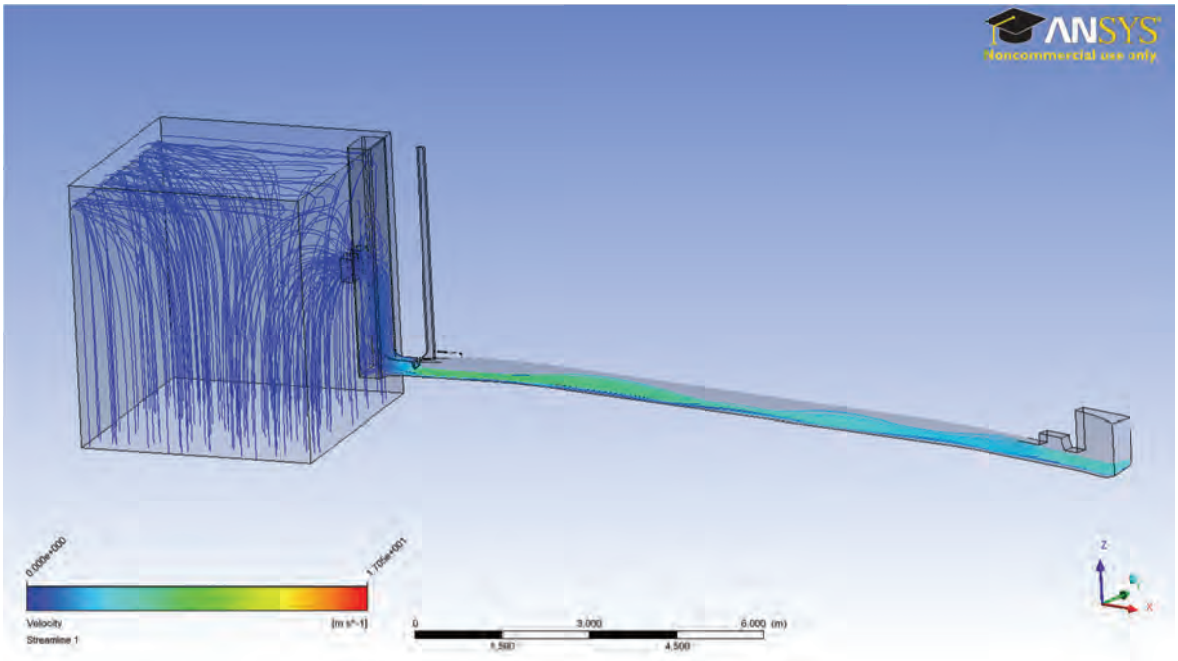

Figure 5-36: Velocity streamlines for 50% emergency gate opening

The figures also show the high velocities of the water at the emergency gate and the reduced velocities as it flows through the conduit. This may be attributed to the variation in flow area.

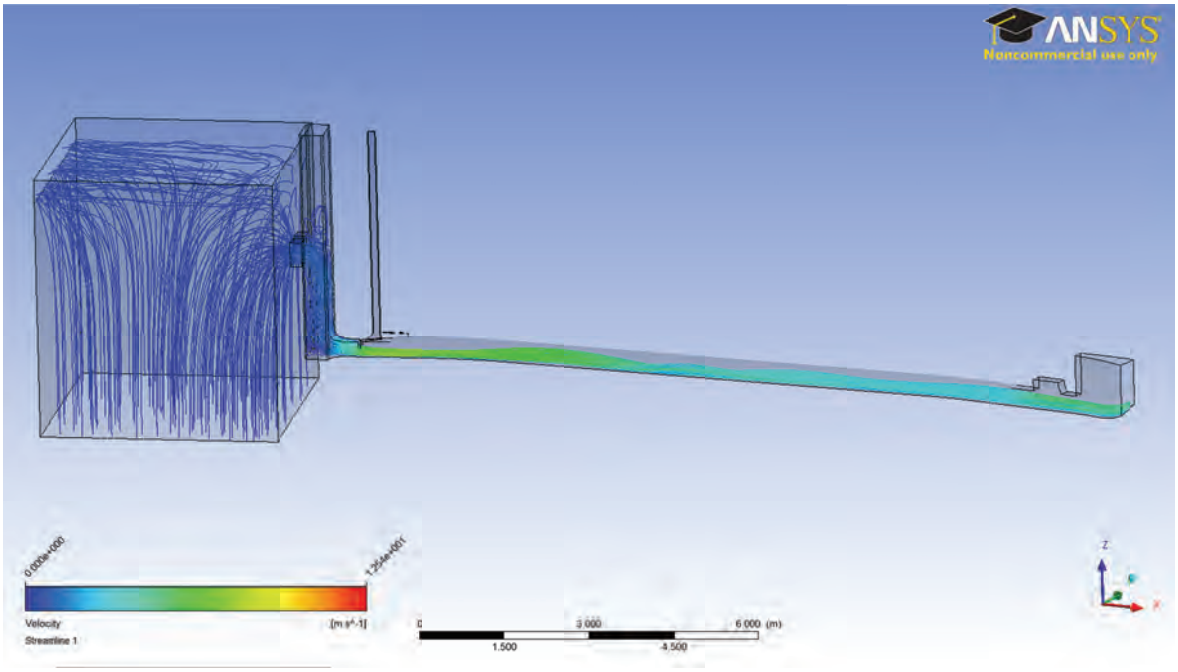

Figure 5-37: Velocity streamlines for 60% emergency gate opening

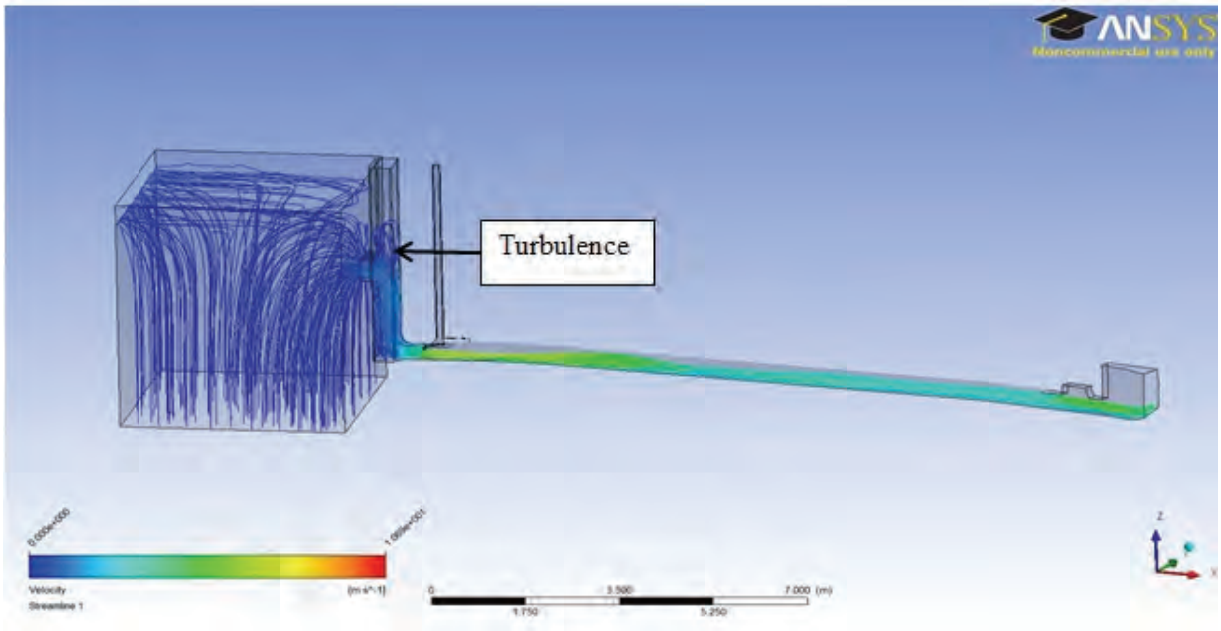

Figure 5-38: Velocity streamlines for 70% emergency gate opening

5.1.8 Flow Patterns at the Bends

The figures below show the velocity vectors, coloured by density, at the first bend (12 degrees) downstream of the emergency gate and at the second bend (8 degrees) upstream of the radial gate housing for the various emergency gate openings.

The figures also show the nature of flow in the wet well tower above. For some gate openings it was possible to see the swirling effect of the flow in the tower.

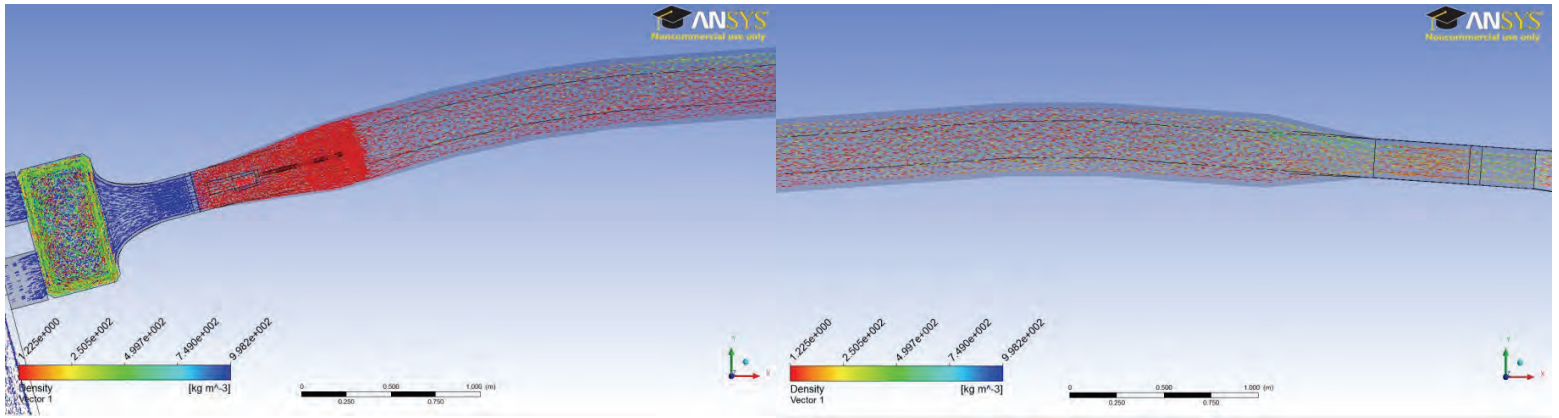

Figure 5-39: Plan view of velocity vectors at bends and wet well for 20% emergency gate opening

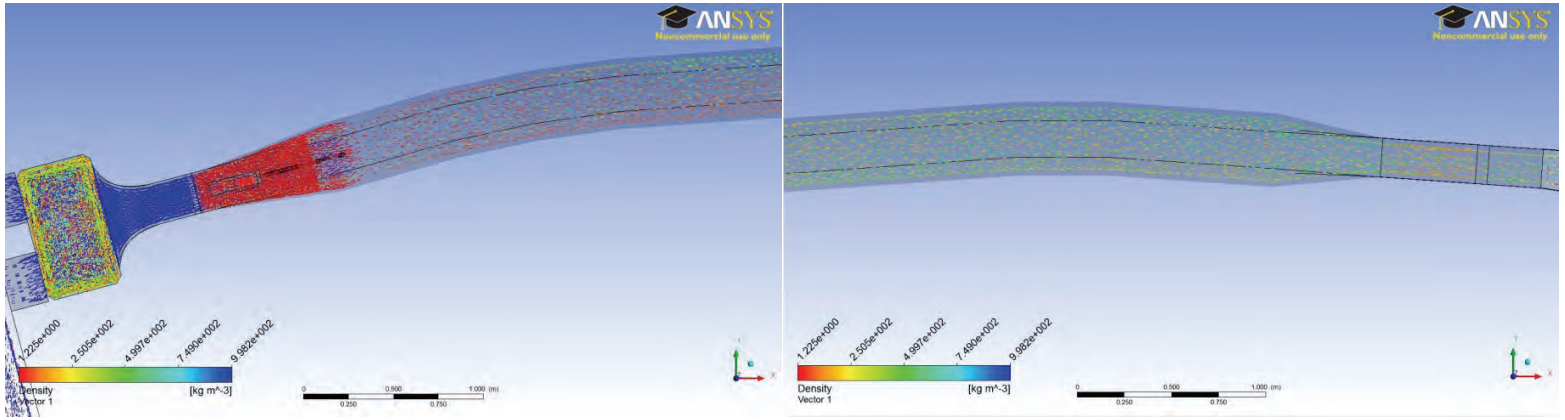

Figure 5-40: Plan view of velocity vectors at bends and wet well for 30% emergency gate opening

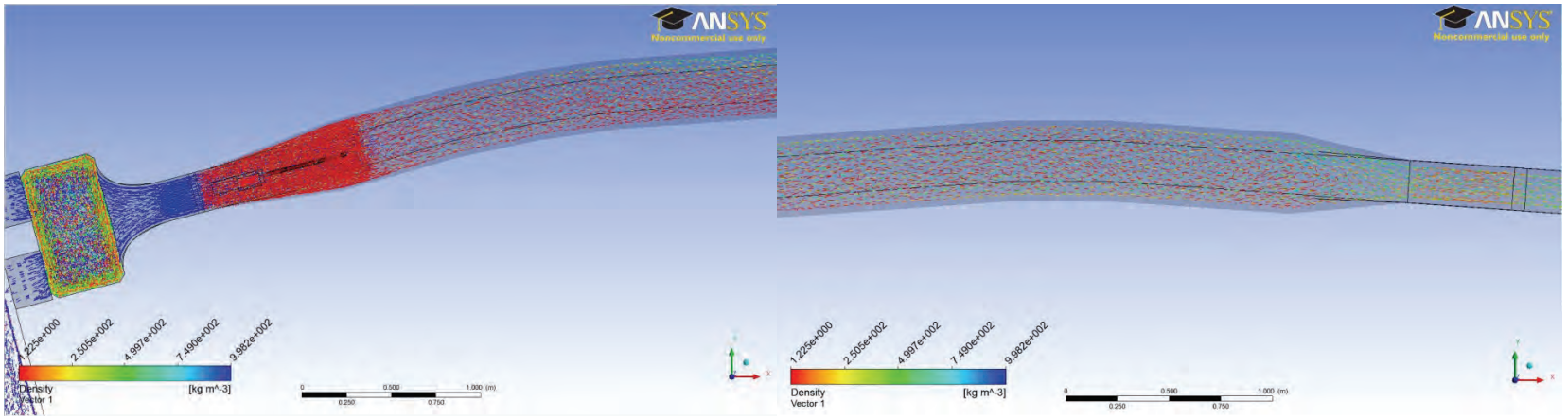

Figure 5-41: Plan view of velocity vectors at bends and wet well for 40% emergency gate opening

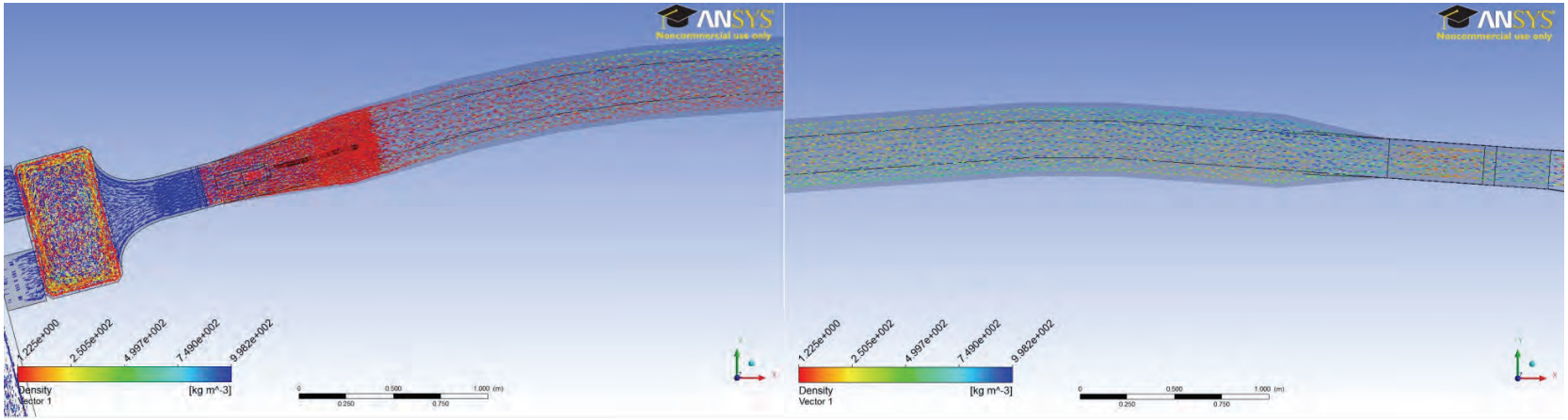

Figure 5-42: Plan view of velocity vectors at bends and wet well for 50% emergency gate opening

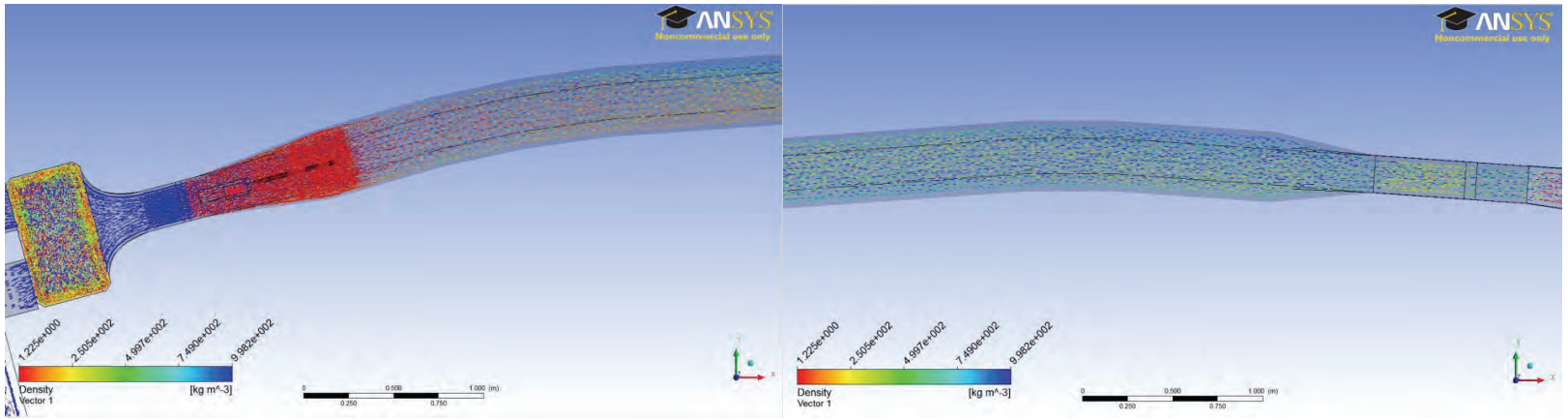

Figure 5-43: Plan view of velocity vectors at bends and wet well for 60% emergency gate opening

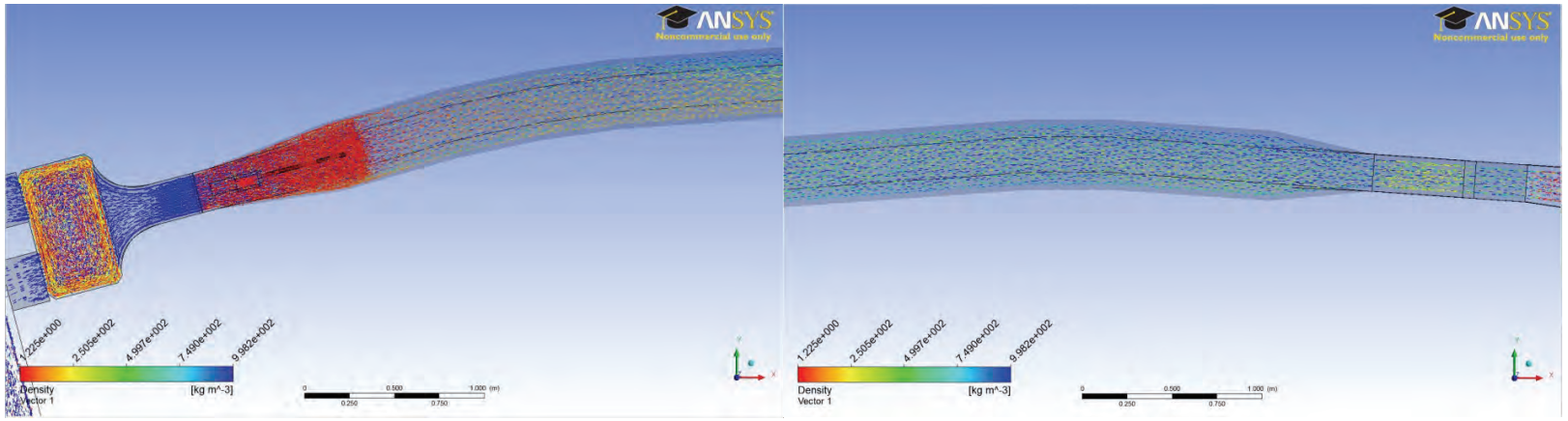

Figure 5-44: Plan view of velocity vectors at bends and wet well for 70% emergency gate opening

The purpose of showing the flow at the bends was to establish whether they influenced the nature of the flow in the conduit.

At 20% and 30% emergency gate openings, Figures 5-39 and 5-40 the results showed that the first and second bends introduced slight changes in flow density possibly on account of the super elevation and cross waves that would occur.

For gate openings of 40% and more (Figures 5-41 to 5-44), the flow across the bends appeared undisturbed. There was damming of highly aerated flow at different parts of the conduit that could be mistaken for a hydraulic jump it was established that the flow in the outlet structure was supercritical. The fluid in the wet well was shown to be rotational and swirly. Such behaviour of the flow could contribute to the formation of vortices that are known to entrap a lot of air (Borodina, 1969). From the animations created of the simulations, no vortices were observed in the wet well but there was horizontal rotational flow on the surface of the water in the tower.

5.2 Graphical and Tabulated Results

5.2.1 Discharge

For the CFD numerical model, the discharge into the wet well from the reservoir was determined by placing three velocity point monitors at the selector gates at the entrance to the wet well and the average of these results used to determine the discharge. The same method was also used to determine the discharge at the emergency gate. Results showed that there were unexpected differences in the obtained values although steady state had been attained. The results are shown in Table 5-2 below and graphically represented in Figure 5-45

Table 5-2: Comparison of discharges from the numerical and the physical model

CFD Numerical model results								(1)	(2)
Emergency gate opening (%)	**Emergency gate velocity (m/s)**	**Emergency gate area (m²)**	**Emergency gate discharge (m³/s)**	**Selector gate velocity (m/s)**	**Selector gate area (m²)**	**Selector gate discharge (m³/s)**	**Physical model discharge (m³/s)**	**Percentage discharge error at Emergency gate (%)**	**Percentage discharge error at selector gates (%)**
20	8.13	0.01	0.10	0.50	0.24	0.12	0.070	30	42
30	7.56	0.02	0.14	0.75	0.24	0.18	0.107	23	41
40	7.99	0.02	0.20	0.90	0.24	0.22	0.141	28	35
50	6.49	0.03	0.20	1.05	0.24	0.25	0.170	15	33
60	6	0.04	0.22	1.50	0.24	0.36	0.203	8	44
70	5.79	0.04	0.25	1.74	0.24	0.42	0.240	4	43

(1) CFD Emergency gate discharge and Measured Physical model discharge:

$$100 \times \left(\frac{CFD\ Emergency\ gate\ discharge - Measured\ Physical\ model\ discharge}{CFD\ Emergency\ gate\ discharge}\right)$$

(2) CFD Selector gates discharge and Measured Physical model discharge:

$$100 \times \left(\frac{CFD\ Selector\ gates\ discharge - Measured\ Physical\ model\ discharge}{CFD\ Selector\ gates\ discharge}\right)$$

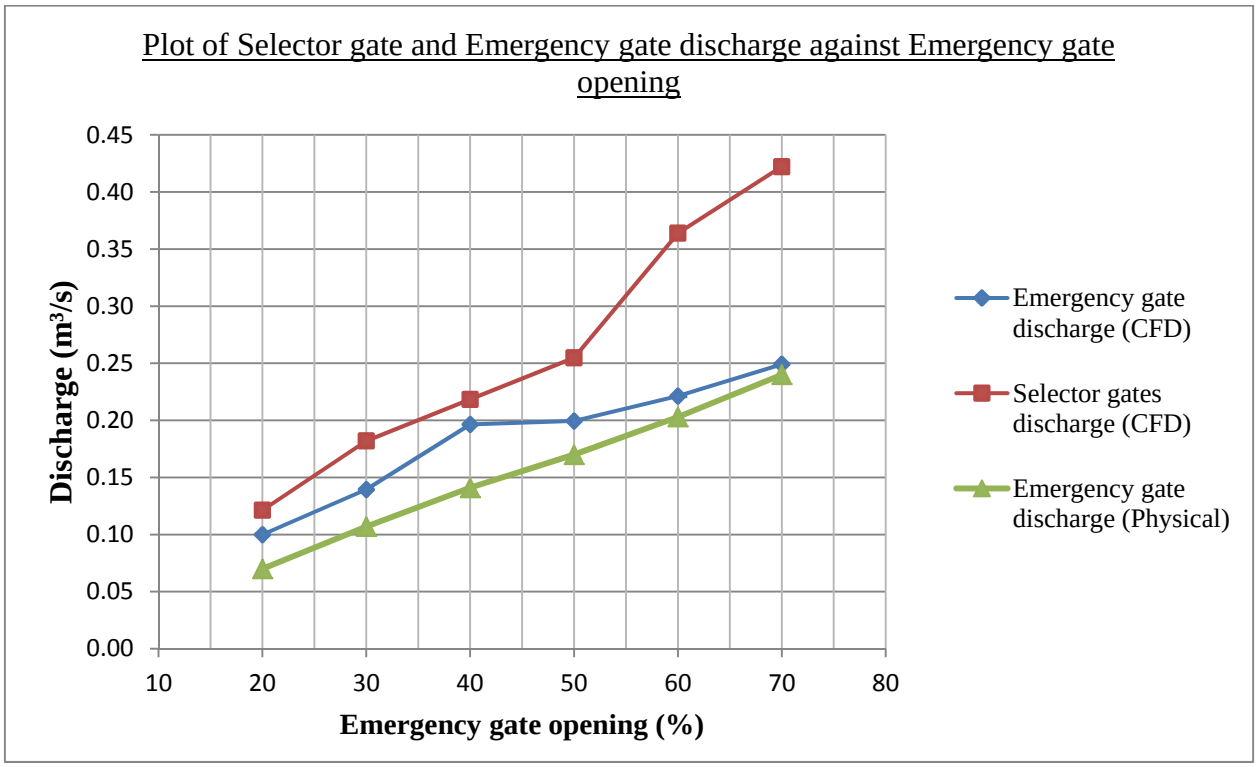

Figure 5-45: Discharge through selector and emergency gate

Whereas as the trend in results is similar (Figure 5-45), there are significant differences in discharge results especially for the CFD selector gate discharge and the measured emergency gate discharge. It is not certain why there are such large differences in the CFD discharge results at the selector gates and the emergency gate of the CFD model since mass balance was attained before results were extracted from the simulations. A viable excuse would be the errors and uncertainties of CFD modelling as explained in Section 3.3 (Veersteg et al., 2007). The CFD results also differ from the measured discharge results probably due to errors in measurement of the flows in the physical model. However, the numerical results for the emergency gate discharge are closer to those from the physical model.

The CFD emergency gate discharge results were chosen for comparison to the physical and empirical calculated results because they were closer to those for the physical model which was used as a validation instrument in the research. Also, flow discharge underneath the gate directly affected the air discharge downstream of the emergency gate.

5.2.2 Air Entrainment

Results for the discharge, air velocity in the air vent, and aeration demand, from the CFD model were compared to those from the physical model and also to those generated from the empirical formulae for gate openings in bottom outlet structures based on the literature review cited above. Tables 5-3 and 5-4 show the air velocities determined for the CFD model and the physical model respectively.

Table 5-3: Air velocities in the air vent from the CFD model

Emergency gate opening (%)	Emergency gate discharge (m^3/s)	Emergency gate velocity (m/s)	Emergency gate discharge (m^3/s)	Air vent velocity (m/s)	Air vent area (m^2)	Air vent discharge (m^3/s)	Aeration ratio (β)	Contracted flow depth (m)	Froude number, Fr
20	0.0999	8.13	0.0999	23.4100	0.0091	0.2130	2.1312	0.0330	14.2978
30	0.1394	7.56	0.1394	21.5600	0.0091	0.1961	1.4072	0.0494	10.8556
40	0.1964	7.99	0.1964	20.1500	0.0091	0.1833	0.9333	0.0659	9.9360
50	0.1994	6.49	0.1994	15.7800	0.0091	0.1436	0.7198	0.0824	7.2186
60	0.2213	6	0.2213	11.5300	0.0091	0.1049	0.4741	0.0989	6.0921
70	0.2491	5.79	0.2491	9.9200	0.0091	0.0902	0.3623	0.1154	5.4428

Table 5-4: Air velocities in the air vent from the physical model

Emergency gate opening (%)	Emergency gate discharge (m^3/s)	Emergency gate velocity (m/s)	Air vent velocity (m/s)	Air vent area (m^2)	Air vent discharge (m^3/s)	Aeration ratio (β)	Contracted flow depth (m)	Froude number, Fr
20	0.070	5.6948	4.2550	0.0091	0.0387	0.5530	0.0330	10.0151
30	0.107	5.8032	5.5050	0.0091	0.0501	0.4681	0.0494	8.3330
40	0.141	5.7354	1.8770	0.0091	0.0171	0.1211	0.0659	7.1323
50	0.170	5.5321	3.1160	0.0091	0.0283	0.1668	0.0824	6.1531
60	0.203	5.5049	1.2500	0.0091	0.0114	0.0560	0.0989	5.5895
70	0.240	5.5785	0.2000	0.0091	0.0018	0.0076	0.1154	5.2440

In the empirical calculation, the discharge had to be determined first and then used to establish the air velocities in the air vent unlike in the numerical and physical models where the discharge was known. Table 5-5 shows the empirical calculations described before.

able 5-5: Air velocities in the air vent from empirical calculations

Emergency gate opening (%)	Prototype emergency gate opening (m)	Scaled head on emergency gate (m)	Scaled gate opening (m)	Emergency gate discharge (m^3/s)	Emergency gate velocity (m/s)	Contracted flow depth (m)	Froude number (F)	Aeration ratio (β)	Air vent velocity (m/s)
20	0.76	2.825	0.054	0.055	4.515	0.033	7.940	0.362	2.205
30	1.14	2.798	0.081	0.083	4.480	0.049	6.433	0.257	2.329
40	1.52	2.771	0.108	0.109	4.444	0.066	5.527	0.199	2.387
50	1.9	2.744	0.135	0.135	4.408	0.082	4.903	0.162	2.405
60	2.28	2.717	0.162	0.161	4.372	0.099	4.439	0.135	2.398
70	2.66	2.690	0.189	0.187	4.336	0.115	4.076	0.116	2.372

The CFD model results, the measured physical model results and the empirical results are compared in the figures below. Figure 5-46 plots the discharge through the emergency gate; Figure 5-47 plots the velocity in the air vent and Figure 5-48 plots the aeration ratios.

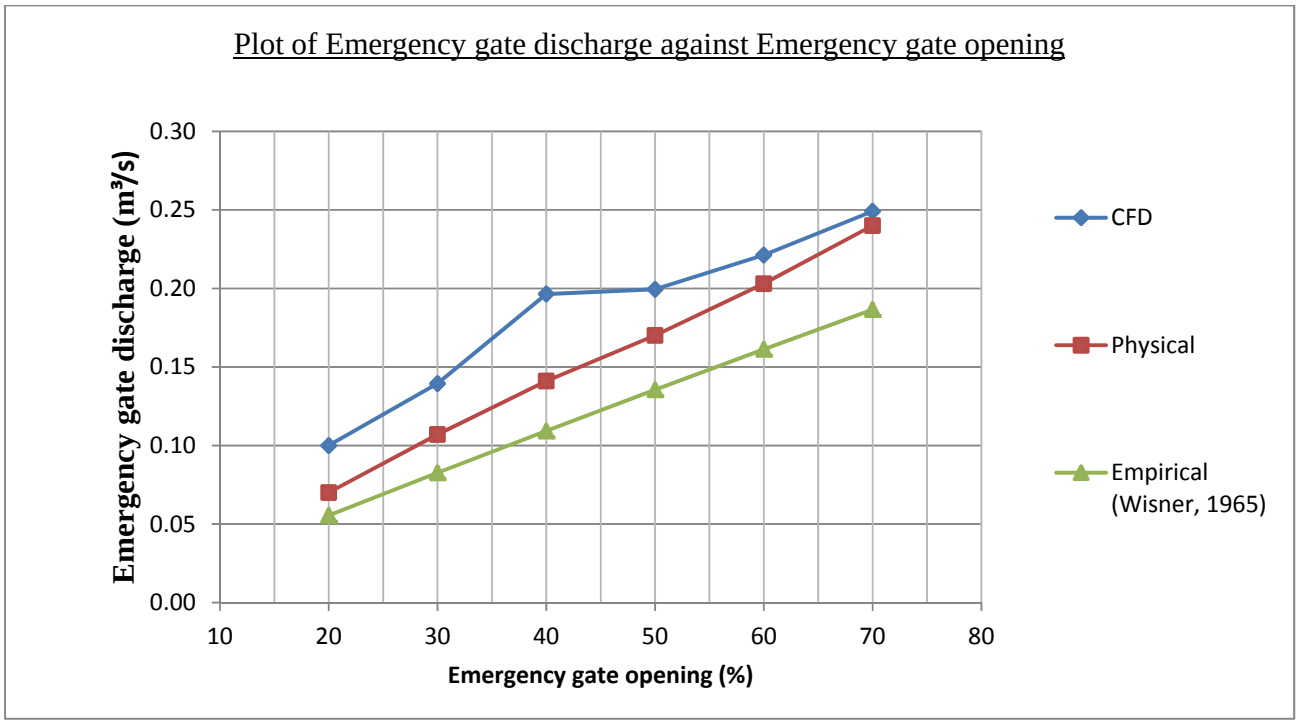

Figure 5-46: Discharge of the flow for different emergency gate openings

Figure 5-46 shows that the trend in results of the CFD model is similar to that for the physical model and the empirical calculations. However, the CFD model indicates higher results. These variations may be attributed to the errors and uncertainties common to most CFD models (Veersteg et al., 2007).

Figure 5-46 also shows that he discharge increases with increasing emergency gate opening, but did not vary with time since simulations were for steady state. The CFD discharge results compared more closely with the physical model results for emergency gate openings larger than 50% whereas the empirical results compared better for gate openings less than 50%.

Figure 5-47 compares air flows in the air vent as determined with the CFD model, measured in the physical model and calculated empirically.

For the CFD model air flows in the air vent were determined from the velocity calculated at three locations in the mid-section of the air vent. The average of these velocities results was used for comparison with those from the physical model and calculated empirical.

The air velocity in the physical model was determined by placing an anemometer in the mid-section of the air vent which digitally sensed and recorded the air velocities. However, the anemometer was not able to record the direction of air flow so this was monitored by placing a piece of plastic sheet in the mid-section of the air vent which blew upward or downward depending on the direction of air flow.

Figure 5-47 below shows the air velocities in the air vent for the CFD model, the physical model and the empirical calculations.

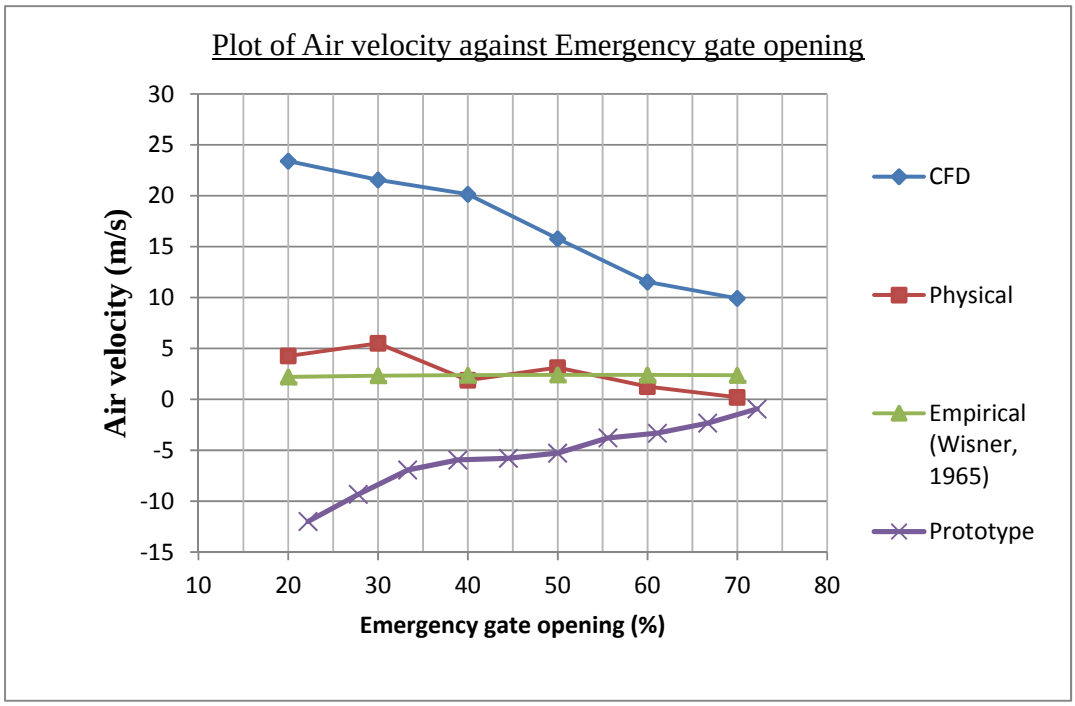

Figure 5-47: Air velocity in air vent for different emergency gate openings (Note: Positive velocity indicates air flow into the model)

In Figure 5-47, it can be seen that there is great variation in the air velocity values from the numerical model and those from the physical model despite the similar trend. The variation in values is probably partially due to the higher discharges from the numerical model. The air velocity decreases with increasing gate opening which implies that the aeration demand decreases with increasing gate opening. This is understandable because as the emergency gate openings increase, the pipe begins to flow full and there is less air entrained in the flow. It should be noted that in all cases (CFD and physical models), air was sucked into the air vent and not blown out as was the case with the prototype. The release of air from the prototype

occurred under dynamic gate closure conditions when the reservoir was not full. The prototype results adjusted by scale factor for the physical model as also plotted on Figure 5-47

Based on cited literature that quotes an air velocity limitation of 45 m/s for prototype values, the CFD model would render the air vent inadequate for all emergency gate openings below 50%, since the prototype velocities would be quite higher than the said values for these gate openings.

The graph below shows the aeration demand of the flow for the CFD model, physical model and empirical calculations (Wisner, 1965).

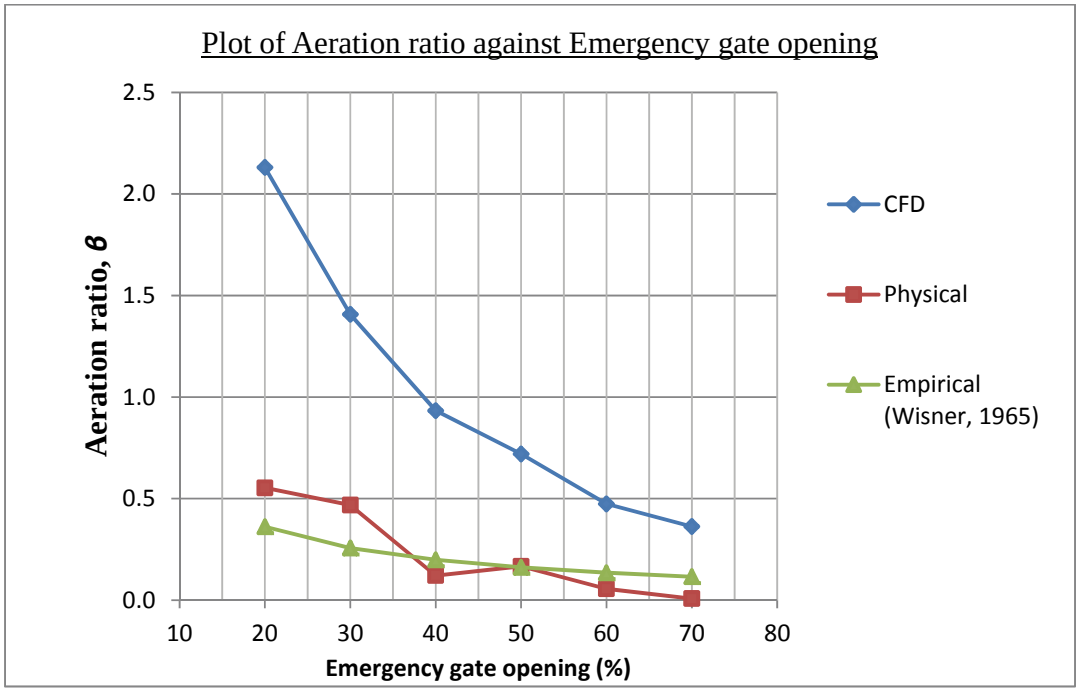

Figure 5-48: Aeration demand for the different emergency gate openings (Note: β = Qa/Qw where Qa is the air discharge and Qw is the water discharge at the emergency gate)

The aeration demands determined from the CFD model are much higher than those measured in the physical model and those determined by the empirical calculations. However, they all appear to follow the same trend with the demand decreasing with increasing emergency gate openings. Thus, the smaller the gate opening the greater the amount of air sucked into the conduit downstream of the emergency gate.

The results from the CFD model where compared to those from a previous research project by Najafi et al. (2007) on the numerical simulation of air-water flow in gated tunnels. Figure 5-49 below shows a graph extracted from the research paper.

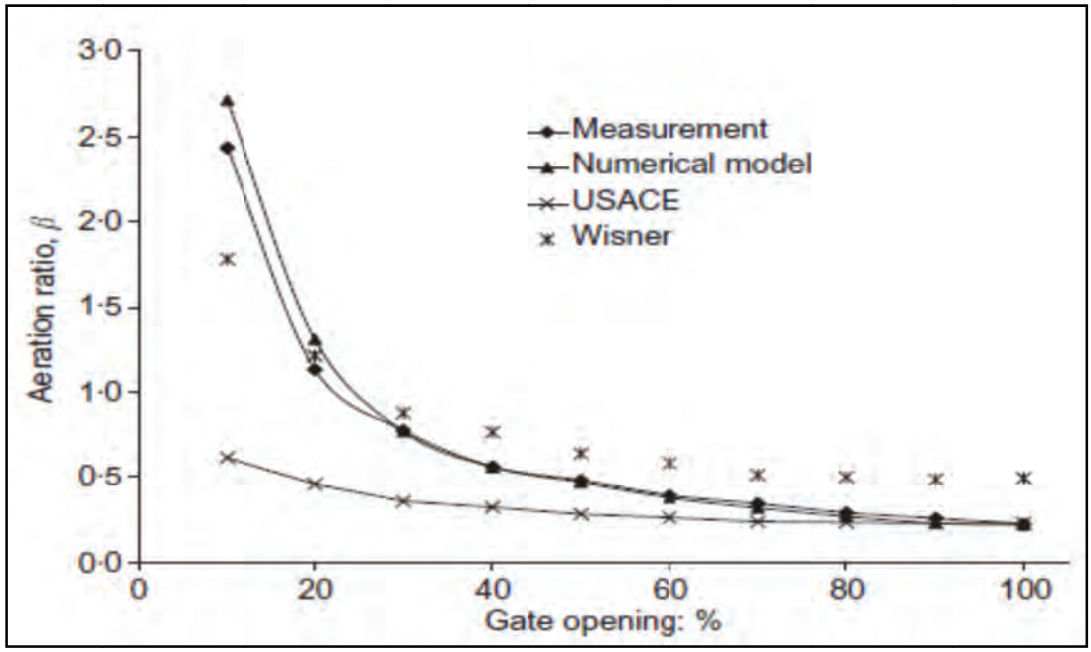

Figure 5-49: Aeration demand from research by Najafi et al. (2007).

The results from the research work follow a similar trend as those for the CFD model described above with differences of course since the models are not geometrically the same. The research study entailed a 1:17 scaled numerical and physical model and only the section of emergency gate was studied. This is another important validation that shows that the CFD modelling of the Berg River Dam provided similar results to those of another research project.

5.2.3 Froude Number

The flow velocities through the emergency gate for all gate openings shown in the Tables 5-3, 5-4 and 5-5 above were used to establish and the Froude number, thus confirming the nature of the flow.

The Froude number was calculated using the formula common for rectangular sections seen below.

$$Fr = V/(gy)^{1/2}$$

Where,

V is the flow velocity at the vena contracta

y is the water depth at the vena contracta

Figure 5-50 below shows the Froude numbers determined for the CFD model, the physical model and those calculated empirically.

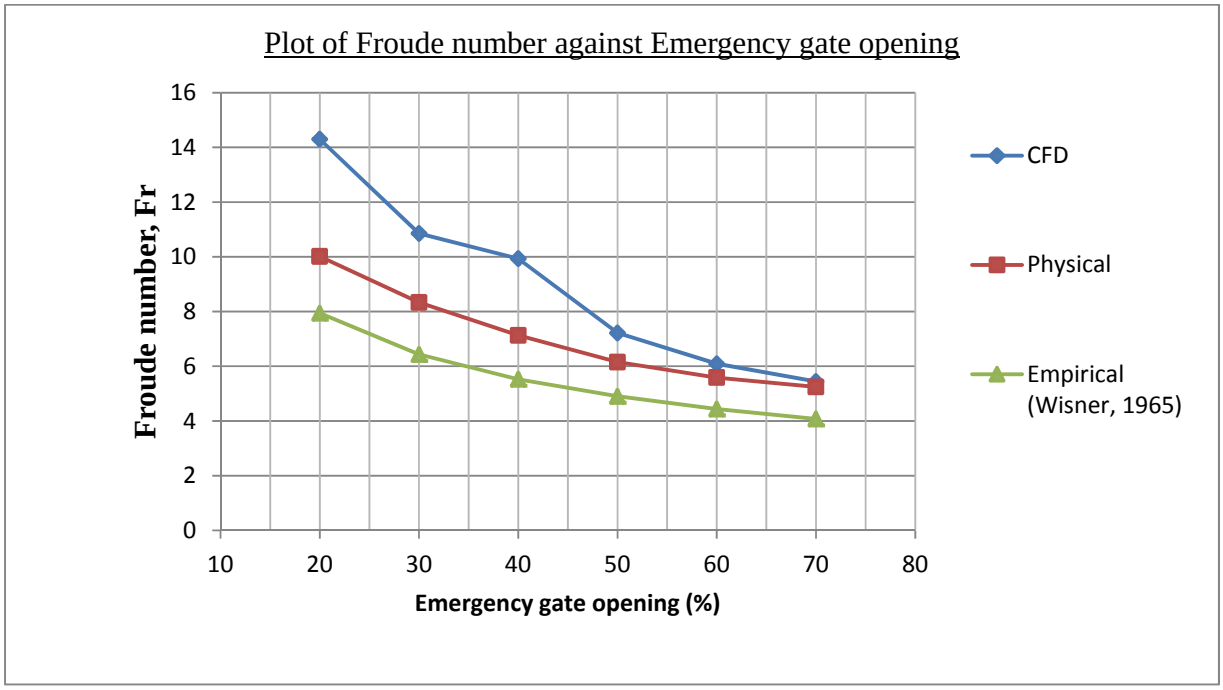

Figure 5-50: Plot of Froude number at the emergency gate

Froude number plotted in Figure 5-50 closely follow the same trend and also confirm supercritical flow since all values are greater than 1.

It was noticed that as the flow downstream progressed in the conduit structure, highly aerated damming of fluid in the conduit was observed at 50% and 60% gate openings. These masses resembled hydraulic jumps, so in order to determine whether any hydraulic jump was actually formed in the conduit, the Froude Numbers at various points along the conduit were established to determine whether the flow transitioned from supercritical to subcritical.

The points monitored included the first bend, midway between the first and second bends, and at the second bend. Table 5-6 shows the results obtained from calculated Froude numbers.

Table 5-6: Froude number at different parts of the floor of the conduit section

Emergency gate opening (%)	Velocity at Bend 1 (m/s)	Velocity at Mid-section (m/s)	Velocity at Bend 2 (m/s)	Froude number at Bend 1	Froude number at Mid-section	Froude number at Bend 2
20	7.5	6.25	6.25	8.86	4.67	6.03
30	6.93	5.04	3.78	6.69	3.44	2.58
40	7.99	6.85	6.85	7.71	4.33	5.12
50	7.42	5.56	3.71	6.20	3.51	2.34
60	8	5	4	5.98	2.79	2.11
70	7.53	4.6	3.47	5.63	2.43	1.83

With the Froude number for all emergency gate openings being more than 1, it was concluded that there was no formation of hydraulic jumps in the conduit since for a hydraulic jump to occur, the flow has to transition from super-critical to sub-critical flow.

6. CONCLUSIONS AND RECOMMENDATIONS OF FIXED GATE OPENINGS STUDY

The purpose of the 3-dimensional CFD study was to investigate the occurrence of the sudden air up-surge in the air vent of the Berg River Dam outlet structure as experienced at the 2008 commissioning tests. The initial assumption was that there was a gate opening during which the aeration demand was not adequately satisfied. The 3-dimensional study was used to investigate the case study and steady state simulations were conducted for static gate openings to investigate the adequacy of the air vent for a range of fixed gate openings.

Simulation results were compared with those from the physical hydraulic model tests. The physical model with a scale of 1:14.066 was tested at the University of Stellenbosch hydraulics laboratory.

The CFD study of steady state fixed gate openings simulated positive air flow down the air vent which agreed with the physical model tests. In the physical model tests, negative air flow could only be obtained while the gate was closing.

The results obtained from the steady state simulations were similar to those of the physical model. However, the numerical model produced higher air flow than the physical model, although the trend in results was the same. Because the simulations were steady state, it was not possible to monitor the variation of parameters with time. Even with the similarity in results from the physical model and numerical model, it was not possible to simulate the sudden air up surge that was experienced in the prototype.

Even though the steady state simulations did not produce the required result, they were not in vain. They enabled not only the establishment and determination of the variables required for further research work but also provided direction for future work.

The steady state simulations helped establish that at static gate opening, the aeration demand could be adequately satisfied since the discharge was constant for specific gate openings.

Since the steady state simulations were not able to produce time dependent results of the varying pressures and velocities that occur during the testing of the Berg River Dam prototype, it

is recommended that transient simulations be conducted for a moving gate setting. The results of the transient simulations would create a basis for the comparison of time varying parameters. As a first step the simulations may be performed with fixed gate openings as in the steady state set up and in a further step the creation of a moving gate into the existing geometry should be incorporated.

Further research done with a dynamic gate for transient simulations would cause the discharge to vary rapidly with time. As the gate closes, the discharge decreases and the demand for air increases. Inadequacy of the air vent to provide the required aeration demand might force the system to solicit air from the ski jump, a situation that could lead to sudden upstream flow of air.
Increased flow simulation times must be used to ensure that the model is stable and that conservation of mass has been established before results can be extracted for analysis. There may be changes to the flow patterns even after the flow has reached the ski jump. To guarantee the accuracy of the solutions from the simulation, finer meshes should be used although this would require more calculation time, and the quality of the mesh must be kept within acceptable limits.

Smaller time steps are recommended to ensure that divergence of the solution is avoided.
It should be noted, however, that transient simulations will require more processing time since the solutions have to be calculated for time varying parameters.

STAGE 2: SIMULATION OF CONTINUOUS GATE CLOSURE

7. MODEL SET-UP FOR CONTINUOUS GATE CLOSURE

7.1 Methodology for Modelling of Continuous Gate Closure

At the outset, the aim was to set up a CFD model (of the same scale as the physical model) with a continuously closing gate and then run simulations of a number of physical model tests and directly compare the results. This would involve:

- Modifying the existing CFD model (WRC, 2011) to run transient simulations with a continuously closing gate using a user defined function (UDF).
- Getting a simulation to run stably to completion and produce realistic results, initially with a 10 second closing time (equivalent to 37 seconds in the prototype) to reduce computation time, while monitoring the pressures at certain points on the floor of the conduit and the air velocity in the airshaft; and
- Running simulations for various closing rates at various reservoir water levels, as done in the laboratory with the physical model, and directly comparing the results (pressures and air velocities).

However, becoming familiar with the modelling software, setting up the model and getting a stable simulation to run proved more difficult and time-consuming than originally anticipated and it was not possible, in the time available, to complete more than the initial trial simulation with a 10 second closing time. The third step of the method above was therefore adjusted to:

- Comparing the results of this 10 second simulation to the best available laboratory test data, and to results from literature.

7.2 Adapting the Mesh Geometry

In the second phase of the study, the three dimensional mesh used in the first phase was adapted to model a continuously closing gate by means of a dynamic mesh controlled by a user defined function (UDF).

In order to reduce computation time and simplify the problem, the reservoir and selector gates from the original mesh were deleted and the wet well was cut-off 1.5 m above the floor level (21 m in the prototype). It can be seen in the results of the previous simulations (for example see section 5.1.2) that the flow upstream of this point has virtually no effect on the aeration downstream of the gate. A constant pressure inlet was used at the wet well instead of the

velocity inlet and overflow in the reservoir of the original model. Figure 7-1 and Figure 7-2 below show the original and new meshes respectively.

The adapted mesh consisted of 73 546 nodes and 352 502 tetrahedral or triangular cells, ranging in height from approximately 1.5 mm to 40 mm. The mesh is finest in the region immediately surrounding the gate and coarsest in the downstream conduit.

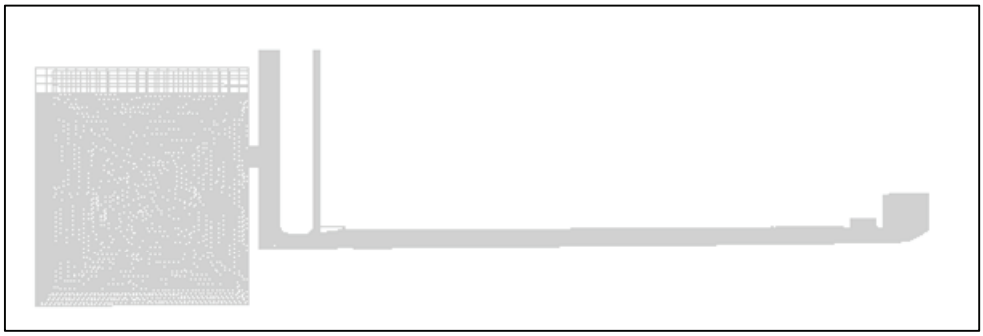

Figure 7-1: Side View of Original Mesh used for first Berg river Dam Simulations

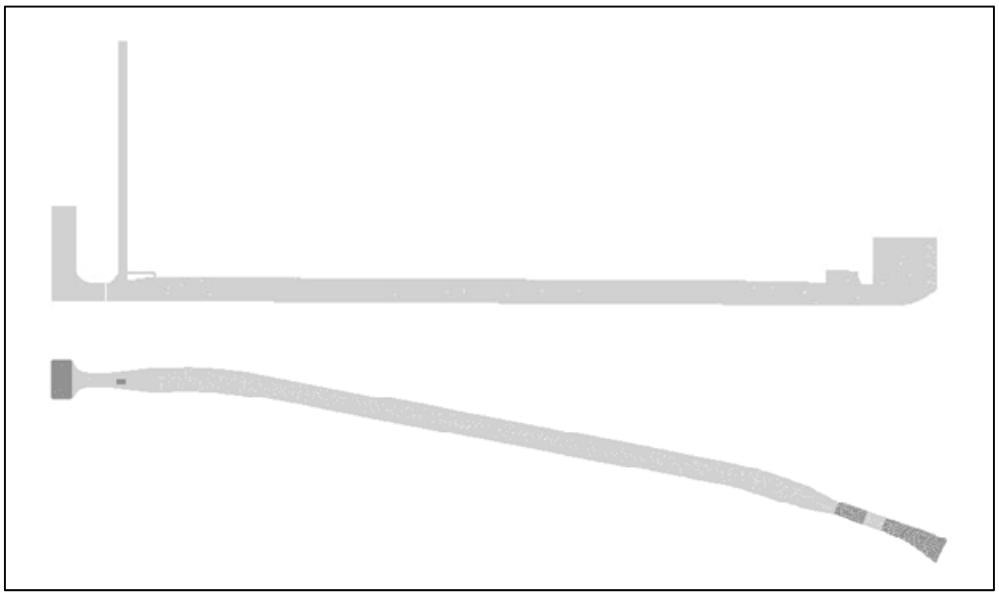

Figure 7-2: Side and Top Views of Adapted Mesh

7.3 Creating the Dynamic Mesh

To create a dynamic mesh in FLUENT, interfaces must be defined between the moving and non-moving parts. To create these the model was split into two separate meshes: one for the fluid region directly below the gate (gate zone – shown in blue in Figure 7-3 and Figure 7-4) , and another for the rest of the model (shown in black). Both meshes were imported into FLUENT and the interfaces between them were defined. The side walls of the gate zone are defined as deforming zones and the top is given a constant downwards velocity, specified with a simple UDF (See Figure 7-5). FLUENT's remeshing and smoothing methods were used for updating the mesh at each time step.

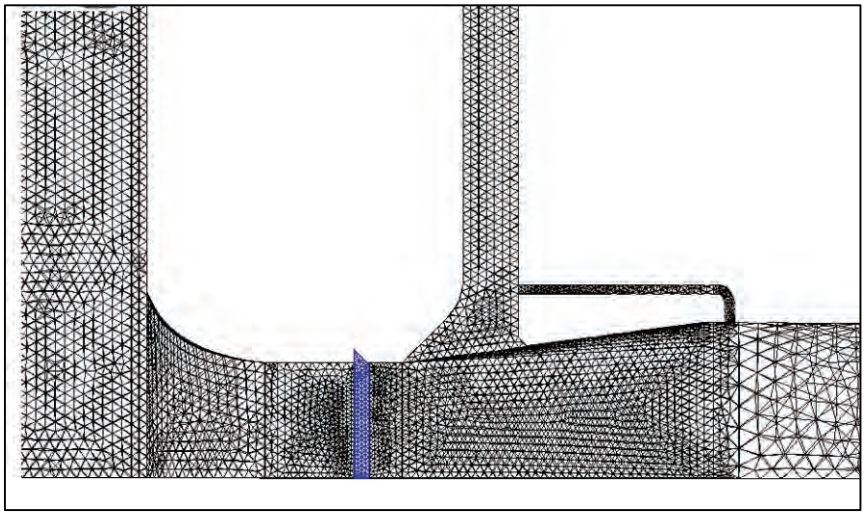

Figure 7-3: Mesh for completely open gate showing separate gate zone in blue

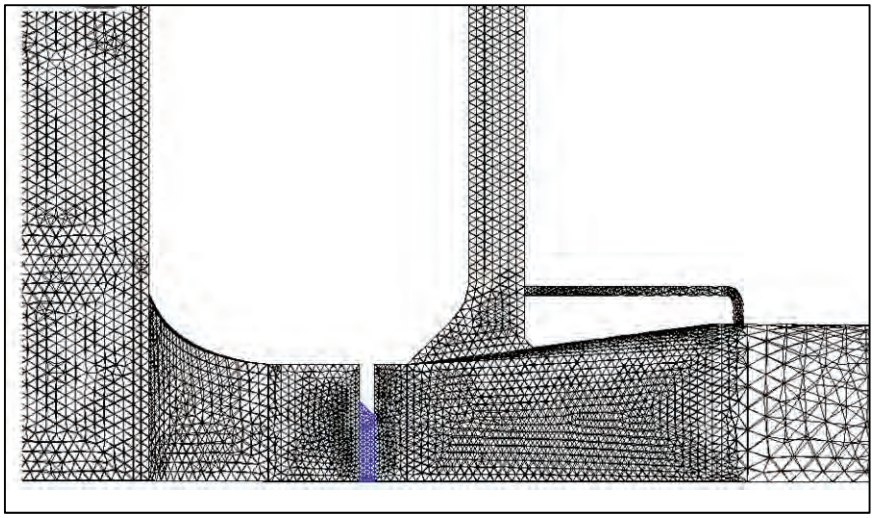

Figure 7-4: Mesh for partially closed gate

```
#include "udf.h"

DEFINE_CG_MOTION(motion_solid, dt, vel, omega, time, dtime)
{
 real velocity;
 vel[2]=-0.0270515;
}

// The gate is 0.27015 m high
// Z-velocity = -0.270515m /10s = 0.0270515 m/s
```

Figure 7-5: UDF function for Gate Closure in 10 seconds

7.4 Solver Settings

The FLUENT Volume of Fluid (VOF) Model for multiphase flow (described in 3.5.3), with a pressure based solver and absolute velocity formation was used to perform the required transient simulations. An explicit scheme was used with automatically adjusted time-steps based on a prescribed Courant number[1]. Turbulence was modelled using the k-epsilon RNG model (see 3.5.2) with standard wall functions.

The full FLUENT input summary for the 10 second closure simulation is attached in Appendix A.

7.5 Operating and Boundary Conditions

Instead of using a velocity inlet and overflow as was done in the first simulations, a constant water level in the wet well was assumed, and the water inflow at the wet well was modelled as a pressure inlet with the volume-fraction of water equal to 1 (only water is allowed in). The inlet pressure (given as total gauge pressure in Pascal) is calculated from the height of the water above the point where the model is cut off (i.e. total height of the water in the wet well, minus 1.5 m).

The outflow at the front of the ski jump was modelled as a pressure outlet, with a gauge pressure of zero and a backflow volume-fraction of water equal to zero (only air can flow back into the model from this boundary).

[1] The dimensionless Courant number is a measure of the number of cells a particle moves through in a single time step. It is defined as $Cr = \frac{v\Delta t}{\Delta x}$ where v is the local velocity, Δt is the time step and Δx is the cell size.

The top of the airshaft, top of the radial gate, and top of the ski jump are all open to the atmosphere and were modelled as outlet vents, also with a gauge pressure of zero and a backflow volume-fraction of water equal to zero.

The turbulence conditions at the inlets and outlets were set by specifying the hydraulic diameter and turbulence intensity[2]. The hydraulic diameters of the various boundaries are the same as those given in Section 4.4 and the turbulence intensity was assumed to be 5%.

The inlet and outlet boundaries are shown schematically in Figure 7-6 below.

As for the steady-state simulations, the operating pressure for this model was 101 325 Pa (average atmospheric pressure) and gravitational acceleration was applied in the negative z-direction. The walls of the model were set as “wall” boundaries, with a roughness height of 0.003 mm, the estimated roughness of Perspex (Chadwick, Morfett, & Borthwick, 2004), the wall material used for the physical model.

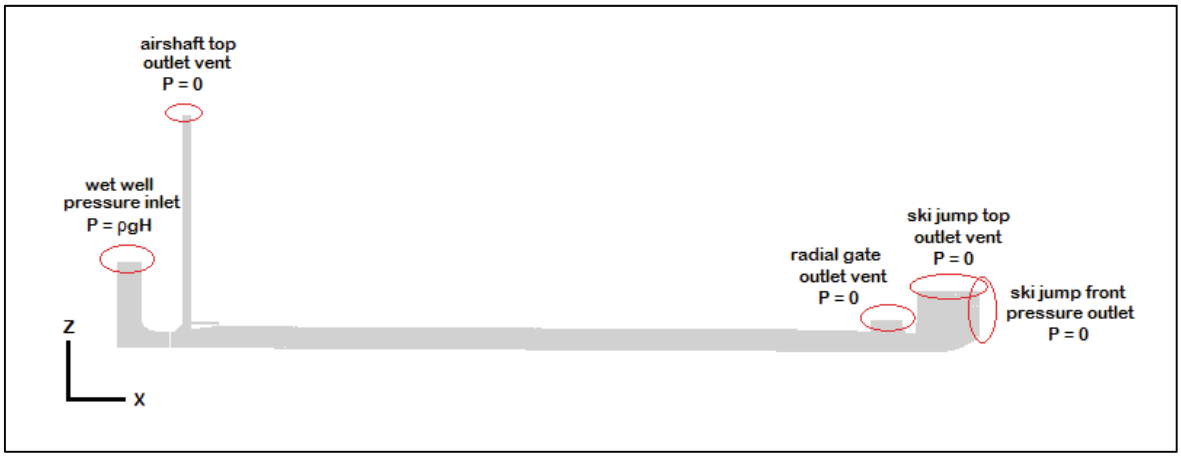

Figure 7-6: Inlet and Outlet Boundary Conditions

[2] Turbulence Intensity, I, is the ratio of the root-mean-square of velocity fluctuations, v', to the mean flow velocity, v_{avg}: $I = \frac{v'}{v_{avg}}$
A turbulence intensity, I <1% is considered low and I >10% is considered high. A moderate turbulence intensity is assumed here.

7.6 Results Monitors

For transient simulations result monitors are required to record parameters over time. In this model point monitors were created to record the static pressures[3] in the centre of the floor of the conduit at six points along its length, corresponding to the positions of the piezometers in the physical model (see Volume I, Section 4.5.1). A surface monitor was created to record the air flow velocity at the top of the airshaft, where the anemometer was placed in the physical monitor (see Volume I, Section 4.5.2). This monitor tracked the area-weighted-average velocity through the total boundary area. Figure 7-7 below shows the positions of the monitors and their coordinates.

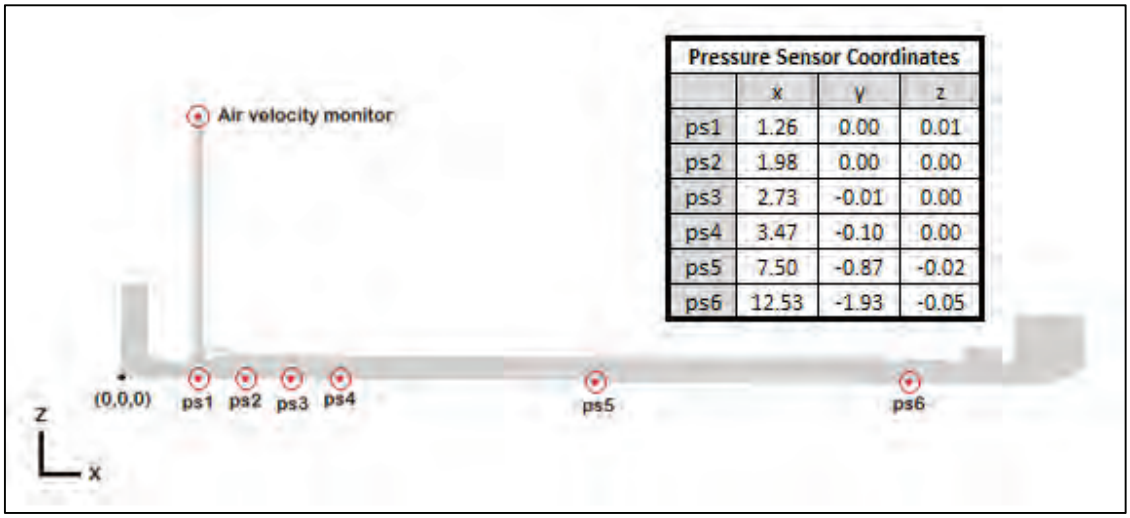

Pressure Sensor Coordinates			
	x	y	z
ps1	1.26	0.00	0.01
ps2	1.98	0.00	0.00
ps3	2.73	-0.01	0.00
ps4	3.47	-0.10	0.00
ps5	7.50	-0.87	-0.02
ps6	12.53	-1.93	-0.05

Figure 7-7: Positions of Pressure and Velocity Monitors

[3] In fluid dynamics total pressure, P_0, is defined as $P_0 = P + \frac{1}{2}\rho v^2$, where the pressure, P, is called static pressure to distinguish it from the total pressure and $\frac{1}{2}\rho v^2$ which is called the dynamic pressure.

8. SIMULATIONS

8.1 Open Gate Simulation with Inlet Pressure of 10 000 Pa

Before the moving gate could be started the situation with the gate completely open had to be modelled. A stable solution with an open gate was then used as the starting condition for the moving gate simulation.

For the first trial simulation 10 000Pa (approximately 1 m water) was used as the inlet pressure at the wet well (giving a total water column height in the wet well of 2.5 m). The model was initially patched with air in the airshaft and top parts of the radial gate and ski jump, and the rest of the domain was filled with stationary water. As the simulation starts the pressure is suddenly applied and a wave passes through the model forcing water up and out the top of the airshaft. The water level in the air shaft then drops all the way down to the bottom and starts oscillating up and down by about 1.5 m. The amplitude of the oscillations remains fairly constant after 10 seconds of flow time. The simulation was run for 33 seconds. Freeze-frames from this simulation are shown in Appendix B. The pressure and air velocity monitor results are shown in section 9.1 below. The final steady water flow rate through the model was approximately 0.38 m^3/s.
Videos of the physical model tests in the laboratory also show an oscillating water level in the airshaft while the conduit is flowing completely full.

8.2 Continuous Gate Closure in 10 seconds

Transient simulations on three-dimensional models with thousands of cells require very long computation times when run on normal computers and a fair amount of trial and error is involved when first developing a model. For this reason a very fast closing time of 10 seconds (equivalent to 37 seconds in the prototype) was chosen for the first closing gate simulation to keep simulation time relatively short while the model was still being developed.

The open gate simulation above was used as a starting condition. The UDF for the moving gate (see Figure 7-5) was then compiled in FLUENT and the dynamic mesh was activated to start continuous closure of the gate.

The rapidly closing gate resulted in highly unstable flow patterns underneath the gate and the solution diverged many times during the simulation. Each time the simulation was restarted

from the last stable point and adjustments were made to the time step. The time step was initially set to be variable with a prescribed Courant Number, but after the solution diverged a number of times a fixed time step was chosen instead for more control (this was recommended by ANSYS). Some parts of the simulation would only run successfully with a time step as small as 0.00001 seconds (with this time step the simulation gained only about 0.3 seconds of flow time in 24 hours). In order to minimise the time taken for the simulation the time step was increased as much as possible whenever the solution seemed to be converging quickly with each time step. If the solution became unstable again and diverged, then the simulation had to be started again from the last stable point and a part of the simulation had to be re-run with a smaller time step.

The simulation was run in this way until the gate was completely closed for a few seconds. The animations and results were then analysed and some parts of the simulation were re-run where strange results occurred, with a very small time step.

8.3 Open Gate Simulation with Inlet Pressure of 13 506 Pa

At the 2008 Berg River Dam emergency gate commissioning test the reservoir water level was 40.5 m above the floor of the wet well. This translates to 2.88 m in the 1:14.066 scale model. In the CFD model this is 1.38 m above the wet well inlet (1.5 m high), which is equivalent to an inlet pressure of 13 506 Pa (gauge).

The open gate simulation discussed in 8.1 above was repeated with this commissioning level inlet pressure. This simulation can be used as a starting point for future moving gate simulations of the physical model tests.

The behaviour of this simulation was strangely different to that with the slightly lower inlet pressure. The first few seconds of simulation were similar but the amplitude of the oscillations in the air shaft reduced very quickly and the water level was almost stationary within 25 seconds.

The pressure and air velocity results with this commissioning inlet pressure were compared to those with the first inlet pressure of 10 000 Pa. The results were then used to adapt the continuous gate closure pressure results so that they could be more closely compared to

physical model tests conducted at the commissioning water level. These results are shown in Section 9.1 below.

9. RESULTS FROM CFD MODEL

9.1 Open Gate Simulations

9.1.1 Static Pressures

A graph of static pressure versus flow time for each of the pressure monitors is shown in Figure 9-1 for both inlet pressures simulated (10 000 Pa and 13 506 Pa).

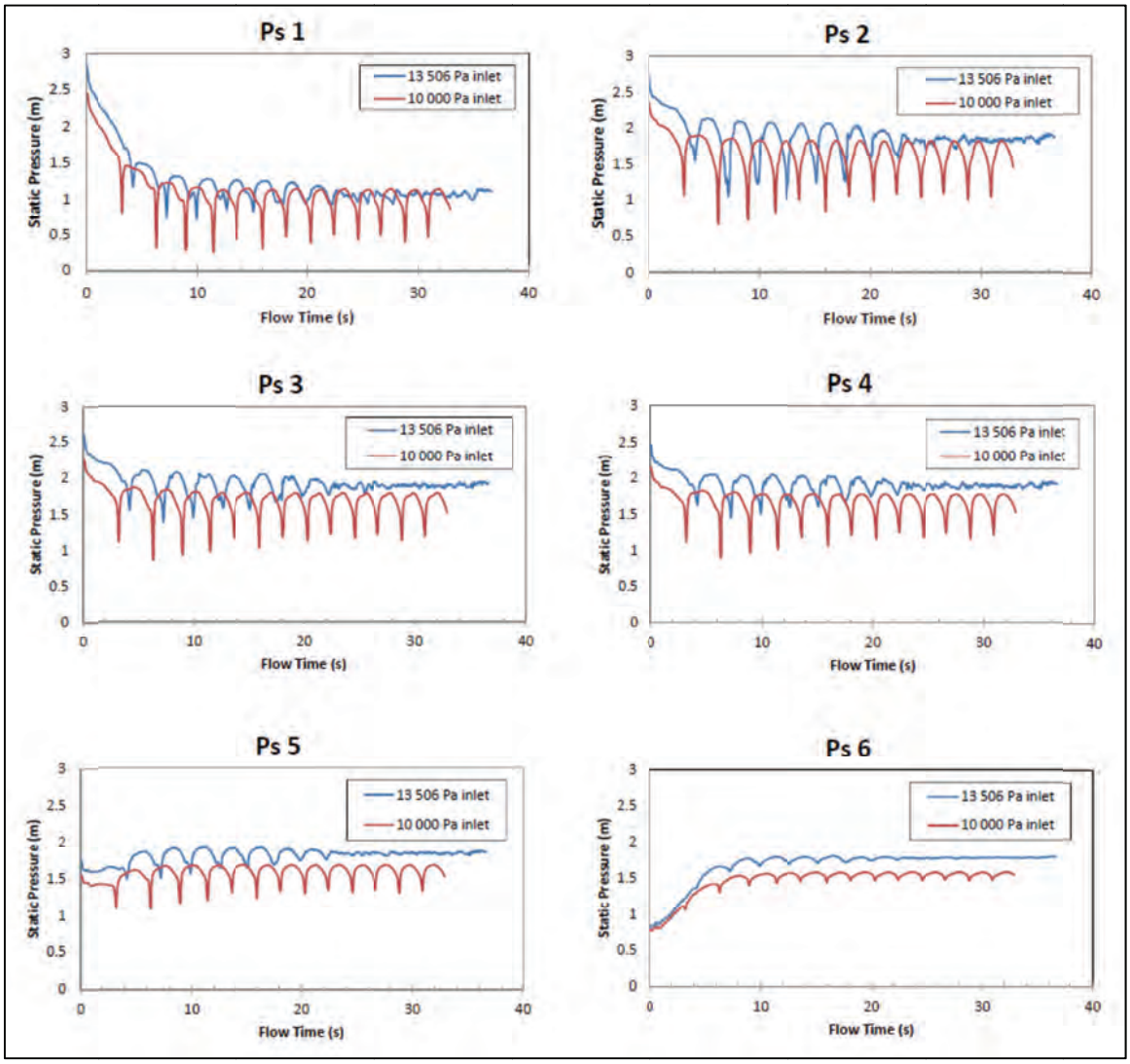

Figure 9-1: Static Pressure Results for Open Gate Simulation

These graphs clearly show pressure fluctuations associated with the oscillating water level in the air shaft (discussed in section 8 above). It can be seen that the higher inlet pressure causes a solution which stabilises to an almost constant state within 25 seconds, while the

lower inlet pressure leads to cyclical oscillations with no significant decrease in amplitude from 15 to 30 seconds of flow time.

The average static pressure at each monitor for the full flowing conduit was determined by averaging the pressure values recorded from 25 seconds of flow time to when the simulation was stopped. These values are shown in Table 9-1 and Figure 9-2 below.

Table 9-1: Average static pressures at each pressure monitor for full flowing conduit

	Average Static Pressures – P(m)					
	ps1	**ps2**	**ps3**	**ps4**	**ps5**	**ps6**
10 000 Pa inlet	0.967	1.613	1.655	1.651	1.610	1.557
13 506 Pa inlet	1.042	1.839	1.896	1.893	1.854	1.790
Difference (ΔP)	*0.074*	*0.226*	*0.240*	*0.242*	*0.243*	*0.233*

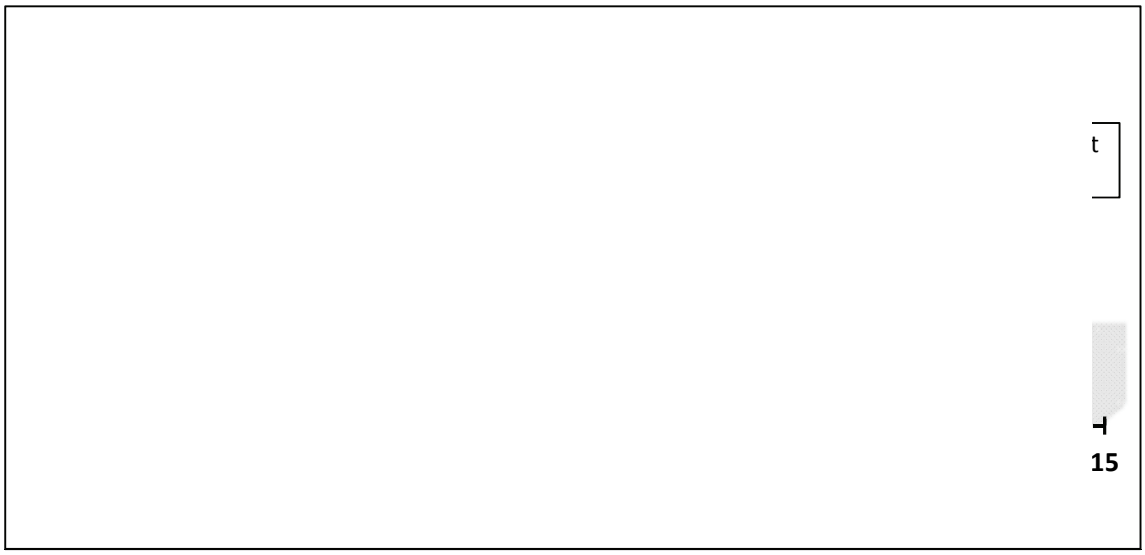

9.1.2 Airshaft Velocities

The air velocity in the airshaft is shown in Figure 9-3 below. The positive direction indicates air flowing up out of the airshaft (positive z-direction). The oscillating water level in the air shaft causes air above it to be moved up and down cyclically. The air velocities in the 13 506 Pa model decrease with the airshaft water level fluctuations.

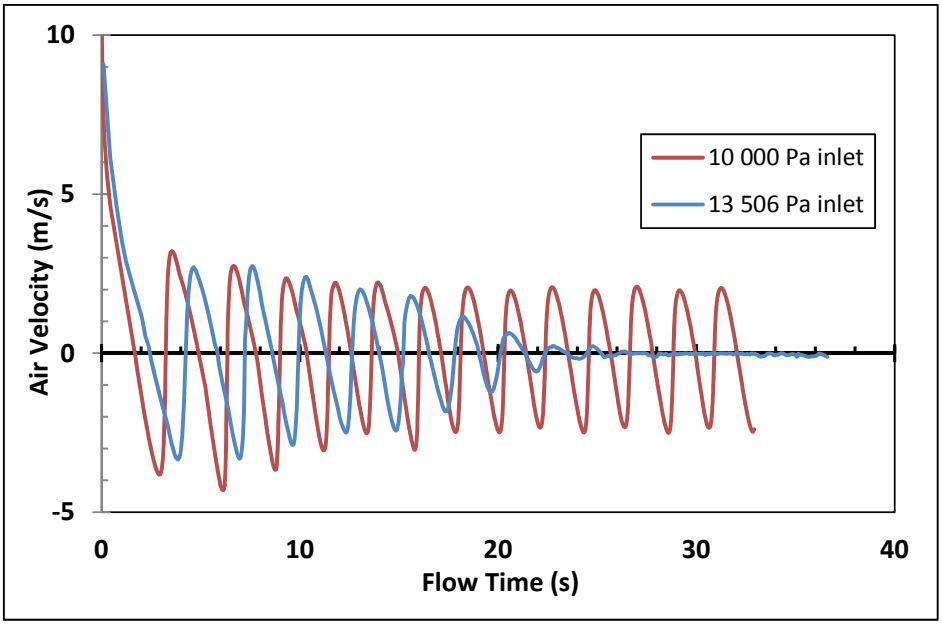

Figure 9-3: Air Velocity in the airshaft for full flowing conduit

9.2 Continuous Gate Closure Simulation

9.2.1 Static Pressures

Figure 9-4 below shows the results of all pressure sensor monitors for the 10 second closure simulation (run from the 10 000 Pa inlet pressure). It can be seen that the pressures closest to the gate and the airshaft drop quickest as the gate begins to close.

A negative pressure of up to -0.25 m is shown at ps2: the first bend in the conduit about 0.3 m downstream of the airshaft. This translates to -3.5 m pressure head in the prototype.

The simulation was run for about 12.5 seconds. During the first 10 seconds the gate closed completely, in the last few seconds the water began to drain out the model. From the pressure results it can be seen that when the simulation was stopped pressure sensors ps1-ps4 were almost dry, while the last of the water was not yet past ps5 and ps6.

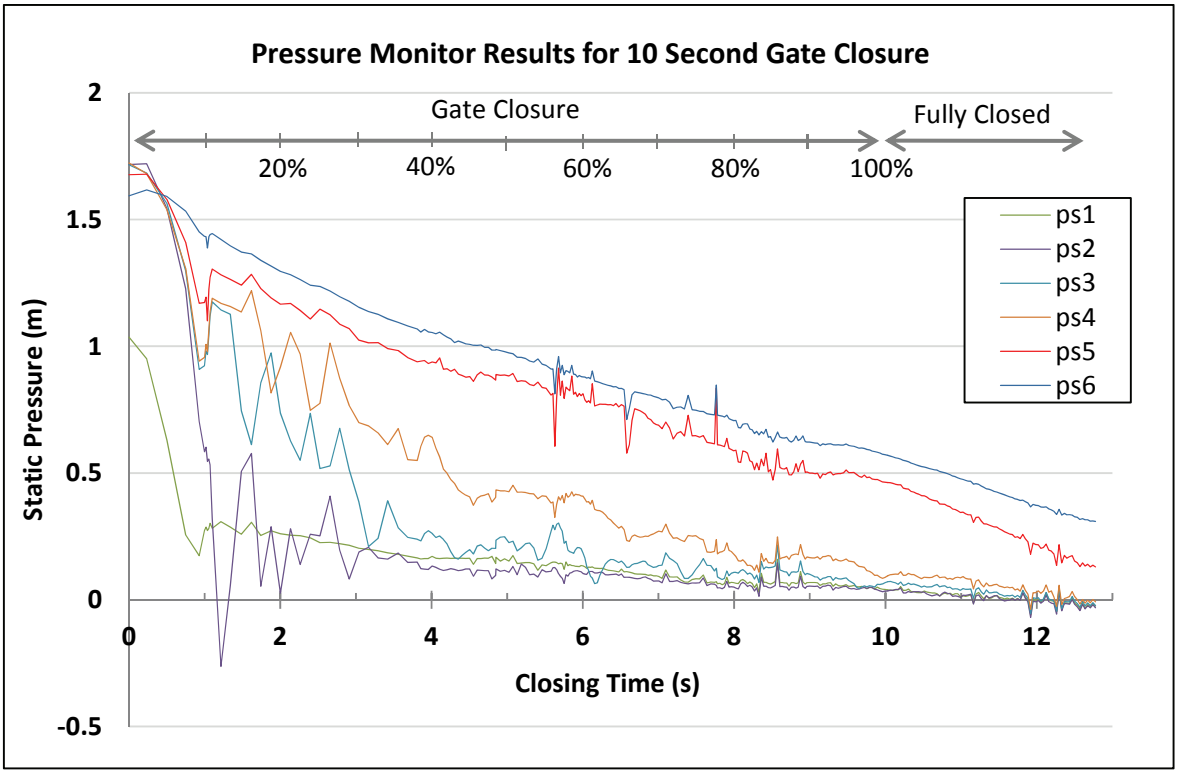

Figure 9-4: Pressure monitor results for 10 second gate closure

9.2.2 Airshaft Velocity

The airshaft velocity results are shown in Figure 9-5 below. Here the positive direction refers to air flowing into the model, down the airshaft. The maximum air velocity is recorded after the gate is completely closed, at the very end of the simulation. This is to be expected for such a fast closing time. Once the gate is completely closed there is still a large amount of water in the model flowing with a high velocity which forces large volumes of air to be sucked into the model. The maximum recorded velocity in the model was 19.8 m/s which translates to a velocity of 74.2 m/s in the prototype.

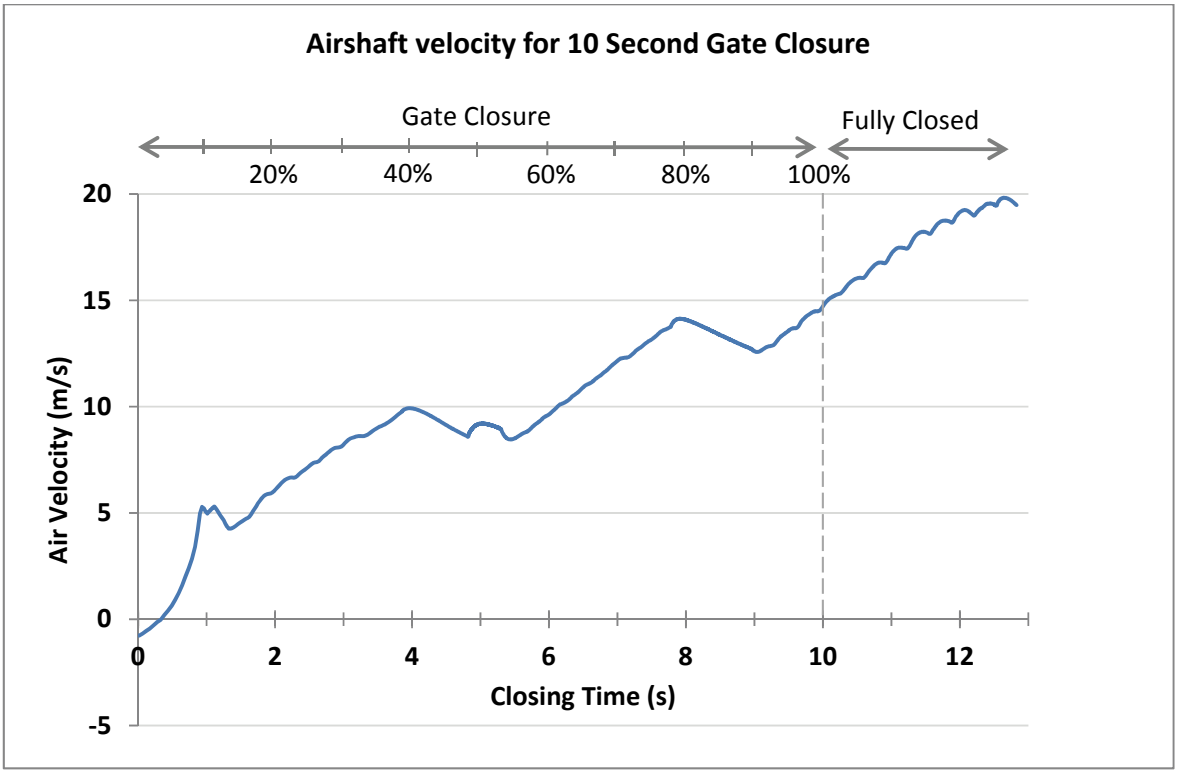

Figure 9-5: Airshaft velocity for 10 second gate closure

10. COMPARISON WITH PHYSICAL MODEL RESULTS AND DISCUSSION

10.1 Physical Model Tests used for Comparison

The results of four tests on the physical model with a gate closure time of roughly 40 seconds were obtained for comparison with the CFD model results. This was the shortest possible closing time for the gate motor on the physical model. The tests were run on 15 September 2011 in Stellenbosch University's Civil Engineering hydraulics laboratory. A description of the physical model and testing procedure are given in Chapter 4 and 5 of Volume I of this report.

10.2 Comparison of Discharge

The discharge was not recorded in all of the physical model tests. On one particular day two measurements were made for the full flowing conduit (gate 100% open) at the commissioning water level, of 290 l/s and 319 l/s respectively. In previous studies on the same physical model with fixed gate openings it was found that the discharge varied linearly with gate opening, and extrapolating these results gives a discharge of 335 l/s. The average of these three values was taken as the physical model estimate in Table 10-1 below. In this table the model values are converted to prototype values to put them into perspective.

Table 10-1: Comparison of Discharges of CFD and Physical Models

Model		Model Q (l/s)	scale factor 14.066^(5/2) /1000	Prototype Q (m^3/s)
CFD	10 000 Pa inlet	385	0.742039	*286*
	13 506 Pa inlet	391	0.742039	*290*
Physical		315	0.742039	*233*

Compared to the physical model, the CFD model (13 506 Pa inlet) over estimates discharge by 24%. The reason for this overestimation of flow by the CFD model is not known. It may be that a finer mesh is needed in certain areas of the model, that some input parameters need to be changed, or that different solution methods are needed to make the model more accurate.

10.3 Comparison of Static Pressures

Figure 10-1 below shows graphs of the static pressures for each pressure monitor as measured in the four physical model tests (at about 40 s closing time) and in the continuously closing CFD model (10 s). From here it can be seen that there is a significant difference in the static pressures even at a completely open gate (before the different rates of closure could have an effect). Table 6-2 and Figure 10-2 (on the following page) show a comparison between the applicable open gate simulation and the starting state of the physical model. The ps4 and ps5 results are excluded in Figure 6-2 as they are outside the range of the pressure sensor.

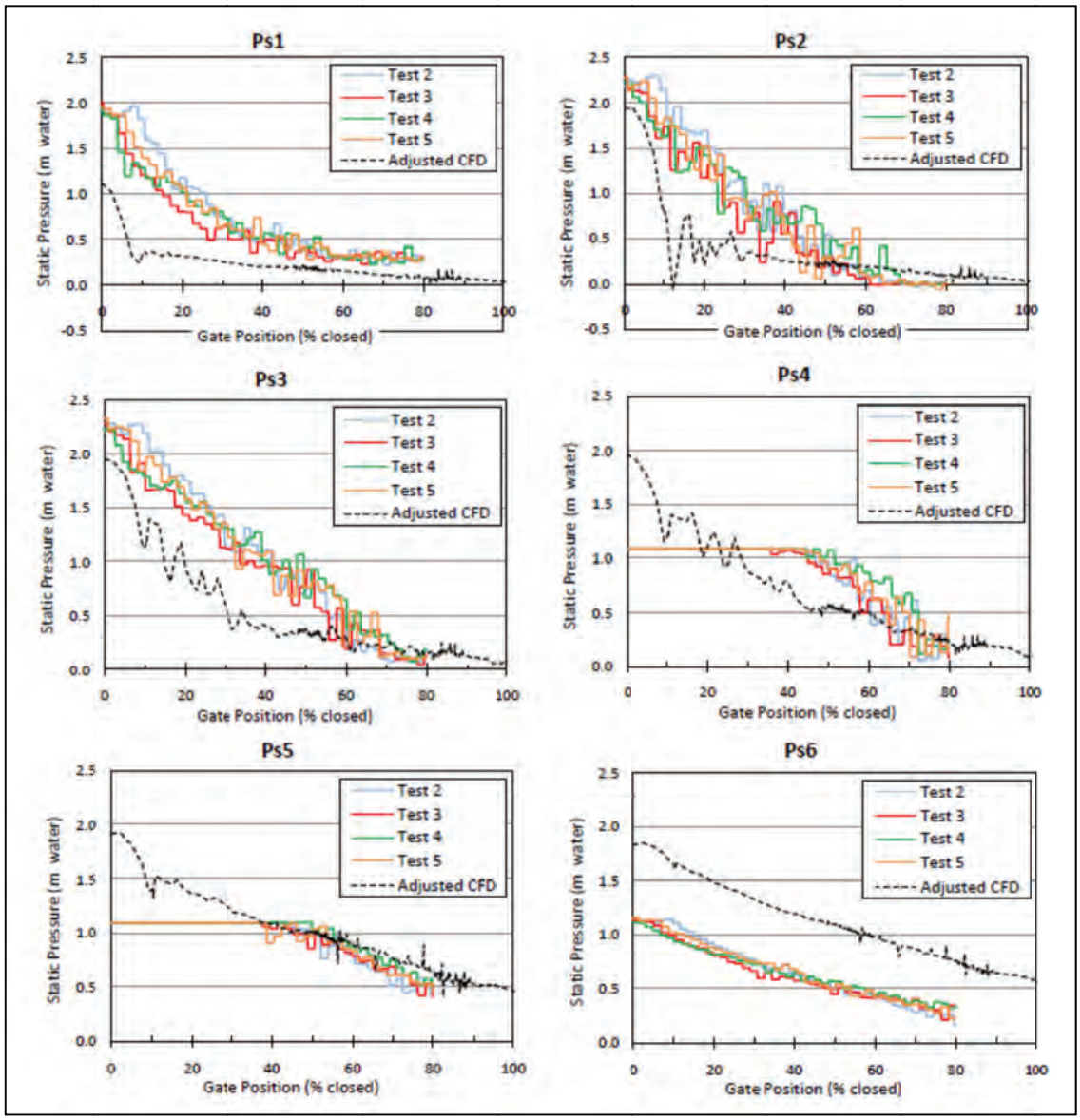

Figure 10-1: Comparison of CFD and Physical Model Static Pressures

Table 10-2: Comparison between CFD Model and Physical Model Pressures at Fully Open Gate

	Average Static Pressures (m)					
	ps1	**ps2**	**ps3**	**ps4**	**ps5**	**ps6**
Phys. Model Avg	1.998	2.309	2.310	~~1.104~~	~~1.104~~	1.131
CFD -13 506 Pa inlet	1.042	1.839	1.896	1.893	1.854	1.790
Diff. btwn Phys. & CFD -13 506 Pa	*-0.957*	*-0.471*	*-0.414*	-	-	*0.659*
CFD Error	*-47.9%*	*-20.4%*	*-17.9%*	-	-	*58.3%*

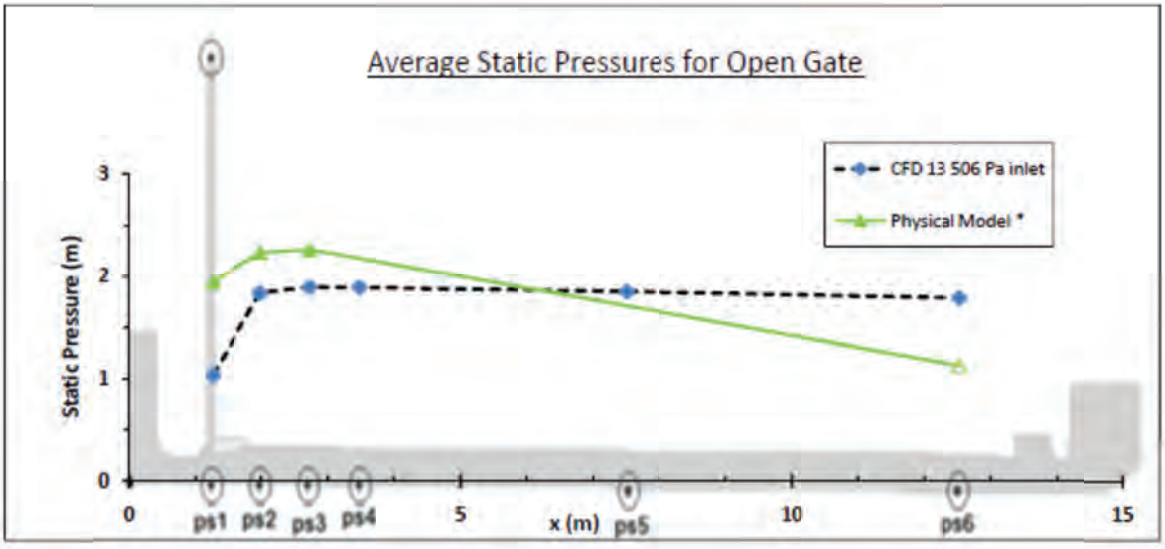

Figure 10-2: Graphical Comparison between CFD and Physical Pressure Results with Open Gate

In Figure 6-1 the "Adjusted CFD" lines show the results from the 10 s closure CFD model corrected for inlet pressure. An inlet pressure of 13 506 Pa corresponds to the water level used for the physical model tests (commissioning level), but the CFD closing gate simulation was run with an inlet pressure of 10 000 Pa. The difference between the pressures in the 2 open gate simulations, ΔP, (see Table 5-1) was therefore used to adjust the closing gate simulation pressures for each pressure sensor. The full difference was added where the gate was 100% open and a linearly decreasing adjustment was made to the rest of the simulation:

$$P_{adjusted\ CFD} = P_{CFD} + \Delta P(1 - \frac{\%closed}{100})$$

While the results of the closing gate simulation cannot be expected to match those of the physical model results because of the difference in closing speed, the results of the open gate simulations can be directly compared to the starting point of the physical model tests. This comparison is shown in Table 10-1 and Figure 10-2 above. A poor correlation between CFD results and those of the physical model can be seen. Assuming the physical model pressures are correct, the CFD model underestimates the pressures at the start of the conduit by 48% and overestimates the pressures at the end of the conduit by 58%. This seems to be an indication that the physical model underestimates the energy losses in the conduit.

An underestimation of the losses in the conduit results in a higher discharge for a given inlet total pressure. A higher discharge has a higher velocity and dynamic pressure and therefore a lower static pressure for a constant total pressure. At the inlet the total energy and total pressure in the CFD model is set to be the same as that in the physical model. The static pressure at the CFD model inlet is therefore underestimated. Subsequently, the static pressures predicted at ps1, ps2 and ps3 (located close to the inlet) are also underestimated.

As the flow moves downstream the contribution of the energy losses becomes significant. Since the CFD model underestimates these losses the predicted downstream pressure gradually becomes higher than in the physical case.

As the gate begins to close (see Figure 10-1) the pressures close to the gate (at ps1, ps2 and ps3) decrease much more rapidly in the CFD model than in the physical model. This is to be expected as the rate of closure is much faster for the CFD model.

10.4 Comparison of Airshaft Velocities

The physical and CFD models produce very different airshaft velocities as shown in Figure 10-3 (note that the positive direction in this figure refers to inflow velocity, down the airshaft). The CFD mode simulation, with 10 second closure, has a much higher velocity than any of the physical model tests run with a 40 second closure, which is unsurprising.

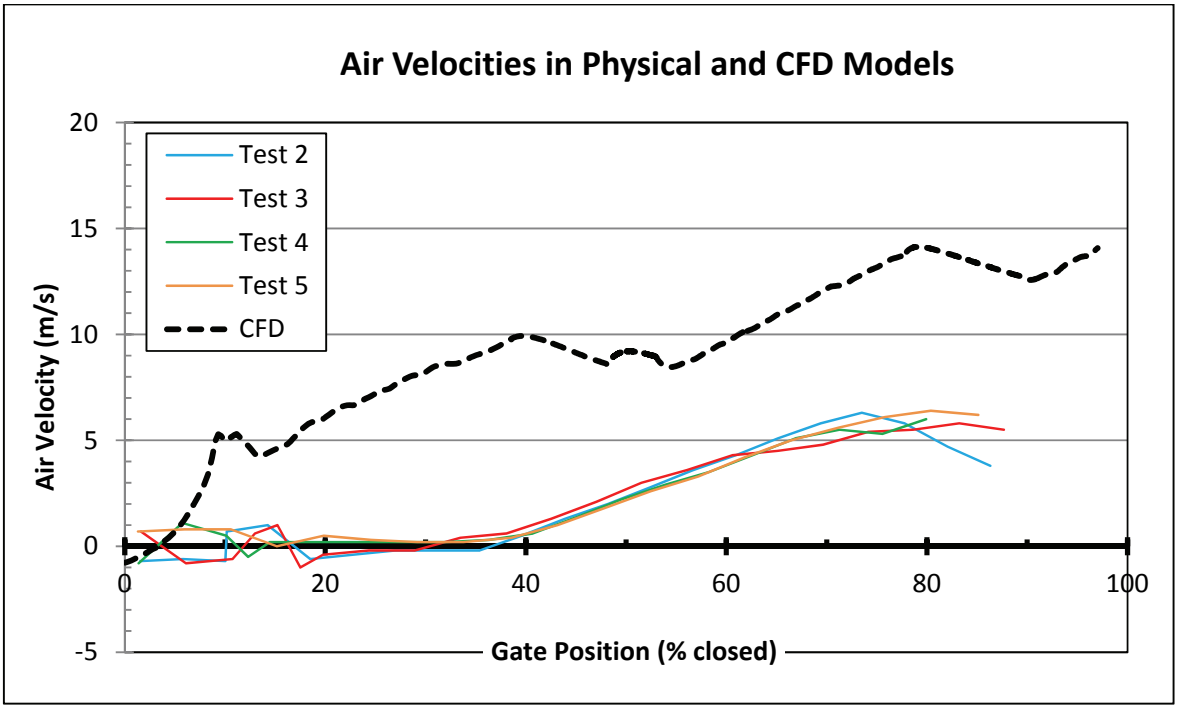

Figure 10-3: Comparison of Airshaft Velocities in Physical and CFD Model

Both the CFD and physical model results show some outflow of air at low velocities in the early stages of closure. This is as a result of the oscillating water level in the airshaft which occurs when the gate is fully open which continues as the gate first begins to close (see Figure 9-3 for full flow air velocities), and is not analogous to the high outflow velocities observed in the commissioning tests.

Considering only the closing part of the CFD simulation the peak airshaft velocity, airflow and the air demand ratio are shown in Table 10-3 below. In both models the maximum air demand (during closure) occurs when the gate is approximately 20% open (80% closed).

Table 10-3: Air demand for Physical and CFD Models

	Max. Discharge (l/s)	Max. Velocity (m/s)	Air Flow Rate Qa (l/s)	Gate Closure	Water Discharge Qw (l/s)	β = Qa/Qw
Physical Model (±40 s closure)	315	6.4	58.2	76%	78.75	0.739
CFD Model (10 s closure)	380	14.14	128.6	80%	76	1.693

10.5 Possible Reason for Underestimation of Energy Losses

10.5.1 General Mesh Considerations for Turbulence Modelling

Turbulent flows are susceptible to mesh dependence, and it is therefore important that regions where the mean flow velocity changes rapidly are meshed with suitably fine resolution (ANSYS Inc., 2009). Further, the k-ε and many other turbulence models are derived for fully turbulent core flows and special treatment is therefore needed for near-wall regions. In FLUENT this is provided by wall functions, which provide laws for the boundary layer. For wall functions to be valid the near wall cells must be within a suitable size range. These sizes are given in terms of the dimensionless y^+ value,

$$y^+ = \frac{\rho u_t y}{\mu}$$

Where: y = cell height

ρ = density

μ = viscosity

u_t = local frictional velocity

For standard wall functions with a k-ε turbulence model y^+ for the cells adjacent to the wall should be between 30 and 300 (ANSYS Inc., 2009). The y^+ value for any cell is dependent on the solution so it is often difficult to estimate the required mesh size accurately when a mesh is created. FLUENT can report the y^+ values for a solution and has a tool to refine or coarsen a mesh (mesh adaption) to satisfy a prescribed y^+ range once a solution has been reached.

10.5.2 Application to this Study

One anticipated reason for the underestimated energy losses and overestimated discharge in the CFD model was that the mesh was not fine enough. To check if this was the case, a mesh adaption was performed in Fluent (for the fully open gate stable solution) to satisfy $30 < y^+ < 300$, the condition required for reliable wall treatment for a k-ε turbulence model with standard wall functions.

The adaption increased the number of nodes from approximately 75 000 to 170 000, and the number of cells from 359 000 to 561 000. This represents a significant refinement of the mesh. Images of the original and adapted meshes (shown in Figures 6-4 and 6-5 below respectively) show that a significantly finer mesh is required along the walls of the gate region and conduit for accurate application of the turbulence wall functions. Unfortunately this problem was only recognised late into the project and there was not time available to re-run these simulations with the refined mesh.

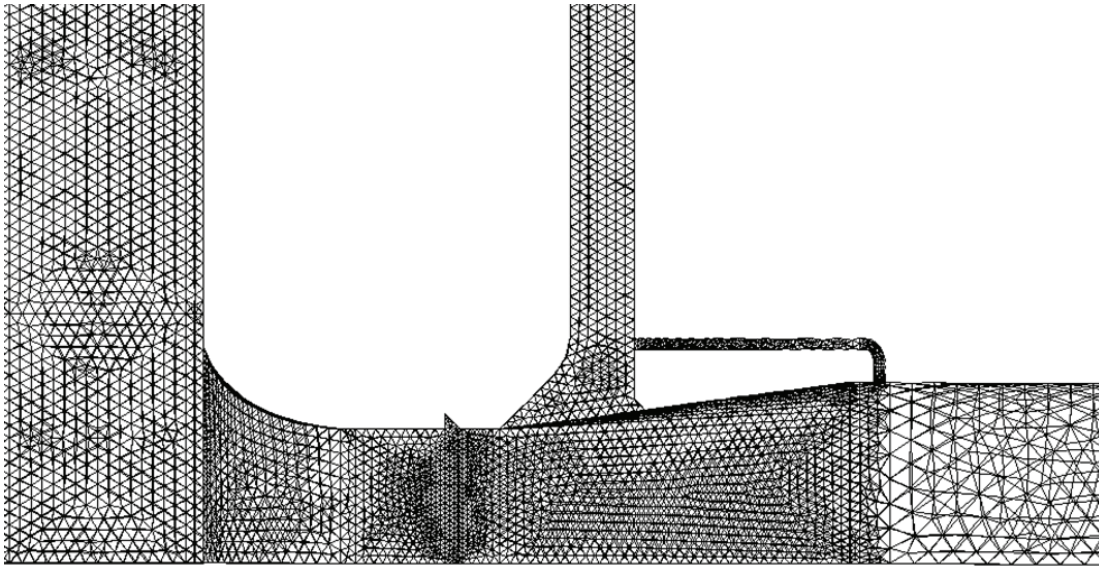

Figure 10-4: Original Mesh

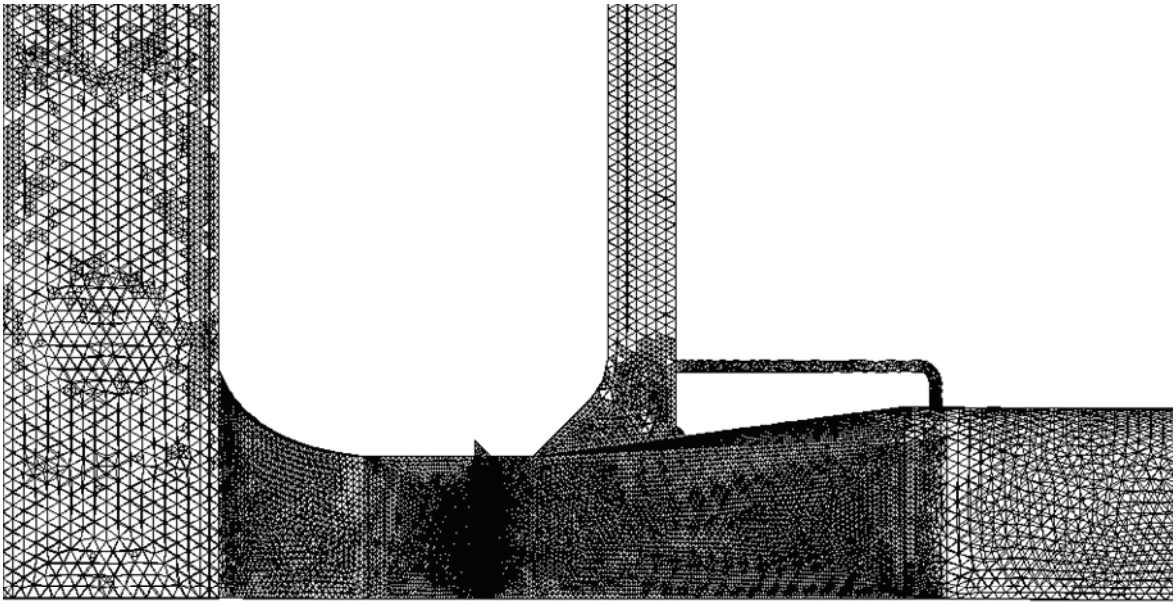

Figure 10-5: Mesh Adapted for $30 < y^+ < 300$

11. CONCLUSIONS AND RECOMMENDATIONS OF CONTINUOUS GATE CLOSURE STUDY

11.1 Conclusions

The three dimensional CFD model was successfully modified to model transient simulations with a dynamic mesh, simulating continuous gate closure.

A simulation of complete gate closure over 10 seconds was completed. The static pressure and airshaft velocity results from this CFD simulation were compared to those from physical model tests with a 40 second gate closure (the fastest possible closure of the physical model). The air demands were calculated for both the CFD and physical model tests and compared to those predicted by empirical methods from literature.

With a fully open gate, it was found that the CFD model significantly underestimates the energy losses in the model resulting in an overestimation of the discharge by about 25% and a poor correlation with the physical model pressure results. It is expected that this underestimation of losses is partially due to a too coarse mesh in the conduit.

A direct comparison between the CFD and physical model results could not be made for the continuously closing gate due to the large difference in closing speeds. However, apart from the significantly lower losses, the results show similar trends and the behaviour of the model appears realistic.

This study has not developed any further understanding of the behaviour that occurred during the 2008 commissioning test of the Berg River Dam emergency gate due to the limited computer runtime available, but progress has been made in developing the CFD model. It is expected that this model may provide valuable insight into the flow dynamics which resulted in the airshaft expulsions once it is run with a finer mesh with slower rates of closure.

11.2 Recommendations

It is recommended that the mesh is refined and open gate simulations are continued until the CFD model accurately reproduces the discharge and energy losses. Further attention may be needed to the boundary conditions, model dimensions and solver settings as well as to the mesh resolution.

The model should then be run with slower, more realistic closing times that can be compared directly to physical model results. Once verified against the physical model, the CFD model can be scaled up to prototype size to eliminate scale effects, and can be adapted to investigate the effect of changes such as straightening the conduit or removing the ski jump.

Slow simulation speeds are currently a major limitation of the CFD models. Ways of increasing simulation speed should be investigated. These could include acquiring more powerful computers or running simulations on a cluster as well as possibly using different solvers (implicit) which allow larger time steps.

Finally, it is recommended that physical emergency gates are never closed with extremely fast closing times as done in the CFD model in this project because it may result in excessively high airshaft velocities.

12. CONCLUSIONS AND RECOMMENDATIONS AFTER BOTH STAGES

A three-dimensional CFD model was successfully created and results of steady-state simulations of various fixed gate opening were studied in detail and compared to physical model simulations (see Volume I). The flow patterns shown in the CFD model were very similar to those seen in the physical model and the graphical representation of flows provided by the CFD analysis helped give a clear understanding of the flow, although the discharge through the CFD model was found to be greater than that in the physical model.

The model was then successful adapted to perform a closing gate transient simulation. However, the excessive computational time required by the solver meant that only a single simulation of a very fast gate closure could be completed. Further, comparison of pressure results with those from the physical model showed that energy losses are significantly underestimated by the CFD model. The CFD model therefore could not aid in explaining the airshaft expulsions experienced in the commissioning tests.

It has been recommended that simulations of slower gate closure are performed, and the reasons for the discrepancies between the physical and CFD models are further investigated. *Currently a simulation of a 96 second simulation (equivalent to 6 min in the prototype) is underway.*

In order for the potential of CFD analysis to be realised in future hydraulics problems, faster simulation speeds are required.

13. REFERENCES

Abban, B., Shand, M., Kamish, W., Makhabane, M., Van Zyl, B., & Tente, T. (unknown). *Decision Support System for the Berg River Dam and Supplement Scheme.* University of Stellenbosch, South Africa.

ANSYS Inc. (2009). Ansys Fluent 12.0 Theory Guide. ANSYS.

ANSYS Inc. (2009). Ansys Fluent 12.0 User's Guide. USA: ANSYS, Inc.

ASHRAE (1981) – American Society of Heating, Refrigerating and Air Conditioning Engineers, Inc. *ASHRAE Handbook Fundamentals Volume*.

Aydin, I. (2002). Air demand behind high head gates during emergency closure. *Journal Hydraulics Division, vol. 40, 2002, NO. 1*

Borodina, L. K. (1969). Aeration behind low level gates. *Gidrotekhnicheskoe Stroitel'stvo, No. 9, pp. 32-37*.

Calitz. J. A. (2009). *Physical and Mathematical Modelling of air Flow with the Emergency Gate Closure of the Berg River dam.* Stellenbosch University, South Africa.

Campbell, F. B. and Guyton, B. (1953). Air Demand in Gated Conduits. *IAHR Symposium, Minneapolis.*

Chadwick, A., Morfett, J., Borthwick, M. 2004. *Hydraulics in Civil and Environmental Engineering*. New York: Spon Press.

Erbisti, P. C. F. (2004). Design of Hydraulic Gates. *Swets and Zeitlinger B. V., Lisse, Balkema Publishers,* Netherlands.

Falvey, H.T. (1980). Air-water flow in hydraulic structures. *US Department of interior, Water and Power Resources Service*, Engineering monograph No.41

Giesecke, J. (1982). Verschlusse in Grundablassen – Funktion and Ausfuhrung. *Wasserwirtscraft* 72(3): 97-104 (in German).

Hydraulics Research Wallingford. (1990). Charts for the Hydraulic Design of Channels and Pipes. 6th Edition. *Thomas Telford Limited. London.*

Kalinske, A. A. and Robertson, J. W. (1943). Entrainment of Air in Flowing Water in Closed conduit flow. ASCE *Transactions 108: 1435-1447*.

Knapp, R. T., Daily J. W., and Hammit, F. G. (1970). Cavitation. McGraw-Hill Book Company, *New York, London.*

Launder, B. E., & Spalding, D. B. (1972). *Lectures in Mathematical Models of Turbulence.* London: Academic Press.

Levin, L. (1965). Calcul Hydraulique des Conduits d'Aeration des Vidanges de Fond et Dispositifs Deversants. *L. Houille Blanche,No. 2* (in French).

Lewin, J. (1995). Hydraulic Gates and Valves in free surface flow and submerged outlets*. T. Telford, London*.

Logan, C., Louwinger, F., Mongili, E., & Lillie, E. (2011). *Confidential Report.*

Najafi, M. R. and Zarrati, A. R. (2007). Numerical simulation of air-water flow in gated tunnels. *Proceedings of the Institution of Civil Engineers. Water management 163 Issue WM6, pp 289-295.*

Naudascher, E. (1991). Hydrodynamic forces. *IAHR Hydraulic Structures Design Manual* 3. Balkema, Rotterdam, the Netherlands.

Novak, P. Moffat, A.I.B. Naluri, C. and Narayanan, R. (2007). Hydraulic Structures. Fourth Edition. Taylor and Francis Group, Oxon.

Rabben, S. L., & Rouvè, G. (1985). Belüftung von Grundablässen. *Wasserwirtschaft 75(9)* , 393-399.

Schmitt, S. (2011). *Personal Communication.*

Sharma, H. R. (1976). Air entrainment in high head gated conduits. *Proceedings of ASCE, Journal of the Hydraulics Division. vol.102, No.11, pp.1629-1646.*

Speerli, J., & Hager, W. H. (2000, June). Air-water flow in bottom outlets. *Canadian Journal of Civil Engineering* , pp. 454-462.

U. S. Army Corps of Engineers. (1964). *Hydraulic Design Criteria*. Air demand, Regulated outlet works, Sheet 050-1.

Van Vuuren, S. (2003). *Berg River Project Hydraulic Model Testing of the Outlet works Model Scale 1:20.* Sinotech CC, South Africa.

Vischer, D. L. and Hager, W. H. (1998). Dam Hydraulics. *Wiley Series in Water Resources Engineering*, England

Versteeg, H. K. and Malalasekera, W. (2007). The Finite Volume Method. *An Introduction to Computational Fluid Dynamics*. Second Edition. *Pearson edition published*, England.

Wisner, P. (1965). On the role of the Froude criterion for the study of air entrainment in high velocity flows. *Proceedings of the 11th IAHR Congree, USSR, Leningrad.*